Thesis for the Degree of Licentiate of Engineering

Nyquist Stability Analysis of a VSC-HVDC System with a Distributed Parameter DC-cable Model

Yujiao Song

Group of Automatic Control
Department of Signals and Systems
Chalmers University of Technology
Göteborg, Sweden 2015

Nyquist Stability Analysis of a VSC-HVDC System with a Distributed Parameter DC-cable Model

Yujiao Song

Technical report number: XXXX/2015
ISSN 1403-266X

Group of Automatic Control
Department of Signals and Systems
Chalmers University of Technology
SE–412 96 Göteborg
Sweden

Telephone: +46 (0)31 – 772 1000

Email: yujiao@chalmers.se

Typeset by the author using LaTeX.

Chalmers Reproservice
Göteborg, Sweden 2015

to my parents

Abstract

Voltage source converter based high voltage direct current (VSC-HVDC) transmission systems have now been in operation since 1997 as it is a reliable and flexible method of power transmission. This thesis focuses on small signal dynamics of such systems, emphasizing stability properties. When modeling such systems, the DC-cable is most often approximated by a single Π-section and there are questions if this is accurate enough to decide on if a certain VSC-HVDC system is stable or not. To be independent of this approximation, we propose the use of a distributed parameter cable model, based on the damped wave equation.

Under assumption of strong grid AC environment, the VSC-HVDC system with distributed parameter DC cable model can be described by two cascaded blocks. The first block is a transfer function that will be different, due to which input and output variables that are considered but is in all realistic cases stable. The second block is a feedback loop, where the forward path is a rational function and the return path is a dissipative infinite dimensional function, that remains the same in all cases. The stability is then analyzed using the Nyquist criterion in a straight forward manner.

The stability analysis of two terminal VSC-HVDC systems embedded in a weak AC-grid can be separated into two parts: the active power controlled VSC and the VSC-HVDC system while the active power controlled VSC is under steady state. The stability of the first part is analyzed by the small gain theorem. The second part is analyzed by the Nyquist criterion. Similar to the strong AC-grid case, the system can be described by two cascaded blocks. The first block is a transfer function and the second block is a feedback loop. Note that all blocks, however, will be a bit more complicated than in the strong AC-grid case. One example is given, showing that the VSC-HVDC system with a single Π-section cable model is sufficient to prove system stability, independently of the DC-cable length and impedance density.

Keywords: Electric power transmission, VSC-HVDC system, Distributed parameter cable model, Nyquist stability analysis, Weak AC-grid, Small gain theorem.

Acknowledgments

I would like to thank my examiner and supervisor Professor Claes Breitholtz who worked with me closely during my PhD studies. I'm very grateful for the enormous time he spend and effort he made to teach me how to give presentations, to write papers, and to do research. I would also like to thank my co-supervisor Professor Lina Bertling-Tjernberg for her encouragement, support and discussion of this study. I have been very fortunate to have the chance to collaborate with the researchers at Electric power Department, including Professor Massimo Bongiorno and Georgios Stamatiou. I thank all of them for the fruitful collaboration and stimulating discussions. The financial support provided by the Chalmers Energy Initiative research program is gratefully acknowledged.

Many thanks to the reference group members, Tuan Ahn Le and Per Norberg from Chalmers, Lennart Harnefors and Bertil Berggren from ABB, Emil Hillberg from STRI, Anders Manikoff formerly from SP, Abdel-Aty Edris from Quanta Technology, Wang Feng and Gustavo Pinares, for their ideas and passionate discussion during the reference meetings.

Working at the division of Automatic control, Automation and Mechatronics has been an exciting experience. I would like to thank all colleagues for making this such a nice environment to work in. I would also like to thank my friend Yinan Yu for providing me various kinds of help and I will always remember the time we spent together.

Finally, I want to thank my parents. Thank you for the constant support, consideration, patience and endless love.

Yujiao Song
Göteborg, June 2015

List of publications

This thesis is based on the following appended papers:

Paper 1

Y. Song and C. Breitholtz, Nyquist stability analysis of a VSC-HVDC system using a distributed parameter DC-cable model, *19th World Congress of the International Federation of Automatic Control*, August 2014, Cape Town, South Africa.

Paper 2

Y. Song and C. Breitholtz, Nyquist Stability Analysis of an AC-grid connected VSC-HVDC System Using a Distributed Parameter DC-cable Model, *submitted for publications in IEEE Tran. on Power Delivery, special issue: HVDC transmission systems for large offshore wind power plants.*

Other publications

In addition to the appended papers, the following paper by the thesis author are related to the topic of the thesis:

G. Stamatiou, Y. Song, M. Bongiorno and C. Breitholtz, Analytical investigation of poorly damped resonance conditions in HVDC systems, *submitted for publications in IEEE Tran. on Power Delivery, special issue: HVDC transmission systems for large offshore wind power plants.*

List of Abbreviations

abc-frame	Three phase reference frame
AC	Alternating current
DC	Direct current
dq-frame	Direct-Quadrature reference frame
HVDC	High voltage direct current
LCC	Line commuted converter
LPF	Low pass filter
PCC	Point of common coupling
PI-controller	Proportional Integral controller
PLL	Phase locked loop
p.u.	Per unit
PWM	Pulse width modulation
SCR	Short circuit ratio
TF	Transfer function
VSC	Voltage source converter
VSC-HVDC	Voltage source converter based high voltage direct current

List of Symbols

x^{ref}	Reference signals of variable x
x_0	Steady state value of variable x
Δx	Small variation of variable x
x_i	Variable x at the i-th VSC side, where $i = 1, 2$
$\tilde{x}$	Laplace transform of the time domain variable x
v_{sd}	d-axis of the AC source voltage v_s
v_{sq}	q-axis of the AC source voltage v_s
E	PCC voltage in the dq-frame
E^{abc}	PCC voltage in the abc-frame
E_{cd}	Converter measured PCC voltage E_c in the d-axis
E_{cq}	Converter measured PCC voltage E_c in the q-axis
v_c^{abc}	Converter voltage in the abc-frame
v_{cd}	d-axis of the converter voltage v_c
v_{cq}	q-axis of the converter voltage v_c
i	Converter input current in the dq-frame
i^{abc}	Converter input current in the abc-frame
i_{cd}	Converter measured input current i_c in the d-axis
i_{cq}	Converter measured input current i_c in the q-axis
L	Series inductance of the VSC phase reactor
R	Series resistance of the VSC phase reactor
Z_g	Series AC-grid impedance matrix in the dq-frame
L_g	Series AC-grid inductance
R_g	Series AC-grid resistance
C	DC-side shunt capacitor
f_0	Fundamental AC-grid frequency
ω_0	Fundamental AC-grid angular velocity $\omega_0 = 2\pi f_0$
f_{sw}	Switching frequency of the PWM
T_{sw}	Time delay due to the switching action of the PWM
P	Active power absorbed by the VSC from the AC-grid
Q	Reactive power absorbed by the VSC from the AC-grid
P_{load}	Active power absorbed from the VSC to the DC-grid

i_{DC}	Direct current flow into the DC-grid
v_{DC}	Direct voltage of the VSC's DC shunt capacitor
K_p	Proportional gain of the inner current PI-controller
K_i	Integral gain of the inner current PI-controller
α_c	Bandwidth of the inner current control loop
K_{pd}	Proportional gain of the DC-voltage PI-controller
K_{id}	Integral gain of the DC-voltage PI-controller
α_d	Bandwidth of the DC-voltage control loop
α_f	Bandwidth of the LPF of the DC load power P_{load}
$\hat{C}$	Approximate shunt capacitor at the DC-side of VSC
ζ	Damping ratio of the DC-voltage control loop
ω_{nd}	Natural frequency of the DC-voltage control loop
K_{pp}	Proportional gain of the active power PI-controller
K_{ip}	Integral gain of the active power PI-controller
α_p	Bandwidth of the active power control loop
K_{pa}	Proportional gain of the AC-voltage P-controller
θ	AC-grid phase angle estimated by the PLL
$K_{p,pll}$	Proportional gain of the PLL PI-controller
$K_{i,pll}$	Integral gain of the PLL PI-controller
α_{pll}	Bandwidth of the PLL
r	Resistance density of the DC-cable
l	Inductance density of the DC-cable
c	Capacitance density of the DC-cable
g	Conductance density of the DC-cable
d	Length of the DC-cable
L_{DC}	Equivalent inductance of the single Π-section DC-cable model
R_{DC}	Equivalent resistance of the single Π-section DC-cable model
C_{DC}	Equivalent capacitance of the single Π-section DC-cable model at each terminal
$\gamma(s)$	Characteristic wave complex damping factor of the DC-cable
$Y_0(s)$	Characteristic wave admittance of the DC-cable
$h_i(s)$	TF of the distributed parameter DC-cable model, $i = 1, 2$
$h_{\pi i}(s)$	Equivalent TF of the single Π-section DC-cable model, $i = 1, 2$
$g_0(s)$	Forward block TF of the VSC-HVDC system block diagram
$g_1(s)$	Forward TF of the feedback loop of the block diagram
$g_{ij}(s)$	TF from the i-th input to the j-th output of the VSC-HVDC system under weak AC-grid
$\hat{g}_{ij}(s)$	TF from the i-th input to the j-th output of the VSC-HVDC system under strong AC-grid
w	Disturbance input variables due to AC-grid dynamics

Contents

II Included papers

Part I

Introductory chapters

Chapter 1

Overview

1.1 Background

Voltage source converter based high voltage direct current (VSC-HVDC) transmission systems have now been in operation since 1997 as it is a reliable and flexible method of power transmission [1]. In principle, the operation of VSCs don't rely on the strength of the connected AC systems compared with the line commuted converter (LCC-HVDC) transmission technology. Furthermore, it provides independent control of the reactive power at the two ends and independently of the active power transfer over the DC transmission [2]. A typical application of a VSC-HVDC system would be the integration of renewable energy resources over large geographical areas, such as wind farms [3].

Various control aspects of these VSC-HVDC systems have been addressed, especially focusing on the control strategy and small signal stability analysis. Without considering the DC load dynamics, the stability and control strategy of a single DC-voltage controlled VSC have been analyzed by [4], which is based on passivity analysis of the input-admittance matrix. In [5], a robust controller is applied to an active power controlled VSC with linearized models in 94 different power and network impedance operating points, which shows that with the synthesized lower order multi-performance controllers, a better overall performance have been achieved compared with standard Glover-McFarlane loop shaping procedure controller. For multi-terminal HVDC systems, a distributed controller is applied to maintain the voltage levels of the converters close to the nominal voltages, while at the same time, the injected current is fairly shared amongst the converters [6].

From the system theory point of view the VSCs involve several linear subsystems, for example PI-controllers and linear circuit elements, but also nonlinear subsystems, due to the relations between power and voltage (or

current). If large changes in voltage levels should be taken into account, for example due to severe system faults, nonlinear dynamical models must be used in analysis as well as in simulation. A major interest has been in the dynamics close to steady state (implying sinusoidal steady state at the AC-side and constant steady state at the DC-side). Consequently, linearized dynamical models have been much in focus [7].

However, little attention has so far been paid to evaluate the influence of DC cable dynamics of VSC-HVDC systems, especially when embedded within weak AC-environment. Typically, DC-cables have been modeled by a single Π-section and thus the stability of linearized multi-terminal or two-terminal VSC-HVDC systems could be analyzed by straightforward calculation of the system eigenvalues [8] [9]. This is often sufficient, at least when considering dynamics of short cables and low frequencies. If more general results are required, for example fast system excitation caused by abrupt disturbances and perhaps in submarine cables (due to increased impedance density i.e. inductance density, capacitance density and resistance density), it would be more appropriate to use a distributed parameter cable model together with transfer functions (or finite order state-space) in the linearized VSC-models.

1.2 Main contribution of the thesis

The main contributions of this research are the following:

1. Transfer function approach to model the linearized VSC-HVDC system, permitting the use of a distributed parameter cable model.

   Schemes and equations are deduced in this thesis and simulation results in frequency domain will be showed as well. The purpose is to provide a tool for small signal analysis of the total VSC-HVDC system, including a cable model that is valid independently of cable length and impedance density or which frequencies that can be considered due to the cable model approximation.

2. Using the infinite dimensional VSC-HVDC model to investigate small signal stability by use of the Nyquist criterion.

   The system can be described by two cascaded blocks: One is a forward combination of transfer functions that will be different, due to which input signal and which output signal that are considered. In cases of VSC-HVDC system embedded in the strong AC-grid, the first block is input to output stable. The second block is a feedback system, where the forward subsystem is finite dimensional and the return subsystem

only depends on the infinite dimensional cable model. The stability of this feedback system, which remains the same for all combinations of input and output signals, is analyzed by use of the Nyquist criterion.

3. Extending the stability analysis to a VSC-HVDC system embedded in an uncertain weak AC-grid by use of the small gain theorem.

   The investigation that is based on a distributed parameter DC-cable model, does to a large extent justify the use of a single Π-section for over all system stability assessments of the VSC-HVDC system.

1.3 Thesis outline

Chapter 1 provides the introduction to the topic, where the background and contributions are presented. In Chapter 2, the VSC-HVDC system topology, the local controllers around the VSC's, at the AC- as well as the DC-sides, and the grid dynamics are presented to explain the system functions. Chapter 3 continues with the block diagram of the constructed VSC-HVDC system dynamics, which can be made to take the form of a forward combination of transfer functions cascaded by a feedback system. The simulation and stability analyses of the VSC-HVDC system are presented in Chapter 4. Finally, the thesis ends with conclusions and summary of the attached papers, which are given in Chapter 5 and Chapter 6 respectively.

Chapter 2

VSC-HVDC system

The intention of this chapter is to provide the reader with a VSC-HVDC transmission scheme and the main control technologies applied to the VSC. Following to that, the most important elements of a VSC is presented. Then, the principles of the inner current control loop, the active power and DC voltage control loops, the reactive power and AC voltage control loops, and the phase locked loop (PLL) are described in detail. Finally, the DC cable model and the AC grid dynamics are presented.

2.1 Introduction

The system under study is depicted in Fig. 2.1. The source voltage, the point of common coupling (PCC) voltage, the converter voltage and the converter input current are denoted by v_s, E, v_c and i respectively. Weak AC-grids are modeled by the impedance matrices $Z_{g1}(s)$ and $Z_{g1}(s)$ at the synchronous dq-frame respectively. The so-called synchronous frame is oriented to be in alignment with the voltage direction, due to the PLL [10]. The PLL dynamics will be considered to build converter grid interconnection.

At the AC-side of the VSCs, the series inductances ($L_1,\ L_2$) and resistances ($R_1,\ R_2$) represent the AC phase reactors and the power losses in the converters. The phase reactors serve the function both of stabilizing the AC current and to enable the control of active and reactive output power from the VSC separately. The DC shunt capacitors at the terminals are denoted by $C_1,\ C_2$ respectively, which serve the purpose of stabilizing the DC voltage and to reduce the ripple introduced by the harmonics injected by the VSC [2].

In standard VSC-HVDC systems, one converter station (VSC1) is assigned the duty as the DC voltage controller to secure the stability of the DC-Bus voltage; the other station (VSC2) operates as the active power

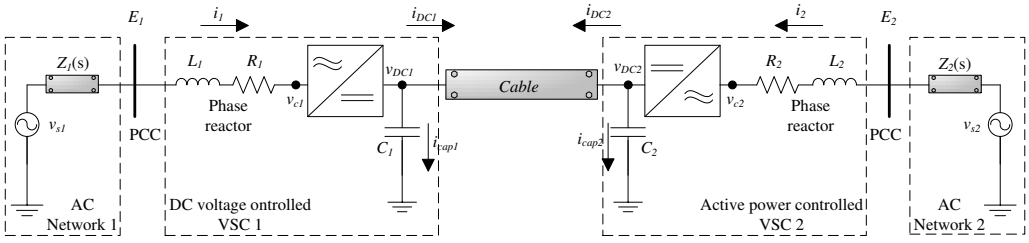

Figure 2.1: Standard HVDC-VSC system embedded in a weak AC environment. v_s is the source voltage; E is the PCC voltage; i is the converter input current; v_c is the converter voltage; E_c is the converter measured PCC voltage; i_c is the converter measured input current; $Z(s)$ is the AC-grid impedance.

controller to guarantee and balance the power exchanges [11]. Moreover, in each VSC, it is possible to control the grid voltage at the AC side, which in this thesis is performed by a P-controller.

If the DC cable is modeled by a single Π-section, the stability of the system can be investigated by an eigenvalue calculation. However, the high frequency information is not necessarily well interpreted by the single Π-section cable model and thus potentially inconvenient to analyze the real dynamic influence of the DC cable. The new standard VSC-HVDC model includes the distributed parameter cable model and formulates the transfer function into the block diagram which enables that the stability of the linearized system can be analyzed by use of the Nyquist criterion [12] [13].

2.2 VSC control system

In this section, the VSC model is derived in the so-called power invariant dq reference frame [14], where the frame is chosen to be in align with the PCC voltage direction i.e. $E_{cq10} = E_{cq20} = 0$. E_{10} and E_{20} are the steady states of the converter measured PCC voltage. The two VSCs are assumed to be ideal and symmetrical, having a switching frequency of 1 [kHz]. In the following, the units for voltage, current and active power are [kV], [kA] and [MW] respectively and all reference signals x are expressed as x^{ref}, the differential operator with respect to time is denoted 'p' and the Laplace transform of a time domain variable $x(t)$ is denoted $\tilde{x}(s)$.

The AC-grid frequency is assumed to be constant i.e. $\omega_0 = 2\pi f_0$ and $f_0 = 50$ [Hz]. Since the VSCs are assumed symmetric, the variables and parameters in this section are not subscribed by the numbers 1 and 2, used to denote the different VSCs.

The local controller of the VSC is separated into two cascaded parts:

inner current controller and outer controller. The inner current controller provides the voltage reference (v_{cd}^{ref} and v_{cq}^{ref}) to the pulse width modulator (PWM). The d-axis outer controller is used to track the reference of either the DC voltage or the active power and generates the d-axis current reference (i_d^{ref}) to the inner current loop; The q-axis outer P-controller is used to decrease the voltage drop of the PCC voltage [4] and it therefore generates a reference for the q-axis current (i_q^{ref}).

Vector current control method

The principle of the VSC controller is to control the magnitude and phase of the fundamental frequency component of the AC voltage at the valve side of the series inductive interface (v_c), in such a way that the converter input current (i) through the phase reactor has the desired phase and magnitude as well.

With the vector control method, three phase currents are transformed to d and q axis quantities based on the Park transformation [14]. Similarly, the desired current d and q quantities can be calculated by the desired current magnitude and phase in the three phase system. Since the dq frame is chosen to be in align with the PCC voltage, the active power P^{ref} and the reactive power Q^{ref} are thus determined by i_{cd} and i_{cq} separately [2].

Applying the voltage Kirchhoff law to the phase reactor at the AC side of the VSC

$$L \cdot \frac{\mathrm{d}i^{abc}}{\mathrm{d}t} = -R \cdot i^{abc} + E^{abc} - v_c^{abc} \tag{2.1}$$

where the relation between the abc and dq reference frames is given by Park's transformation:

$$x^{abc} = P^{-1} x_{dq0} \tag{2.2}$$

$$P = \frac{2}{3} \begin{bmatrix} \cos(\omega t) & \cos(\omega t - \frac{2\pi}{3}) & \cos(\omega t + \frac{2\pi}{3}) \\ -\sin(\omega t) & -\sin(\omega t - \frac{2\pi}{3}) & -\sin(\omega t + \frac{2\pi}{3}) \\ \frac{1}{2} & \frac{1}{2} & \frac{1}{2} \end{bmatrix}$$

Applying the Park transformation to (2.1), the dq frame model of current dynamics is obtained:

$$L \cdot \frac{\mathrm{d}i_{cd}}{\mathrm{d}t} = -R \cdot i_{cd} + \omega_0 L \cdot i_{cq} + E_{cd} - v_{cd} \tag{2.3}$$

$$L \cdot \frac{\mathrm{d}i_{cq}}{\mathrm{d}t} = -R \cdot i_{cq} - \omega_0 L \cdot i_{cd} + E_{cq} - v_{cq} \tag{2.4}$$

The current controller consists of one PI-controller and two feed forward signals, i.e. the PCC voltage and the cross coupling current [15]. The

reference voltages (v_{cd}^{ref}, v_{cq}^{ref}) are given by:

$$v_{cd}^{ref} = -(K_p + \frac{K_i}{p})(i_d^{ref} - i_{cd}) + E_{cd} + \omega_0 L \cdot i_{cq} \tag{2.5}$$

$$v_{cq}^{ref} = -(K_p + \frac{K_i}{p})(i_q^{ref} - i_{cq}) + E_{cq} - \omega_0 L \cdot i_{cd} \tag{2.6}$$

Due to the switching action of PWM inside the converter, a delay of half a switching period appears, where $T_{sw} = 1/(2f_{sw}) = 0.5$ [ms]. After having designed the inner current loop relatively slow, the delay is reasonable to ignore in the analysis of system dynamics i.e. $v_{cd}^{ref} \approx v_{cd}$ and $v_{cq}^{ref} \approx v_{cq}$ [4]. Consequently, the dynamics between the d- and q-axis is decoupled at the inner current loop.

The PI-parameters are designed as $K_p = \alpha_c L$ and $K_i = \alpha_c R$, where α_c is the desired bandwidth of the inner current loop and the phase reactor pole of $-R/L$ is thus canceled by the inner current PI-controller. Note that the unavoidable uncertainties in the AC side model parameters, L and R, from a practical point of view are assumed to be quite small. Hence these uncertainties will have only a minor impact on the inner current loop performance. In addition, since the outer loop bandwidth usually is designed to be at least ten times smaller than α_c, the effect caused by the inner loop parameter uncertainty will not influence the entire system dynamics very much. Therefore, the design of the inner current loop PI-controller based on model parameters is well justified. Consequently, the linearized inner current closed loop in the Laplace domain is:

$$\Delta\tilde{i}_{cd}(s) = \frac{\alpha_c}{s + \alpha_c}\Delta\tilde{i}_d^{ref}(s) \tag{2.7}$$

$$\Delta\tilde{i}_{cq}(s) = \frac{\alpha_c}{s + \alpha_c}\Delta\tilde{i}_q^{ref}(s) \tag{2.8}$$

2.2.1 Direct voltage controller

The DC voltage is determined by the capacitor charging power that is the difference between the input active power to the VSC (assuming that the VSC in itself is power lossless) and the DC load power:

$$\frac{\mathrm{d}}{\mathrm{d}t}(\frac{1}{2}C \cdot v_{DC}^2) = P - P_{load} \tag{2.9}$$

$$\Rightarrow \quad C \cdot v_{DC0} \cdot \frac{\mathrm{d}\Delta v_{DC}}{\mathrm{d}t} = \Delta P - \Delta P_{load} \tag{2.10}$$

Therefore, the linearized expression of the input active power and the

DC load power are required, where the conjugate of x is denoted by x^*:

$$\begin{aligned} P &= Re\{(E_0 + \Delta E_{cd} + j\Delta E_{cq})(i_{d0} + \Delta i_{cd} + j(i_{q0} + \Delta i_{cq}))^*\} \\ &\approx \underbrace{E_0 i_{d0}}_{P_0} + \underbrace{E_0\Delta i_{cd} + i_{d0}\Delta E_{cd} + i_{q0}\Delta E_{cq}}_{\Delta P} \end{aligned} \tag{2.11}$$

$$\begin{aligned} P_{load} &= (v_{DC0} + \Delta v_{DC})(i_{DC0} + \Delta i_{DC}) \\ &\approx \underbrace{v_{DC0} i_{DC0}}_{P_{load0}} + \underbrace{v_{DC0}\Delta i_{DC} + i_{DC0}\Delta v_{DC}}_{\Delta P_{load}} \end{aligned} \tag{2.12}$$

Equation (2.11) shows that ΔP is proportional to Δi_{cd} and independent of Δi_{cq}. Therefore, the output of the DC voltage controller i.e. the d-axis reference current, can be provided through the reference input active power. The reference input active power is the sum of the output from a PI-controller operating on the error of the DC voltage square and the filtered feed forward DC load power (with bandwidth α_f):

$$P^{ref} = (K_{pd} + \frac{K_{id}}{p}) \cdot \nu + \frac{\alpha_f}{p + \alpha_f} P_{load} \tag{2.13}$$

$$\nu = \frac{(v_{DC}^{ref})^2 - v_{DC}^2}{2} \text{ and } i_d^{ref} = \frac{P^{ref}}{E_{cd}} \tag{2.14}$$

$$\Delta\tilde{P}^{ref} = v_{DC0} F_d(\Delta\tilde{v}_{DC}^{ref} - \Delta\tilde{v}_{DC}) + F_f \Delta\tilde{P}_{load} \tag{2.15}$$

$$F_d = K_{pd} + \frac{K_{id}}{s} \text{ and } F_f = \frac{\alpha_f}{s + \alpha_f}$$

$$\Delta\tilde{i}_d^{ref} = \frac{1}{E_0}\Delta\tilde{P}^{ref} - \frac{P_0}{E_0^2}\Delta\tilde{E}_{cd} \tag{2.16}$$

After ignoring both the low-pass filter in (2.15) and the inner current loop dynamics i.e. $\Delta i_{cd} = \Delta i_d^{ref}$, designing the PI-controller parameters as $K_{pd} = 2\hat{C}\zeta\omega_{nd}$ and $K_{id} = \hat{C}\omega_{nd}^2$, the transfer function from $\Delta\tilde{v}_{DC}^{ref}$ to $\Delta\tilde{v}_{DC}$ is:

$$\frac{\Delta\tilde{v}_{DC}}{\Delta\tilde{v}_{DC}^{ref}} \approx \frac{2\zeta\omega_{nd}\frac{\hat{C}}{C}s + \omega_{nd}^2\frac{\hat{C}}{C}}{s^2 + 2\zeta\omega_{nd}\frac{\hat{C}}{C}s + \omega_{nd}^2\frac{\hat{C}}{C}} \tag{2.17}$$

The approximation is based on the fact that the inner current loop dynamics is designed ten times faster than the DC voltage loop and also assume that the DC load power signal has lower magnitude in the higher frequency band.

$\hat{C}$ is the estimated DC-shunt capacitance and C is the actual physical shunt capacitance. The damping ratio ζ and natural frequency ω_{nd} are amplified by $\sqrt{\hat{C}/C}$ compared to the designed parameters. Since the physical shunt capacitance C contains an impact from the DC-cable distributed

shunt capacitance, and is assumed to be a bit larger than $\hat{C}$; then ζ and ω_{nd} should be a bit higher than the designed value in order to compensate for the error. In this thesis, the influence of such parameter uncertainty of C is not considered. ζ and ω_{nd} are chosen to be 1 and $0.4\alpha_d$, which guarantees that the DC-voltage loop bandwidth of (2.17) is α_d.

2.2.2 Active power controller

For the outer controller of transmitted active power, again a PI-controller is used. The controller parameters are designed by inner current loop pole cancelation i.e. $K_{pp} = \alpha_p/\alpha_c$, $K_{ip} = \alpha_p$. The bandwidth of the outer loop is chosen as $\alpha_p = 0.2\alpha_d$. Therefore, the DC voltage would not display large oscillations during the variations of transmitted active power. The linearized differential equations (where $E_{c0} = E_0$) of the active power control loop are derived as follows:

$$i_d^{ref} = (K_{pp} + \frac{K_{ip}}{p})(P^{ref} - P)/E_c \tag{2.18}$$

$$\Rightarrow \Delta\tilde{i}_d^{ref} = \frac{1}{E_0}(K_{pp} + \frac{K_{ip}}{s})(\Delta\tilde{P}^{ref} - \Delta\tilde{P}) \tag{2.19}$$

2.2.3 Reactive power and Alternating voltage controller

The idea of the AC-voltage or reactive power controller is to compensate for the AC-voltage drop i.e. to increase the reactive power at PCC while the AC-voltage is lower than the reference PCC voltage [16]. In this thesis, a P-controller is applied and thus the q-axis reference current is:

$$\Delta\tilde{i}_q^{ref} = K_{pa} * (\Delta\tilde{E}^{ref} - \Delta\tilde{E}_{cd}) \tag{2.20}$$

It is also possible to use a PI-controller instead of a P-controller. The reason not to is that there is no accuracy specification for the AC voltage control and that the insert of an extra integral control action will not promote system stability. Therefore, in this thesis, a P-controller is applied to control the AC voltage.

2.2.4 Phase Locked Loop

A PLL is applied to track the rotating phase angle θ^{ref}, which is used for transforming the converter dq frame from the stationary $\alpha\beta$ frame. At steady state, the converter dq frame coincides with the grid dq frame. E_s, E and E_c are the PCC voltages in the $\alpha\beta$ frame, grid dq frame and converter dq frame respectively. θ^{ref} and θ are the grid phase angle and converter

phase angle (tracked through PLL). At steady state, $\theta = \theta^{ref}$. The frame transformation gives: $E_s = e^{j\theta^{ref}}E$ and $E_s = e^{j\theta}E_c$. Introducing $\Delta\theta = \theta - \theta^{ref}$, obviously E_c is expressed as $E_c = e^{-j\Delta\theta}E$.

Since the phase angle and the AC frequency cannot be measured directly, the measured sinusoidal PCC voltage is used to track the phase angle together with one PI-controller, $F_{pll}(s) = \left(K_{p,pll} + \frac{K_{i,pll}}{s}\right)$. The block diagram of the nonlinear PLL is shown at Fig. 2.2. At steady state, $\Delta\theta = 0$ and the imaginary part (q-axis) of the PCC voltage in the converter dq frame is zero as well, i.e., at steady state, $E_c = E_0$. The linearized equations are given as follows, where $e^{-j\Delta\theta} \approx 1 - j\cdot\Delta\theta$ if $|\Delta\theta| \leq \varepsilon$, where ε is very small.

$$\begin{aligned} E_c &= E\cdot e^{-j\Delta\theta} \approx (E_0 + \Delta E)\cdot(1 - j\cdot\Delta\theta) \\ &\approx E_0 + \Delta E - jE_0\cdot\Delta\theta \qquad (2.21) \\ \Delta\omega &= \left(K_{p,pll} + \frac{K_{i,pll}}{p}\right)\cdot \mathrm{Im}\{E_c\} \\ &= F_{pll}(p)\cdot(\mathrm{Im}\{\Delta E\} - E_0\cdot\Delta\theta) \qquad (2.22) \\ \frac{\mathrm{d}\Delta\theta}{\mathrm{d}t} &= \frac{\mathrm{d}(\theta - \theta^{ref})}{\mathrm{d}t} = \omega - \omega^{ref} \\ &= \omega_0 + F_{pll}(p)\cdot(\mathrm{Im}\{\Delta E\} - E_0\cdot\Delta\theta) - \omega^{ref} \qquad (2.23) \end{aligned}$$

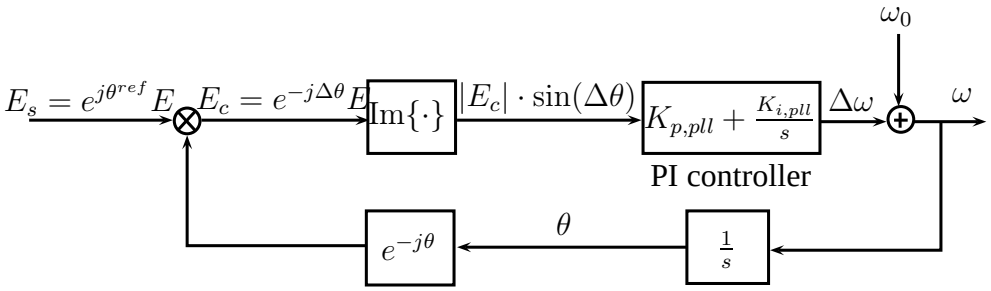

Figure 2.2: Model of Phase Locked Loop

As $\omega^{ref} = \omega_0$, a P-controller is enough to reach zero steady state error, which implies that the integral action of the PI-controller is used to compensate for the grid frequency approximation. In this thesis, we assume that $\omega^{ref} = \omega_0$ and design $K_{i,pll} = 0$, $K_{p,pll} = \alpha_{pll}/E_0$. The transfer function from $\mathrm{Im}\{\Delta E\}$ to $\Delta\theta$ is $G_{pll}(s) = \frac{\alpha_{pll}/E_0}{s+\alpha_{pll}}$. The bandwidth of the PLL, α_{pll}, should satisfy: $\alpha_{pll} < 0.1\alpha_c$, where α_c is the bandwidth of the inner current loop [17].

As we discussed above, at steady state, the converter dq frame coincides with the grid dq frame, i.e. $E_{c0} = E_0$ and $i_{c0} = i_0$. Besides, $E_c = e^{-j\Delta\theta}E$ and $i = e^{j\Delta\theta}i_c$. After considering the transfer function $G_{pll}(s)$ and the

approximation $e^{-j\Delta\theta} \approx 1 - j \cdot \Delta\theta$, the linearized relations are given as follows:

$$\begin{aligned} E_c &= E \cdot e^{-j\Delta\theta} \approx (E_0 + \Delta E) \cdot (1 - j \cdot \Delta\theta) \\ &\approx E_0 + \Delta E - jE_0 \cdot \Delta\theta \qquad (2.24) \\ \Delta E_c &= \Delta E - jE_0 \cdot \Delta\theta \\ &= \Delta E - jE_0 \cdot G_{pll}(p) \cdot \mathrm{Im}\{\Delta E\} \qquad (2.25) \\ i &= i_c \cdot e^{j\Delta\theta} \approx (i_0 + \Delta i_c) \cdot (1 + j \cdot \Delta\theta) \\ &\approx i_0 + \Delta i_c + ji_0 \cdot \Delta\theta \qquad (2.26) \\ \Delta i &= \Delta i_c + ji_0 \cdot \Delta\theta \\ &= \Delta i_c + ji_0 \cdot G_{pll}(p) \cdot \mathrm{Im}\{\Delta E\} \qquad (2.27) \end{aligned}$$

In the Laplace form, the relations are given as:

$$\begin{aligned} \Delta\tilde{E}_{cd} &= \Delta\tilde{E}_d \qquad (2.28) \\ \Delta\tilde{E}_{cq} &= (1 - E_0 G_{pll}(s)) \cdot \Delta\tilde{E}_q \qquad (2.29) \\ \Delta\tilde{i}_d &= \Delta\tilde{i}_{cd} - i_0^q G_{pll}(s) \cdot \Delta\tilde{E}_q = \Delta\tilde{i}_{cd} + \frac{Q_0}{E_0} G_{pll}(s) \cdot \Delta\tilde{E}_q \qquad (2.30) \\ \Delta\tilde{i}_q &= \Delta\tilde{i}_{cq} + i_0^d G_{pll}(s) \cdot \Delta\tilde{E}_q = \Delta\tilde{i}_{cd} + \frac{P_0}{E_0} G_{pll}(s) \cdot \Delta\tilde{E}_q \qquad (2.31) \end{aligned}$$

The equilibriums of the PLL are $\Delta\omega = 0$ and $\Delta\theta = k\pi$ (k is odd implies unstable equilibrium and k is even implies stable equilibrium), thus the initial value of $\Delta\theta$ should be bounded within $[-\pi\ \pi]$ in order to reach equilibrium $\Delta\omega = 0$ and $\Delta\theta = 0$. For the strong AC grid case, the PLL dynamics is ignored, which implies $G_{pll}(s) = \frac{\alpha_{pll}/E_0}{s+\alpha_{pll}} \approx 1/E_0$.

2.3 AC grid model

The AC grid model is not unique. In this thesis, the AC grid is modeled by the series $R_g L_g$-circuit. The strength of the AC grid is represented by the short circuit ratio (SCR), which is the ratio between short circuit power and rated power. If the base power unit is set as the rated power, SCR=$1/Z_g$, where Z_g is the AC grid impedance in per unit [18]. For the series connected AC grid, since the transmission line typically has a Q-value ($\omega L_g/R_g$) that exceeds 10, the grid resistance R_g can be ignored when calculating SCR, i.e. SCR$\approx 1/(\omega L_g)$ where ωL_g is the grid reactance in per unit. For a strong grid, L_g is ignored, implying that SCR approaches infinity. The least SCR value which has been practically experienced by the end of year 2004 is 1.3 [2]. There is no particular limit on SCR, however, as the transmittable maximum active power is limited by a smaller SCR.

The dynamics of the series R_gL_g-circuit modeled in the synchronous dq-frame is:

$$\Delta\tilde{v}_{sd} - \Delta\tilde{E}_d = (L_g s + R_g)\Delta\tilde{i}_d - \omega_0 L_g \Delta\tilde{i}_q \tag{2.32}$$

$$\Delta\tilde{v}_{sq} - \Delta\tilde{E}_q = \omega_0 L_g \Delta\tilde{i}_d + (L_g s + R_g)\Delta\tilde{i}_q \tag{2.33}$$

2.4 DC cable model

2.4.1 Distributed parameter DC cable model

The conventional method of approximating a transmission line is to replace the line by cascaded lumped RLCG-sections, which is shown in Fig. 2.3. The terminal voltage and current are represented by v_{DC1}, v_{DC2}, i_{DC1} and i_{DC2}. The cable parameters are given by r, l, c, g and d, which are the cable densities of resistance, inductance, capacitance, conductance, and the cable length.

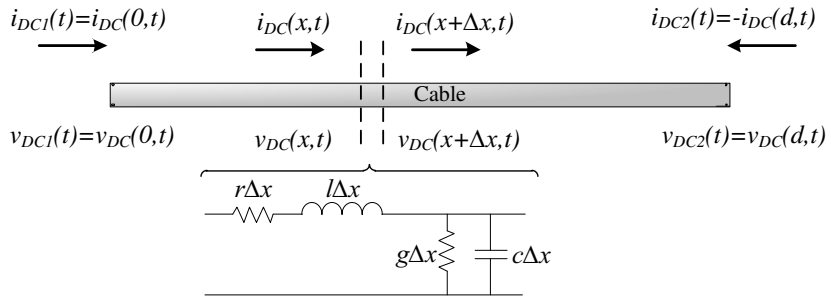

Figure 2.3: DC cable model: since the current from the AC to DC side is defined as positive, $i_{DC1} = i_{DC}(0,t)$ and $i_{DC2} = -i_{DC}(d,t)$

Define the current from the AC to the DC side as a positive current. At arbitrary distance 'x' from terminal 1, the voltage v_{DC} and current i_{DC} obey the following two equations:

$$v_{DC}(x+\Delta x,t) = v_{DC}(x,t) - r\Delta x \cdot i_{DC}(x,t) - l\Delta x \cdot \frac{\partial i_{DC}(x,t)}{\partial t} \tag{2.34}$$

$$i_{DC}(x+\Delta x,t) = i_{DC}(x,t) - g\Delta x \cdot v_{DC}(x+\Delta x,t) - c\Delta x \cdot \frac{\partial v_{DC}(x+\Delta x,t)}{\partial t} \tag{2.35}$$

After dividing by Δx and letting Δx approaches zero, we have the resulting coupled linear partial differential equations for current and voltage

distribution:

$$\frac{\partial v_{DC}(x,t)}{\partial x} + r \cdot i_{DC}(x,t) + l \cdot \frac{\partial i_{DC}(x,t)}{\partial t} = 0 \tag{2.36}$$

$$\frac{\partial i_{DC}(x,t)}{\partial x} + g \cdot v_{DC}(x,t) + c \cdot \frac{\partial v_{DC}(x,t)}{\partial t} = 0 \tag{2.37}$$

Taking Laplace transforms of each term in the above equations, gives:

$$\frac{\mathrm{d}\tilde{v}_{DC}(x,s)}{\mathrm{d}x} + (r + l \cdot s) \cdot \tilde{i}_{DC}(x,s) = 0 \tag{2.38}$$

$$\frac{\mathrm{d}\tilde{i}_{DC}(x,s)}{\mathrm{d}x} + (g + c \cdot s) \cdot \tilde{v}_{DC}(x,s) = 0 \tag{2.39}$$

Differentiate each term in (2.38) with respect to x and replace $\mathrm{d}\tilde{i}_{DC}/\mathrm{d}x$ by use of (2.39). The Laplace transformed version of the damped wave equation is then obtained:

$$\frac{\mathrm{d}^2\tilde{v}_{DC}(x,s)}{\mathrm{d}x^2} - (r + l \cdot s)(g + c \cdot s) \cdot \tilde{v}_{DC}(x,s) = 0 \tag{2.40}$$

Letting A(s), B(s) be constants of integration, the solutions of (2.38) and (2.39) are given as:

$$\tilde{v}_{DC}(x,s) = A(s)\cosh(\gamma(s) \cdot x) + B(s)\sinh(\gamma(s) \cdot x) \tag{2.41}$$

$$\begin{aligned}\tilde{i}_{DC}(x,s) &= -\frac{1}{(r + l \cdot s)}\frac{\mathrm{d}\tilde{v}_{DC}(x,s)}{\mathrm{d}x} \\ &= -\frac{1}{(r + l \cdot s)}(A(s)\gamma(s)\sinh(\gamma(s) \cdot x) + B(s)\gamma(s)\cosh(\gamma(s) \cdot x))\end{aligned} \tag{2.42}$$

A(s) and B(s) are then determined by the boundary conditions:

$$\begin{aligned}&\tilde{v}_{DC}(0,s) = \tilde{v}_{DC1}(s) = A(s) \\ &\Rightarrow A(s) = \tilde{v}_{DC1}(s)\end{aligned} \tag{2.43}$$

$$\begin{aligned}&\tilde{v}_{DC}(d,s) = \tilde{v}_{DC2}(s) = A(s)\cosh(\gamma(s) \cdot d) + B(s)\sinh(\gamma(s) \cdot d) \\ &\Rightarrow B(s) = -\coth(\gamma(s) \cdot d) \cdot \tilde{v}_{DC1}(s) + \frac{1}{\sinh(\gamma(s) \cdot d)}\tilde{v}_{DC2}(s)\end{aligned} \tag{2.44}$$

With the relations of $\tilde{i}_{DC1}(s) = \tilde{i}_{DC}(0,s)$ and $\tilde{i}_{DC2}(s) = -\tilde{i}_{DC}(d,s)$, the terminal voltage and current satisfying the following relations:

$$\tilde{i}_{DC1}(s) = \underbrace{Y_0(s)\coth(\Gamma(s))}_{h_1(s)} \cdot \tilde{v}_{DC1}(s) - \underbrace{Y_0(s)\frac{1}{\sinh(\Gamma(s))}}_{h_2(s)} \cdot \tilde{v}_{DC2}(s) \tag{2.45}$$

$$\tilde{i}_{DC2}(s) = -Y_0(s)\frac{1}{\sinh(\Gamma(s))} \cdot \tilde{v}_{DC1}(s) + Y_0(s)\coth(\Gamma(s)) \cdot \tilde{v}_{DC2}(s) \tag{2.46}$$

In the above equations, $\gamma(s)$ and $Y_0(s)$ denote the characteristic wave complex damping factor and the characteristic wave admittance for the transmission line, respectively. They are defined by:

$$Y_0(s) = \sqrt{\frac{c \cdot s + g}{l \cdot s + r}} \tag{2.47}$$

$$\gamma(s) = d \cdot \sqrt{(c \cdot s + g)(l \cdot s + r)} \text{ and } \Gamma(s) = d \cdot \gamma(s) \tag{2.48}$$

Equivalently, the relation between the terminal terms can be written in the matrix form as:

$$\begin{pmatrix} \tilde{i}_{DC1}(s) \\ \tilde{i}_{DC2}(s) \end{pmatrix} = \begin{pmatrix} h_1(s) & -h_2(s) \\ -h_2(s) & h_1(s) \end{pmatrix} \cdot \begin{pmatrix} \tilde{v}_{DC1}(s) \\ \tilde{v}_{DC2}(s) \end{pmatrix} \tag{2.49}$$

It is worth to be mentioned that $h_1^2(s) - h_2^2(s) = Y_0^2(s) = \frac{c \cdot s + g}{l \cdot s + r}$. $h_1(s)$ and $h_2(s)$ are the short cut admittances at each side.

2.4.2 Single Π-section DC cable model

The single Π-section DC-cable model is depicted in Fig. 2.4.

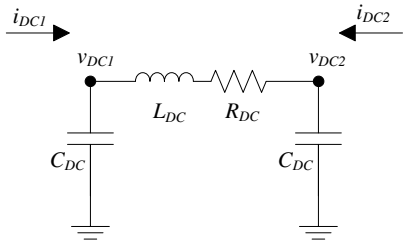

Figure 2.4: Single Π-section DC-cable model: $C_{DC} = d \cdot c/2$, $L_{DC} = d \cdot l$ and $R_{DC} = d \cdot r$.

Similarly, the relation between the terminal voltages and currents can be written in the matrix form as:

$$\begin{pmatrix} \tilde{i}_{DC1}(s) \\ \tilde{i}_{DC2}(s) \end{pmatrix} = \begin{pmatrix} h_{\pi 1}(s) & -h_{\pi 2}(s) \\ -h_{\pi 2}(s) & h_{\pi 1}(s) \end{pmatrix} \cdot \begin{pmatrix} \tilde{v}_{DC1}(s) \\ \tilde{v}_{DC2}(s) \end{pmatrix} \tag{2.50}$$

$$\text{where, } h_{\pi 1}(s) = cs \cdot d/2 + 1/(ls + r)/d$$

$$h_{\pi 2}(s) = 1/(ls + r)/d$$

Chapter 3

Block diagram

In this section, the two terminal VSC-HVDC system embedded in strong or weak AC-environments is considered and transformed into the block diagram in Fig. 3.1.

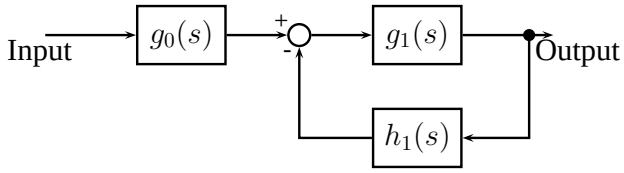

Figure 3.1: Block diagram: g_0 is the forward transfer function, g_1h_1 is the open loop function of the feedback loop $g_1/(1+g_1h_1)$.

3.1 Weak AC-grid environment

Assuming that both VSCs are embedded in a weak AC grid environment, for each VSC system, there are five input signals i.e. Δv_{sd}, Δv_{sq}, Δi_{DC} and reference signals Δv_{DC1}^{ref} or ΔP_2^{ref} and ΔE^{ref}. Note that Δi_{DC} is a state variable in the description of the entire system.

Choose the DC-voltage as the VSC system output. Both Δv_{DC} and Δi_{DC} constitute the interconnection between the VSC and the DC grid. The preliminary transfer functions from those five inputs to the DC voltage are given by

$$\begin{aligned}\Delta\tilde{v}_{DC1} =& g_{11}(s)\Delta\tilde{v}_{DC1}^{ref} + g_{12}(s)\Delta\tilde{E}_1^{ref} + g_{13}(s)\Delta\tilde{v}_{sd1} + \\ &+ g_{14}(s)\Delta\tilde{v}_{sq1} + g_{15}(s)\Delta\tilde{i}_{DC1} \qquad (3.1)\\ \Delta\tilde{v}_{DC2} =& g_{21}(s)\Delta\tilde{P}_2^{ref} + g_{22}(s)\Delta\tilde{E}_2^{ref} + g_{23}(s)\Delta\tilde{v}_{sd2} + \\ &+ g_{24}(s)\Delta\tilde{v}_{sq2} + g_{25}(s)\Delta\tilde{i}_{DC2} \qquad (3.2)\end{aligned}$$

where, the transfer functions $g_{ij}(s)$ can be calculated through the state space model given by (4.9)-(4.11) and (4.16) in Section 4.2.

Combining the relationship between the DC-terminal currents and voltages given by (2.49), the two-terminal VSC-HVDC system transfer function matrix is readily obtained from:

$$\Lambda(s)\begin{bmatrix}\Delta\tilde{v}_{DC1}\\ \Delta\tilde{v}_{DC2}\end{bmatrix} = \Phi(s) * u \tag{3.3}$$

$$\Lambda(s) = \begin{bmatrix}1-g_{15}h_1 & g_{15}h_2\\ g_{25}h_2 & 1-g_{25}h_1\end{bmatrix}$$

$$\Phi(s) = \begin{bmatrix}g_{11} & g_{12} & 0 & 0 & g_{13} & g_{14} & 0 & 0\\ 0 & 0 & g_{21} & g_{22} & 0 & 0 & g_{23} & g_{24}\end{bmatrix}$$

where, $u^T = [\Delta\tilde{v}_{dc1}^{ref}\ \Delta\tilde{E}_1^{ref}\ \Delta\tilde{P}_2^{ref}\ \Delta\tilde{E}_2^{ref}\ \Delta\tilde{v}_{sd1}\ \Delta\tilde{v}_{sq1}\ \Delta\tilde{v}_{sd2}\ \Delta\tilde{v}_{sq2}]$. The MIMO transfer function from inputs to outputs is given as follows, where $\mathrm{adj}(\Lambda)$ denotes the adjoint matrix of Λ:

$$\begin{aligned}\begin{bmatrix}\Delta\tilde{v}_{DC1}\\ \Delta\tilde{v}_{DC2}\end{bmatrix} &= \Lambda^{-1}\Phi\cdot u = \frac{1}{\det\Lambda}\mathrm{adj}(\Lambda)\Phi\cdot u\\ &= \underbrace{\frac{-\frac{g_{15}+g_{25}}{1+Y_0^2 g_{15}g_{25}}}{1-\frac{g_{15}+g_{25}}{1+Y_0^2 g_{15}g_{25}}\cdot h_1}}_{\text{Feedback loop } \frac{g_1}{1+g_1h_1}} \underbrace{\frac{-1}{g_{15}+g_{25}}G(s)}_{\text{Forward function } g_0} * u\end{aligned} \tag{3.4}$$

$$\begin{aligned}G(s) &= \mathrm{adj}(\Lambda)\Phi\\ &= \begin{bmatrix}g_{11}(1-g_{25}h_1) & g_{12}(1-g_{25}h_1) & -g_{21}g_{15}h_2 & -g_{22}g_{15}h_2\\ -g_{11}g_{25}h_2 & -g_{12}g_{25}h_2 & g_{21}(1-g_{15}h_1) & g_{22}(1-g_{25}h_1)\\ g_{13}(1-g_{25}h_1) & g_{14}(1-g_{25}h_1) & -g_{23}g_{15}h_2 & -g_{24}g_{15}h_2\\ -g_{13}g_{25}h_2 & -g_{14}g_{25}h_2 & g_{23}(1-g_{25}h_1) & g_{24}(1-g_{25}h_1)\end{bmatrix}\end{aligned} \tag{3.5}$$

The feedback loop $g_1/(1+g_1h_1)$ remains the same for all combinations of input and output signals. Since the DC cable system is dissipative, the poles of h_1 have negative real part and thus are stable. The number of unstable poles of the open loop function of the feedback system (g_1h_1) is then determined by the rational function g_1. Consequently, the Nyquist stability criterion can be applied to analyze the feedback system stability.

The forward path function g_0 is one element of $-G/(g_{15}+g_{25})$, which varies with different input and output signals. Since g_0 will always be a linear non-feedback combination of rational functions and of h_1 or h_2 (h_1 and h_2 have stable poles), the stability of g_0 is determined by a limited number of poles.

Consequently, by transformation into the block diagram in Fig. 3.1, the VSC-HVDC system stability can be analyzed by the above criteria.

3.2 Strong AC-grid environment

While the connected AC grids are well balanced and strong, i.e. the nominal AC grid voltage is as most subject to small variations, the dynamics of the PLL is ignored. In addition, since the q-axis current has no impact on the dynamics at the DC side (after d- and q-dynamics decoupling at the inner current loop), the q-axis current reference (i_q^{ref}) is thus assumed to be zero. Therefore, there are three input signals for each VSC i.e. Δv_{sd}, Δi_{DC} and reference signal Δv_{DC1}^{ref} or ΔP_2^{ref}. As before, choose the DC-voltage as the VSC output, the preliminary transfer functions from those three inputs to its DC terminal voltage are:

$$\Delta\tilde{v}_{DC1} = \hat{g}_{11}(s)\Delta\tilde{v}_{DC1}^{ref} + \hat{g}_{13}(s)\Delta\tilde{v}_{sd1} + \hat{g}_{15}(s)\Delta\tilde{\tilde{i}}_{DC1} \tag{3.6}$$

$$\Delta\tilde{v}_{DC2} = \hat{g}_{21}(s)\Delta\tilde{P}_2^{ref} + \hat{g}_{23}(s)\Delta\tilde{v}_{sd2} + \hat{g}_{25}(s)\Delta\tilde{\tilde{i}}_{DC2} \tag{3.7}$$

where, the corresponding transfer functions of the strong AC grid case are denoted by $\hat{g}_{ij},\ i = 1, 2\ j = 1, 3, 5$.

Combining the DC grid dynamics (2.49), the transfer functions from inputs $\hat{u} = [\Delta\tilde{v}_{DC1}^{ref}\ \Delta\tilde{P}_2^{ref}\ \Delta\tilde{v}_{sd1}\ \Delta\tilde{v}_{sd2}]^T$ to $[\Delta\tilde{v}_{DC1}\ \Delta\tilde{v}_{DC2}]^T$ are:

$$\begin{bmatrix}\Delta\tilde{v}_{DC1}\\ \Delta\tilde{v}_{DC2}\end{bmatrix} = \underbrace{\frac{-\frac{\hat{g}_{15}+\hat{g}_{25}}{1+Y_0^2\hat{g}_{15}\hat{g}_{25}}}{1-\frac{\hat{g}_{15}+\hat{g}_{25}}{1+Y_0^2\hat{g}_{15}\hat{g}_{25}}\cdot h_1}}_{\text{Feedback loop } \frac{\hat{g}_1}{1+\hat{g}_1 h_1}} \underbrace{\frac{-1}{\hat{g}_{15}+\hat{g}_{25}}\hat{G}(s)}_{\text{Forward function } \hat{g}_0} *\hat{u} \tag{3.8}$$

$$\hat{G}(s) = \begin{bmatrix}\hat{g}_{11}(1-\hat{g}_{25}h_1) & -\hat{g}_{21}\hat{g}_{15}h_2 & \hat{g}_{13}(1-\hat{g}_{25}h_1) & -\hat{g}_{23}\hat{g}_{15}h_2\\ -\hat{g}_{11}\hat{g}_{25}h_2 & \hat{g}_{21}(1-\hat{g}_{15}h_1) & -\hat{g}_{13}\hat{g}_{25}h_2 & \hat{g}_{23}(1-\hat{g}_{15}h_1)\end{bmatrix}$$

For both weak and strong AC-environment, the transfer functions of a two-terminal VSC-HVDC system, using a distributed parameter DC cable model, can be written into the form $g_0 \cdot g_1/(1+g_1h_1)$. The forward function g_0 is determined by the choice of input and output signal, while the feedback loop is invariant of this choice. Using this approach, the small-signal stability of the infinite dimensional system can in principle always be analyzed by the Nyquist criterion.

Chapter 4

Stability analysis

In order to guarantee the stability of the entire system, both the feedback loop and the outer forward path should be stable. Even though the forward path transfer function g_0 is determined by an input-output combination, it will always be a linear non-feedback combination of rational functions and of h_1 or h_2. Thus, the stability of g_0 is determined by the sign of the real parts of a limited number of poles. The stability of the feedback loop is analyzed by use of the Nyquist stability criterion.

Assuming that the closed path $\mathcal{C}$ enclosing all of the right half complex s-plane has the clockwise positive direction, we can apply the Nyquist criterion: The number of anti-clockwise encirclements around the point -1 in the $g_1(s)h_1(s)$-plane should, for a stable closed loop system, equal the number of open loop unstable poles of $g_1(s)$, as $h_1(s)$ is already an input to output stable function [12].

4.1 VSC-HVDC system embedded in a strong AC environment

For a VSC-HVDC system embedded in strong AC grid, the preliminary transfer functions from the four input signals $\hat{u} = [\Delta\tilde{v}_{DC1}^{ref}\ \Delta\tilde{P}_2^{ref}\ \Delta\tilde{v}_{sd1}\ \Delta\tilde{v}_{sd2}]^T$ to the DC voltages v_{DC1} and v_{DC2} are given by (3.8) and the preliminary transfer functions are:

$$\hat{g}_{11} = \frac{\alpha_c\omega_{nd}C_1(2\zeta s + \omega_{nd})}{C_1 s^2(s+\alpha_c) + \alpha_c\omega_{nd}C_1(2\zeta s + \omega_{nd}) + \frac{i_{DC10}}{v_{DC10}}s^2} \tag{4.1}$$

$$\hat{g}_{13} = \frac{\frac{P_{10}}{E_{10}v_{DC10}}s^2}{C_1 s^2(s+\alpha_c) + \alpha_c\omega_{nd}C_1(2\zeta s + \omega_{nd}) + \frac{i_{DC10}}{v_{DC10}}s^2} \tag{4.2}$$

$$\hat{g}_{15} = -\frac{s^2}{C_1 s^2(s+\alpha_c) + \alpha_c \omega_{nd} C_1(2\zeta s + \omega_{nd}) + \frac{i_{DC10}}{v_{DC10}} s^2} \tag{4.3}$$

$$\hat{g}_{21} = \frac{\alpha_p}{(C_2 v_{DC20} s + i_{DC20})(s+\alpha_p)} \tag{4.4}$$

$$\hat{g}_{23} = \frac{\frac{P_{20}}{E_{20}} s}{(C_2 v_{DC20} s + i_{DC20})(s+\alpha_p)} \tag{4.5}$$

$$\hat{g}_{25} = -\frac{v_{DC20}}{C_2 v_{DC20} s + i_{DC20}} \tag{4.6}$$

For each single input single output system, the forward path function g_0 is one element of $-\hat{G}/(\hat{g}_{15} + \hat{g}_{25})$. From (4.1) to (4.6), it shows that $\hat{g}_{11}$, $\hat{g}_{13}$, $\hat{g}_{15}$ have similar pole polynomial and similarly for $\hat{g}_{21}$, $\hat{g}_{23}$ and $\hat{g}_{25}$ except one stable pole $-a_p$. In addition, h_1 and h_2 are stable. The stability of the forward path depends on the zero polynomial $Q_3(s)$ of $\hat{g}_{15} + \hat{g}_{25}$:

$$Q_3(s) = (C_1 + C_2)s^3 + (C_1\alpha_c + \frac{i_{DC10}}{v_{DC10}} + \frac{i_{DC20}}{v_{DC20}})s^2 + \alpha_c K_{pd} s + \alpha_c K_{id} \tag{4.7}$$

To guarantee that the zeros of $Q_3(s)$ are located in the left half plane, the following inequality, resulting from the Routh stability criterion [12], must hold:

$$\frac{C_1\alpha_c + \frac{i_{DC10}}{v_{DC10}} + \frac{i_{DC20}}{v_{DC20}}}{C_1 + C_2} > \frac{K_{id}}{K_{pd}} = \frac{\omega_{nd}}{2\zeta} \tag{4.8}$$

To minimize transmission losses, the DC voltage drop between two terminals should be kept small. Moreover, the bandwidth of the inner current loop α_c is designed to be ten times larger than the DC voltage loop. Therefore the inequality (4.8) holds for all reasonable designs of PI-controllers and the forward path $\hat{g}_0$ for all input-output combinations are thus stable in case of a strong AC-grid environment. The stability of the strong AC grid connected VSC-HVDC system is thus determined by the feedback system $\hat{g}_1/(1 + \hat{g}_1 h_1)$.

In the feedback loop, $\hat{g}_1(s)$ is a rational function with respect to 's' and $h_1(s)$ is input to output stable. Therefore, the number of unstable poles of the open loop transfer function $\hat{g}_1 h_1$ is determined by $\hat{g}_1$, where $\hat{g}_1$ is:

$$\hat{g}_1(s) = \frac{Q_3(s)(ls + r)}{P_5(s)}$$

$$P_5(s) = (ls + r)(C_2 s + \frac{i_{DC20}}{v_{DC20}})[C_1 s^3 + (C_1\alpha_c + \frac{i_{DC10}}{v_{DC10}})s^2 + \alpha_c K_{pd} s + \alpha_c K_{id}] + s^2(cs + g)$$

In the case study setup, the VSC-HVDC system parameters and initial states are listed in Table 4.1; the system bandwidths are listed in Table 4.2. There are two cases that would be discussed in this section: one example is using the rectifier (AC→DC) as DC voltage controller (standard situation) and the other is using the inverter (DC→AC) as DC voltage controller.

Table 4.1: Parameter of VSC-HVDC system

Cable distance	d	50,150,450	km
Cable inductance density	l	0.189	mH/km
Cable capacitance density	c	0.207	μF/km
Cable resistance density	r	0.0376	Ω/km
Cable conductance density	g	0	S/km
Phase reactor inductance	L	53	mH
Phase reactor resistance	R	0.167	Ω
DC shunt capacitor	C	33	μF
Rated AC voltage (dq-frame)	v_{sd0}	200	kV
Rated DC voltage	v_{DC0}	300	kV
Rated transmission power	P_0	600	MW
System frequency	f_0	50	Hz
Weak AC-grid inductance	L_g	53.1	mH
Weak AC-grid resistance	R_g	1.11	Ω

Table 4.2: Bandwidth design of VSC-HVDC system

Inner current loop	α_c	4p.u.	400π [rad/s]
Active power outer loop	α_p	0.1p.u.	10π [rad/s]
DC voltage outer loop	α_d	0.4p.u.	40π [rad/s]
PLL loop	α_{pll}	0.4p.u.	40π [rad/s]

- Rectifier performs as the DC voltage controller

If the rectifier controls the DC voltage and the inverter controls the transmitted active power, the steady states are $v_{DC10} = 300$ [kV] and $P_{20} = -600$ [MW]. The poles of $\hat{g}_1(s)$ with different cable distances are given in Table 4.3. For all three cable distances, there is one unstable pole of the open loop transfer function $\hat{g}_1(s)h_1(s)$.

Table 4.3: Poles of $\hat{g}_1(s)$ with P_{20}=-600MW

d	Poles of $\hat{g}_1(s)$				
50	23.9	-3.3+3.4j	-3.3-3.4j	-206.8+954j	-206.8-954j
150	25.3	-3.3+3.5j	-3.3-3.5j	-204.5+951j	-204.5-951j
450	31.3	-3.3+3.5j	-3.3-3.5j	-194.7+938j	-194.7-938j

The Nyquist plots of the transfer functions $\hat{g}_1(j\omega)h_1(j\omega)$ with different cable distances are given in Fig. 4.1. It shows that for all three cases, $\hat{g}_1(j\omega)h_1(j\omega)$ anti-clockwise encircles the critical point (-1,0) once, which is equal to the number of unstable poles of $\hat{g}_1(s)h_1(s)$. Consequently, for the different cable distances, d = 50 [km], 150 [km], 450 [km], the VSC-HVDC system remains stable at the operational point v_{DC10} = 300 [kV] and P_{20} = -600 [MW]. (For other operating points of both DC-voltage and active power, the VSC-HVDC system still appear to be stable.)

- Inverter performs as the DC voltage controller

If instead the inverter controls the DC voltage and the rectifier controls the transmitted active power, the steady states are v_{DC10} = 300 [kV] and P_{20} = 600 [MW]. The poles of $\hat{g}_1(s)$ with different cable distances are given in Table 4.4. For all three cases, there are two unstable poles of the open loop transfer function $\hat{g}_1(s)h_1(s)$.

Table 4.4: Poles of $\hat{g}_1(s)$ with P_{20}=600 [MW]

d	Poles of $\hat{g}_1(s)$				
50	1.2+11.5j	1.2-11.5j	-3.6	-198+994j	-198-994j
150	1.1+11.3j	1.1-11.3j	-3.6	-195+995j	-195-995j
450	0.95+10.6j	0.95-10.6j	-3.6	-190+996j	-190-996j

The Nyquist plots of the transfer functions $\hat{g}_1(j\omega)h_1(j\omega)$ with different cable distances are given in Fig. 4.2. It shows that for all three cases, $\hat{g}_1(j\omega)h_1(j\omega)$ anti-clockwise encircles the critical point (-1,0) twice, which is equal to the number of unstable poles of $\hat{g}_1(s)h_1(s)$. Consequently, for the different cable distances, d=50 [km], 150 [km], 450 [km], the VSC-HVDC system remains stable at the operational point v_{DC10}=300kV and P_{20}=600MW.

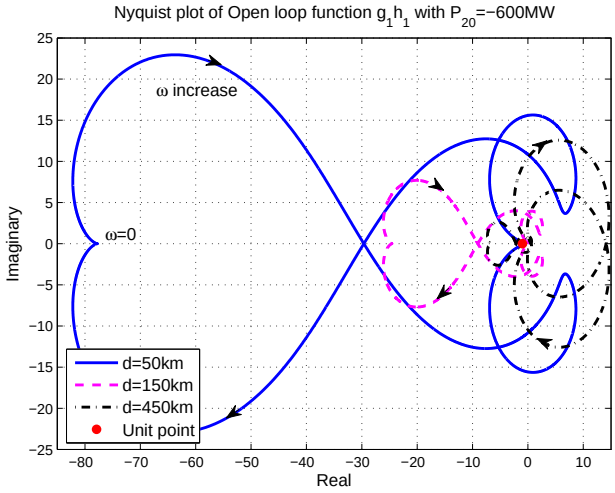

(a)Full curve

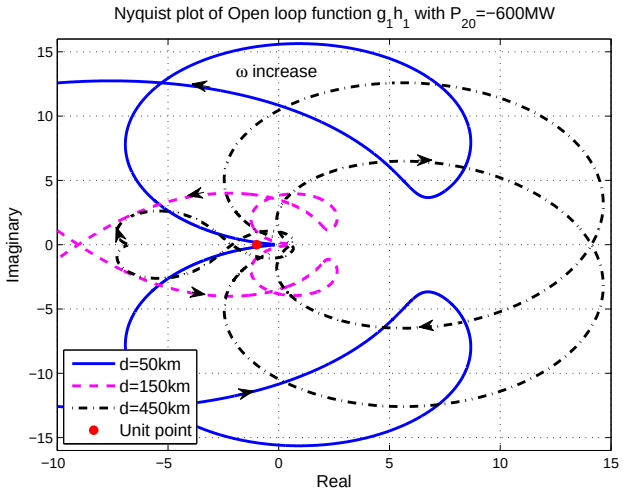

(b)Amplified around critical point (-1,0)

Figure 4.1: Nyquist plot of $\hat{g}_1(j\omega)h_1(j\omega)$ with $P_{20} = -600MW$: blue solid curve is d=50 km; red dashed curve is d=150 km; black dashed dotted curve is d=450 km; the critical point (-1,0) is marked by a red dot.

According to above analysis, the VSC-HVDC system embedded in a strong AC grid will be stable for three different cable distances d=50 [km], 150 [km], 450 [km]. The corresponding conclusion can be made when using the single Π-section cable model. The distributed parameter cable model, hence justifies the use of the single Π-model in most situations.

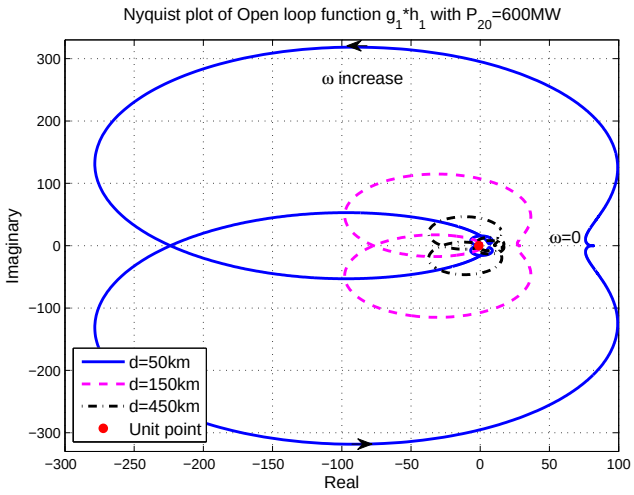

(a)Full curve

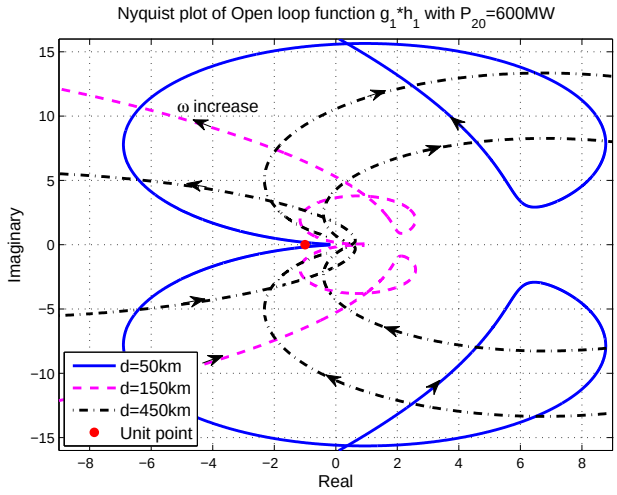

(b)Amplified around critical point (-1,0)

Figure 4.2: Nyquist plot of $\hat{g}_1(j\omega)h_1(j\omega)$ with $P_{20} = 600MW$

4.2 VSC-HVDC system embedded in a weak AC environment

In this section, the stability of the VSC-HVDC system embedded in a weak AC environment is considered. As mentioned in section 2.3, the AC grid is modeled by a series R_gL_g-circuit. In the synchronous coordinates, the AC grid dynamics are given by (2.32-2.33).

For the active power controlled VSC, the transfer function g_{25} from Δi_{DC2} to Δv_{DC2} is the same as the VSC connected to a strong AC-grid. Therefore, $g_{25} = \hat{g}_{25}$ and the feedback loop stability would not be influenced

by the weak AC-grid dynamics at the active power controlled VSC. Similarly, the stability of the active power controlled VSC could be analyzed without considering the DC-side influence. Consequently, the stability analysis of two terminal VSC-HVDC systems embedded in a weak AC-grid can be separated into two parts: the active power controlled VSC and the VSC-HVDC system while the active power controlled VSC is under steady state, which is equivalent as the DC voltage controlled VSC with DC cable.

4.2.1 Stability of Active power controlled VSC

Combining the inner current loop dynamics (2.7),(2.8), active power controlled outer loop dynamics (2.19), AC-voltage controlled outer loop dynamics (2.20) and the PLL dynamics (2.28-2.31), the state-space model of the active power controlled VSC is given by (4.9), (4.11), where the state variables are $x_{ap}^T = [\Delta i_{cd}\ \Delta i_{cq}\ \Delta x_{pll}]$, the input variables are $u_{ap}^T = [\Delta P^{ref}\ \Delta E^{ref}\ \Delta v_{sd}\ \Delta v_{sq}]$ and the disturbance input variables are $w^T = [\Delta E_d\ \Delta E_q]$.

$$\begin{aligned}\dot{x}_{ap} &= A_1 \cdot x_{ap} + B_{u1} \cdot u_{ap} + B_{w1} \cdot w \qquad (4.9)\\ &= \begin{bmatrix} -a_p & 0 & -a_p * \frac{Q_0}{E_0^2} \\ 0 & -a_c & 0 \\ 0 & 0 & -a_{pll} \end{bmatrix} x_{ap} + \begin{bmatrix} \frac{\alpha_p}{E_0} & 0 & 0 & 0 \\ 0 & \alpha_c K_{pa} & 0 & 0 \\ 0 & 0 & 0 & 0 \end{bmatrix} u_{ap} + \\ &\quad + \begin{bmatrix} -a_p * \frac{P_0}{E_0^2} & a_p * \frac{Q_0}{E_0^2} \\ -a_c * K_{pa} & 0 \\ 0 & a_{pll} \end{bmatrix} w\end{aligned}$$

$$w = C_{w1} \cdot x_{ap} + D_{w1} \cdot u_{ap} \qquad (4.10)$$

$$\begin{aligned}C_{w1} &= \frac{L_g}{k_1} \begin{bmatrix} 1 + a_{pll} L_g \frac{P_0}{E_0^2} & -(a_p + a_{pll}) L_g \frac{Q_0}{E_0^2} \\ a_c L_g K_{pa} & 1 - a_p L_g \frac{P_0}{E_0^2} \end{bmatrix} \cdot \\ &\quad \cdot \begin{bmatrix} a_p - \frac{R_g}{L_g} & \omega_0 & \omega_0 \frac{P_0}{E_0^2} + \frac{Q_0}{E_0^2}(a_p + a_{pll} - \frac{R_g}{L_g}) \\ -\omega_0 & a_c - \frac{R_g}{L_g} & (a_{pll} - \frac{R_g}{L_g}) \frac{P_0}{E_0^2} - \frac{Q_0}{E_0^2}\omega_0 \end{bmatrix}\\ D_{w1} &= \frac{1}{k_1} \begin{bmatrix} 1 + a_{pll} L_g \frac{P_0}{E_0^2} & -(a_p + a_{pll}) L_g \frac{Q_0}{E_0^2} \\ a_c L_g K_{pa} & 1 - a_p L_g \frac{P_0}{E_0^2} \end{bmatrix} \cdot \begin{bmatrix} -\frac{ap}{E_0} L_g & 0 & 1 & 0 \\ 0 & -acK_{pa} L_g & 0 & 1 \end{bmatrix}\\ k_1 &= 1 + L_g(a_{pll} - a_p)\frac{P_0}{E_0^2} - L_g^2[a_p a_{pll}\frac{P_0^2}{E_0^4} + a_c(a_p + a_{pll})K_{pa}\frac{Q_0}{E_0^2}]\end{aligned}$$

It appears that while the AC-grid impedance L_g and R_g decrease to zero, $\Delta E_d = \Delta v_{sd}$ and $\Delta E_q = \Delta v_{sq}$ i.e. the connected AC grid is strong. Under strong AC grid environment, the active power controlled VSC is stable and the system poles are $-\alpha_c$, $-\alpha_p$ and $-\alpha_{pll}$. For weak AC grid environment i.e.

non-zero AC grid impedance, the VSC stability depends on the eigenvalues of the disturbed state matrix $A_1 + \Delta A_1$, where $\Delta A_1 = B_{w1}C_{w1}$. C_{w1} is the zero matrix while $L_g = 0$ in the strong AC grid case.

Since the input signals ΔP^{ref}, $DeltaE^{ref}$ are independent of the state variables, the system stability has nothing to do with the value of u_{ap} and thus assume u_{ap} is the zero vector. Under weak-AC environment, the block diagram of the active power controlled VSC with zero input signals is depicted at Fig.4.3, where $G_{ap}(s)$ is stable and ΔA_1 is a constant matrix and thus stable as well.

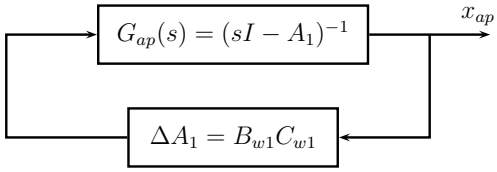

Figure 4.3: Block diagram of VSC

According to the Small Gain Theorem [19], a sufficient condition of a stable VSC system is: for any $\omega \geq 0$, $||G_{ap}(j\omega)||_\infty \cdot ||\Delta A||_\infty < 1$. By denoting the lowest and highest singular value of any matrix M as $\underline{\sigma}(M)$ and $\bar{\sigma}(M)$, the sufficient condition for a stable system is rewritten as:

$$\begin{aligned} & \bar{\sigma}((j\omega I - A_1)^{-1}) \cdot \bar{\sigma}(\Delta A) < 1,\ \omega \in \mathrm{R}^+ \\ \Leftrightarrow\quad & \bar{\sigma}(\Delta A) < \frac{1}{\bar{\sigma}((j\omega I - A_1)^{-1})} = \underline{\sigma}(j\omega I - A_1),\ \omega \in \mathrm{R}^+ \\ \Leftrightarrow\quad & \bar{\sigma}(T^{-1} * \Delta A * T) < \underline{\sigma}(j\omega I - T^{-1} * A_1 * T),\ \omega \in \mathrm{R}^+ \end{aligned} \tag{4.11}$$

The last equivalence holds due to the fact that it is a sufficient condition for a stable equivalent system with state $z = T \cdot x$ as well.

Since the pole corresponding to the state Δi_{cq} is at least ten times further away from the imaginary axis compared to the poles corresponding to the other two states, the dynamics of Δi_{cq} is ignored i.e. $\Delta i_{cq} \approx K_{pa}(\Delta E^{ref} - \Delta E_{cd})$. The reduced order state-space model with new state variables $x_{apn}^T = [\Delta i_{cd}\ x_{pll}]$ is:

$$\begin{aligned} \dot{x}_{apn} &= \tilde{A}_1 \cdot x_{apn} + \tilde{B}_{u1} \cdot u_{ap} + \tilde{B}_{d1} \cdot w \\ &= \begin{bmatrix} -a_p & -a_p * \frac{Q_0}{E_0^2} \\ 0 & -a_{pll} \end{bmatrix} x_{apn} + \begin{bmatrix} \frac{\alpha_p}{E_0} & 0 & 0 & 0 \\ 0 & 0 & 0 & 0 \end{bmatrix} u_{ap} + \\ &\quad + \begin{bmatrix} -a_p * \frac{P_0}{E_0^2} & a_p * \frac{Q_0}{E_0^2} \\ 0 & a_{pll} \end{bmatrix} w \end{aligned} \tag{4.12}$$

$$
\begin{aligned}
w &= \tilde{C}_{w1} \cdot x_{apn} + \tilde{D}_{w1} \cdot u_{ap} \qquad (4.13)\\
\tilde{C}_{w1} &= \frac{L_g}{\tilde{k}_1}\begin{bmatrix} 1 + a_{pll} L_g \frac{P_0}{E_0^2} & -(a_p + a_{pll}) L_g \frac{Q_0}{E_0^2} \\ K_{pa} L_g \frac{R_g}{L_g} & 1 + (\omega_0 K_{pa} - a_p \frac{P_0}{E_0^2}) L_g \end{bmatrix} \cdot \\
&\quad \cdot \begin{bmatrix} a_p - \frac{R_g}{L_g} & \omega_0 \frac{P_0}{E_0^2} + \frac{Q_0}{E_0^2}(a_p + a_{pll} - \frac{R_g}{L_g}) \\ -\omega_0 & (a_{pll} - \frac{R_g}{L_g})\frac{P_0}{E_0^2} - \frac{Q_0}{E_0^2}\omega_0 \end{bmatrix} \\
\tilde{D}_{w1} &= \frac{1}{\tilde{k}_1}\begin{bmatrix} 1 + a_{pll} L_g \frac{P_0}{E_0^2} & -(a_p + a_{pll}) L_g \frac{Q_0}{E_0^2} \\ K_{pa} L_g \frac{R_g}{L_g} & 1 + (\omega_0 K_{pa} - a_p \frac{P_0}{E_0^2}) L_g \end{bmatrix} \cdot \\
&\quad \cdot \begin{bmatrix} -\frac{ap}{E_0} L_g & K_{pa}\omega_0 L_g & 1 & 0 \\ 0 & -\frac{R_g}{L_g} K_{pa} L_g & 0 & 1 \end{bmatrix} \\
\tilde{k}_1 &= 1 + L_g[(a_{pll} - a_p)\frac{P_0}{E_0^2} + \omega_0 K_{pa}] + \\
&\quad + L_g^2[a_{pll}(\omega_0 K_{pa} - a_p \frac{P_0}{E_0^2})\frac{P_0}{E_0^2} + K_{pa}\frac{R_g}{L_g}(a_p + a_{pll})\frac{Q_0}{E_0^2}];
\end{aligned}
$$

For a second order real matrix A with negative real eigenvalues:

$$
\begin{aligned}
A &= \begin{bmatrix} a_{11} & a_{12} \\ a_{21} & a_{22} \end{bmatrix} \\
A \cdot A^T &= \begin{bmatrix} a_{11}^2 + a_{12}^2 & a_{11} \cdot a_{21} + a_{12} \cdot a_{22} \\ a_{11} \cdot a_{21} + a_{12} \cdot a_{22} & a_{21}^2 + a_{22}^2 \end{bmatrix}
\end{aligned}
$$

The singular value of $(j\omega I - A)$ is determined by:

$$
\begin{aligned}
\Psi = j\omega I - A &= \begin{bmatrix} j\omega - a_{11} & -a_{12} \\ -a_{21} & j\omega - a_{22} \end{bmatrix} \\
\Psi\Psi^H &= \begin{bmatrix} a_{11}^2 + a_{12}^2 + \omega^2 & a_{11}a_{21} + a_{12}a_{22} + j\omega(a_{12} - a_{21}) \\ a_{11}a_{21} + a_{12}a_{22} - j\omega(a_{12} - a_{21}) & a_{21}^2 + a_{22}^2 + \omega^2 \end{bmatrix}
\end{aligned}
$$

Since the eigenvalues of A are negative real, the elements of A satisfy: $a_{11} + a_{22} < 0$ and $a_{11}a_{22} - a_{12}a_{21} > 0$. The minimum eigenvalue of $A \cdot A^T$ is $\frac{1}{2}\left[a_{11}^2 + a_{12}^2 + a_{21}^2 + a_{22}^2 - \sqrt{(a_{11}^2 + a_{12}^2 + a_{12}^2 + a_{22}^2)^2 - 4(a_{11}a_{22} - a_{12}a_{21})^2}\right]$. The minimum eigenvalue of $\Psi \cdot \Psi^H$ is $\psi = \omega^2 + \frac{1}{2}\left[a_{11}^2 + a_{12}^2 + a_{21}^2 + a_{22}^2 - \right.$ $\left. - \sqrt{(a_{11}^2 + a_{12}^2 + a_{21}^2 + a_{22}^2)^2 - 4(a_{11}a_{22} - a_{12}a_{21})^2 + 4\omega^2(a_{12} + a_{21})^2}\right]$, where ψ is also the square of the minimum singular value of Ψ and it holds:

$$
\begin{aligned}
&\frac{\partial \psi}{\partial \omega^2}|_{\omega_{opt}} = 0 \;\Rightarrow \\
&1 - \frac{(a_{12} + a_{21})^2}{\sqrt{(a_{11}^2 + a_{12}^2 + a_{21}^2 + a_{22}^2)^2 - 4(a_{11}a_{22} - a_{12}a_{21})^2 + 4\omega_{opt}^2(a_{12} + a_{21})^2}} = 0
\end{aligned}
$$

$$(a_{12}+a_{21})^4 = (a_{11}^2+a_{12}^2+a_{21}^2+a_{22}^2)^2 - 4(a_{11}a_{22}-a_{12}a_{21})^2 + 4\omega_{opt}^2(a_{12}+a_{21})^2$$
$$\Rightarrow \omega_{opt}^2 = -\delta/(a_{12}+a_{21})^2$$
$$\delta = (a_{11}-a_{22})^2[(a_{11}+a_{22})^2+(a_{12}-a_{21})^2] + (a_{12}+a_{21})^2[(a_{11}+a_{22})^2 - 4a_{12}a_{21}]$$

$(a_{11}+a_{22})^2 - 4a_{12}a_{21} > (a_{11}+a_{22})^2 - 4a_{11}a_{22} = (a_{11}-a_{22})^2 > 0$ due to $a_{11}a_{22} - a_{12}a_{21} > 0$, which implies ω_{opt} is negative. Therefore, for any $\omega \in \mathbf{R}^+$, $\frac{\partial \psi}{\partial \omega^2} > 0$. Moreover, the second order partial derivative of ψ with respect to ω^2 is always positive for $\omega \in R^+$ as well, and thus the minimum value of ψ is found at the lower boundary i.e. $\min_{\omega\in\mathbf{R}^+} \underline{\sigma}(j\omega I - A) = \underline{\sigma}(A)$ provided that A is a second order real matrix with negative real eigenvalues.

Consequently, the sufficient condition for a stable active power controlled VSC is:

$$\bar{\sigma}(T^{-1} * \Delta\tilde{A}_1 * T) < \underline{\sigma}(T^{-1} * \tilde{A}_1 * T), \text{ i.e. } \omega = 0 \tag{4.14}$$

Since the differences between the elements of $\Delta\tilde{A}_1$ are large, which provides bigger largest singular value of $\Delta\tilde{A}_1$ and hardly achieve the small gain theorem. Choose the scaling matrix T to be the approximated eigenvectors matrix of $\Delta\tilde{A}_1$:

$$T = \begin{bmatrix} 0.008 & 0.002 \\ -1 & 1 \end{bmatrix}$$

the minimum singular value of $T^{-1}\cdot\tilde{A}_1\cdot T$ and the maximum singular value of $T^{-1}\cdot\Delta\tilde{A}_1\cdot T$ with respect to SCR i.e. SCR=$1/L_g$ p.u. are given in Fig.4.4 and the parameters for the case study are listed in Table 4.2, Table 4.1 and the P-controller parameter of the AC-voltage controller is $K_{pa} = 0.1$.

Since $\tilde{A}_1$ and T are constant matrices, the minimum singular value of $T^{-1}\cdot\tilde{A}_1\cdot T$ is constant and equal to 28.38. As shown in Fig. 4.4., for $SCR > 2.7$, the maximum singular value of $T^{-1}\cdot\Delta\tilde{A}\cdot T$ is smaller than the minimum singular value of $T^{-1}\cdot\tilde{A}_1\cdot T$ and thus the active power controlled VSC is stable. Worth to be mentioned is that, the inequality SCR$>$ 2.7 is a sufficient condition for the stability of the VSC system. For SCR lower than 2.7, however, the system may be stable as well, which can be checked by eigenvalue calculation.

For weak AC grids with other topologies, such as shunt or series L_gC_g-circuits, the small gain theorem could also be applied and get a sufficient condition for stability analysis. However, the disturbance matrix $\Delta\tilde{A}_1$ then needs to be reformulated according to the changed AC grid dynamics.

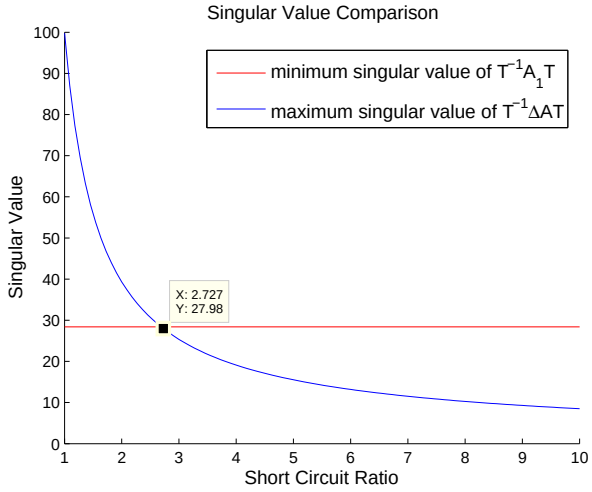

Figure 4.4: Singular value with respect to SCR

4.2.2 Stability of DC voltage controlled VSC with DC cable

As concluded above, the stability of the active power controlled VSC would not influence the stability of the feedback loop $g_1/(1+g_1h_1)$ since $g_{25} = \hat{g}_{25}$. In this subsection, assume that the active power controlled VSC is under steady state. On the other terminal, the DC-voltage controlled VSC is connected to a weak AC-grid, which is modeled by a series L_gR_g-circuit.

- Single Π-section DC-cable model:

While the DC-cable is modeled by one single Π-section, the VSC-HVDC system without considering the dynamics of active power controlled VSC could be modeled by an eighth-order state space model. The state variables are $x_{dv}^T = [\Delta i_{cd}\ \Delta i_{cq}\ \Delta v_{DC}\ x_{dv4}\ x_{dv45}\ x_{pll}\ \Delta i_{DC}\ \Delta v_{DC}^{ap}]$, where x_{dv4} is the integral action of the DC-voltage controller, x_{dv5} is the dynamics of the LPF of the forward DC-load power and Δv_{DC}^{ap} is the DC-voltage at the active power controlled VSC side. The input variables are $u_{dv}^T = [\Delta v_{DC}^{ref}\ \Delta E^{ref}\ \Delta v_{sd}\ \Delta v_{sq}]$ and the disturbance input variables are $w^T = [\Delta E_d\ \Delta E_q]$. u_{dv}^{ref} are the first two reference signals of the input vector u_{dv}.

Combine the inner current loop dynamics (2.7-2.8), the DC-voltage dynamics (2.10), the DC-voltage controlled outer loop dynamics (2.15-2.16), AC-voltage controlled outer loop dynamics (2.20) , the PLL dynamics (2.28-2.31), the DC-current dynamics due to series $R_{DC}L_{DC}$-circuit and the active power controlled VSC dynamics given by $g_{25}(s)$, the state-space model of the VSC-HVDC system with a single Π-section DC-cable model is given below, where $\hat{C} = C + d \cdot c/2 = C + C_{DC}$:

$$\begin{aligned} \dot{x}_{dv} &= A_2 \cdot x_{dv} + B_{u2} \cdot u_{dv}^{ref} + B_{w2} \cdot w \\ w &= C_{w2} \cdot x_{dv} + D_{w2} \cdot u_{dv} \end{aligned} \tag{4.15}$$

$$A_2 = \begin{bmatrix} -a_c & 0 & -2\zeta\omega_{nd}\hat{C}\frac{v_{DC0}}{E_0}a_c & \omega_{nd}^2\hat{C}\frac{v_{DC0}}{E_0}a_c \\ 0 & -a_c & 0 & 0 \\ \frac{E_0}{\hat{C}v_{DC0}} & 0 & -\frac{i_{DC0}}{\hat{C}v_{Dc0}} & 0 \\ 0 & 0 & -1 & 0 \\ a_f E_0 \frac{d\cdot c/2}{\hat{C}} & 0 & a_f i_{DC0}\frac{C}{\hat{C}} & 0 \\ 0 & 0 & 0 & 0 \\ 0 & 0 & \frac{1}{L_{DC}} & 0 \\ 0 & 0 & 0 & 0 \end{bmatrix}$$

$$\begin{bmatrix} \frac{a_c}{E_0} & 0 & 0 & 0 \\ 0 & 0 & 0 & 0 \\ 0 & \frac{E_0}{\hat{C}v_{DC0}}\frac{Q_0}{E_0^2} & -\frac{1}{\hat{C}} & 0 \\ 0 & 0 & 0 & 0 \\ -a_f & a_f E_0 \frac{d\cdot c/2}{\hat{C}}\frac{Q_0}{E_0^2} & a_f v_{DC0}\frac{C}{\hat{C}} & 0 \\ 0 & -a_{pll} & 0 & 0 \\ 0 & 0 & -\frac{R_{DC}}{L_{DC}} & -\frac{1}{L_{DC}} \\ 0 & 0 & \frac{1}{\hat{C}} & \frac{i_{DC0}}{\hat{C}v_{DC0}^{ap}} \end{bmatrix}$$

$$B_{u2}^T = \begin{bmatrix} 2\zeta\omega_{nd}\hat{C}\frac{v_{DC0}}{E_0}a_c & 0 & 0 & 1 & 0 & 0 & 0 & 0 \\ 0 & a_c K_{pa} & 0 & 0 & 0 & 0 & 0 & 0 \end{bmatrix}$$

$$B_{w2}^T = \begin{bmatrix} -a_c\frac{P_0}{E_0^2} & -a_c K_{pa} & \frac{E_0}{\hat{C}v_{DC0}}\frac{P_0}{E_0^2} & 0 & a_f E_0\frac{d\cdot c/2}{\hat{C}}\frac{P_0}{E_0^2} & 0 & 0 & 0 \\ 0 & 0 & -\frac{E_0}{\hat{C}v_{DC0}}\frac{Q_0}{E_0^2} & 0 & -a_f E_0\frac{d\cdot c/2}{\hat{C}}\frac{Q_0}{E_0^2} & a_{pll} & 0 & 0 \end{bmatrix}$$

$$C_{w2} = \frac{L_g}{k_2}\begin{bmatrix} 1 + a_{pll}L_g\frac{P_0}{E_0^2} & -a_{pll}L_g\frac{Q_0}{E_0^2} \\ a_c L_g K_{pa} & 1 - a_c L_g\frac{P_0}{E_0^2} \end{bmatrix} \cdot \begin{bmatrix} a_c - \frac{R_g}{L_g} & \omega_0 & 2\zeta\omega_{nd}\hat{C}\frac{v_{DC0}}{E_0}a_c \\ -\omega_0 & a_c - \frac{R_g}{L_g} & 0 \end{bmatrix}$$

$$\begin{bmatrix} -\omega_{nd}^2\hat{C}\frac{v_{DC0}}{E_0}a_c & -\frac{a_c}{E_0} & \omega_0\frac{P_0}{E_0^2} + \frac{Q_0}{E_0^2}(a_{pll} - \frac{R_g}{L_g}) & 0 & 0 \\ 0 & 0 & (a_{pll} - \frac{R_g}{L_g})\frac{P_0}{E_0^2} - \frac{Q_0}{E_0^2}\omega_0 & 0 & 0 \end{bmatrix}$$

$$D_{w2} = \frac{1}{k_2}\begin{bmatrix} 1 + a_{pll}L_g\frac{P_0}{E_0^2} & -a_{pll}L_g\frac{Q_0}{E_0^2} \\ a_c L_g K_{pa} & 1 - a_c L_g\frac{P_0}{E_0^2} \end{bmatrix} \begin{bmatrix} -2\zeta\omega_{nd}\hat{C}\frac{v_{DC0}}{E_0}a_c L_g & 0 & 1 & 0 \\ 0 & -a_c K_{pa} L_g & 0 & 1 \end{bmatrix}$$

$$k_2 = 1 + L_g(a_{pll} - a_c)\frac{P_0}{E_0^2} + L_g^2 a_{pll} a_c (K_{pa}\frac{Q_0}{E_0^2} - \frac{P_0^2}{E_0^4});$$

A_2, B_{u2} and B_{w2} do not depend on the SCR value. Note, however that C_{w2} and D_{w2} depend on SCR. The parameters of the DC-cable are listed

in Table 4.1, where $L_{DC} = l \cdot d$ and $R_{DC} = r \cdot d$. The stability of the VSC-HVDC system with a single Π-section DC cable model can be analyzed by the eigenvalues of $A_2 + B_{w2}C_{w2}$. It's straight forward to be calculated that for $SCR < 4$, provided the parameter values from Table 4.1, the VSC-HVDC system will become unstable due to the weak AC-grid impedance.

- Distributed parameter DC-cable model:

While the DC-cable is modeled by (2.49), it is hard to use eigenvalue analysis to study the system stability since there are an infinite number of poles. Therefore, the Nyquist criterion is applied to analyze the stability of the system, which has the block diagram in Fig. 3.1.

As claimed in Section 3, the VSC-HVDC system can be described by two cascaded systems: one is a forward combination of transfer functions, which depends on the considered input and output. The second is a feedback loop which is unique for all input-output combinations. For the active power controlled VSC of this study case, the forward functions are stable at least for $SCR > 2.7$. For the DC-voltage controlled VSC, the forward function stability will be analyzed by a case study.

In the case study setup, the VSC-HVDC system parameters and nominal steady states are listed in Table 4.1. However, reset the cable inductance density to be 10.2 [mH/km], which renders the single Π-section cable model based VSC-HVDC system unstable and the SCR of the AC-grid is still chosen to be 4. For the case with distributed parameter DC-cable model, the forward function stability and the function g_{15} are determined by the new state-space model, where x_{dvn} is the first six components of x_{dv}, the input signal is Δi_{DC} and the output signal is Δv_{DC},

$$\begin{aligned} \dot{x}_{dvn} &= A_3 \cdot x_{dvn} + B_3 \cdot \Delta i_{DC} \\ y &= C_3 \cdot x_{dvn} \qquad (4.16) \\ g_{15} &= C_3(sI - A_3)^{-1}B_3 \qquad (4.17) \end{aligned}$$

where A_3 is the sub-square matrix of $A_2 + B_{w2}C_{w2}$ with the first 6 columns and first 6 rows and $c = 0$ [μF] (since the cable capacitance should not be included in the VSC dynamics itself), and B_3, C_3 are:

$$\begin{aligned} B_3^T &= \begin{bmatrix} 0 & 0 & -\frac{1}{C} & 0 & a_f v_{DC0} & 0 \end{bmatrix} \\ C_3 &= \begin{bmatrix} 0 & 0 & 1 & 0 & 0 & 0 \end{bmatrix} \end{aligned}$$

It is straight forward to prove that the above system (4.16) is minimum order, i.e. the system is both controllable and observable. Therefore, the stability of the forward function $g_0 = \frac{-1}{g_{15}+g_{25}}G(s)$ is determined by the zeros

of $g_{15} + g_{25}$. The expression of g_{25} is given by (4.6), as $g_{25} = \hat{g}_{25}$ and the expression of g_{15} is given by (4.17). In this case study, the zeros of $g_{15} + g_{25}$ are -30, $-41 \pm 66j$, -119, -1265, -466180 and thus the forward function $g_0(s)$ is always stable independently of the choice of the input and output signals.

The feedback loop stability is studied by the Nyquist criterion. The number of unstable poles of $g_1 h_1$ is determined by $g_1 = -\frac{g_{15}+g_{25}}{1+Y_0^2 g_{15} g_{25}}$ due to that $h_1(s)$ is dissipative, containing an infinite number of stable poles. The poles of g_1 are: 173, -0.98, $-25 \pm 22j$, -119, -434, -1125 and -449937. Obviously, there is one unstable pole of the open loop function of $g_1/(1 + g_1 h_1)$. In order to guarantee the stability of the closed loop function, the Nyquist plot should anti-clockwise encircle the critical point (-1,0) once. For the single Π-section cable model, the equivalent cable function of $h_1(s)$ is depicted by $h_{\pi 1}(s) = cs \cdot d/2 + 1/(ls + r)/d$. The Nyquist curve of the open loop function $g_1 h_1(j\omega)$ and $g_1 h_{\pi 1}(j\omega)$ is given by Fig. 4.5.

Fig. 4.5 (a) shows that in the low frequency band, both cable models provide similar Nyquist curves. However, in this study case, the Fig. 4.5 (b) shows that for the distributed parameter cable model, the Nyquist curve will anti-clockwise encircle the critical point (-1,0) but for the single Π-section cable model, the Nyquist curve will clockwise encircle the critical point once. Therefore, the VSC-HVDC system with distributed parameter DC cable is stable but the VSC-HVDC system with one single Π-section DC cable model has two unstable poles i.e. $0.7 \pm 1.78j$, which are calculated by the eigenvalue of the weak AC-grid connected VSC-HVDC system state matrix $A_2 + B_{w2} C_{w2}$. This is because, for $\omega < 1/(d\sqrt{lc/2}) = \omega_{rf}$ (resonance frequency of the single Π-section model), $|h_1(j\omega)| > |h_{\pi 1}(j\omega)|$ implying that the VSC-HVDC system with distributed parameter cable model has a larger gain margin.

Fig. 4.6. shows that if the VSC-HVDC system with the single Π-section model is stable, then the phase crossover frequency must be lower than ω_{rf} where $h_1(j\omega)$ is similar to $h_{\pi 1}(j\omega)$ and since $g_1 h_1$ has a larger gain margin, the VSC-HVDC system with the distributed parameter cable model is also stable. Consequently, if the VSC-HVDC system with a single Π-section model is stable, it is sufficient for the VSC-HVDC system with distributed parameter cable model to be stable but not vice versa.

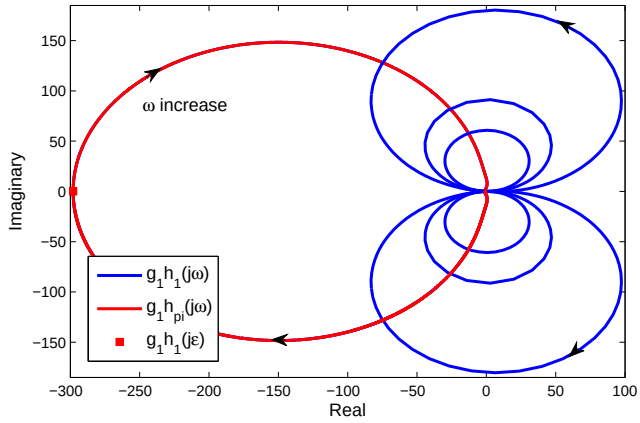

(a)Full curve

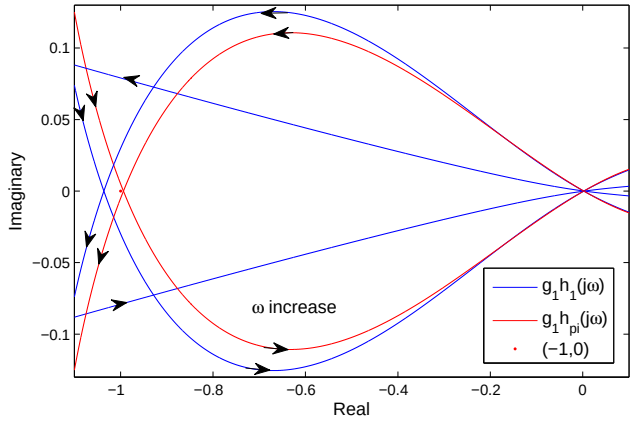

(b)Amplified around critical point (-1,0)

Figure 4.5: Nyquist plot of $g_1(j\omega)h_1(j\omega)$: red curve is the Nyquist plot of VSC-HVDC system with one Π-section DC-cable model; blue curve is the Nyquist plot of the VSC-HVDC system with distributed parameter DC-cable model; $\varepsilon = 0.01$ [rad/s]

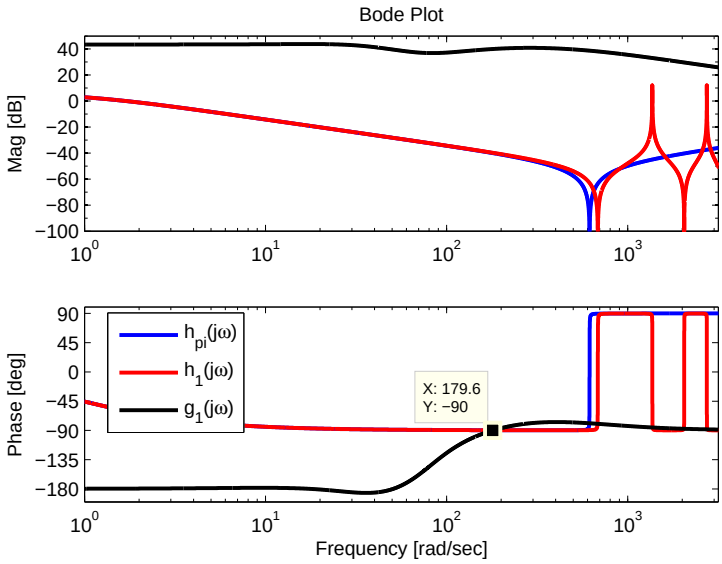

Figure 4.6: Frequency characteristic curve of $g_1(j\omega)$, $h_1(j\omega)$ and $h_{\pi 1}(j\omega)$

Chapter 5

Conclusion

A mathematical model for small-signal stability analysis of a two terminal VSC-HVDC system has been presented. The analysis addresses both the strong and the weak AC grid cases. The system can be separated into two parts: the active power controlled VSC and the DC-voltage controlled VSC with a DC-cable model. For a strong AC grid, the first part will always be stable; for a weak AC grid, the stability of the first part is analyzed by the small gain theorem, which shows that for SCR$>$ 2.7, provided the parameter values from Table 4.1, the active power controlled VSC embedded in a weak AC-environment will always be stable.

The second part is analyzed by the Nyquist criterion. Due to the symmetric properties of the cable model, for arbitrary AC grid dynamics, the block diagram of each input output combination could be rewritten as in Fig. 3.1. $g_0(s)$ is stable with a reasonable design of the DC voltage PI-controller, provided SCR$>$ 4. $g_1(s)$, is a rational function of 's' and the return path $h_1(s)$ is dissipative. For a strong AC grid, two cases have been illustrated, showing that in both cases with either the rectifier or the inverter working as the DC voltage controller, the system is stable for three different cable distances d=50km, 150km, 450km. For weak AC grid, one case study has been illustrated, showing that if the VSC-HVDC system with a single Π-section cable model is stable, then the VSC-HVDC system with distributed parameter DC cable model is also stable provided that $|h_1(j\omega)| > |h_{\pi 1}(j\omega)|$ for $\omega < \omega_{rf}$.

The proposed method enables the VSC-HVDC system stability to be determined with a distributed parameter DC-cable model. It shows that also for long distance VSC-HVDC transmission or larger cable impedance density, the VSC-HVDC system with a single Π-section cable model is sufficient to prove the system stability. Moreover, after utilizing the distributed parameter cable model, the proposed VSC-HVDC system model can be applied for all frequency band analysis.

Chapter 6

Summary of included papers

This chapter provides a brief summary of the papers that constitute the base for this thesis. Full versions of the papers are included in Part II. The papers have been reformatted to increase readability and to comply with the layout of the rest of the thesis.

Paper 1

> Y. Song and C. Breitholtz, Nyquist stability analysis of a VSC-HVDC system using a distributed parameter DC-cable model, *19th World Congress of the International Federation of Automatic Control*, August 2014, Cape Town, South Africa.

In this paper a two terminal VSC-HVDC system embedded in a strong grid AC environment is considered, emphasizing modeling, controller design and small-signal stability analysis.

Under assumption of strong grid AC environment, the dynamics of the PLL and the q-axis of the converter measured input current are ignored. The VSC is modeled as a third order system for the DC-voltage controlled side and as a second system for the active power controlled side. Traditionally, DC cables are most often modeled by a single Π-section and the VSC-HVDC system is consequently modeled as a sixth order system, where the system stability can be investigated through eigenvalue calculation. However, when using Π-section cable model for higher frequencies or in case of transmission over long distances and higher cable impedance density such as submarine cables, approximation accuracy aspects must be considered. In this paper, a distributed parameter cable model, based on the damped wave equation, is used to overcome this limitation.

The VSC-HVDC system with a distributed parameter cable model can be described by two cascaded blocks. The first block is a transfer function

that will be different, due to which input and output variables that are considered, but is in all realistic cases stable. The second block is a feedback loop, where the forward path is a rational function and the return path is a dissipative infinite dimensional function, that remains the same in all cases. For a VSC-HVDC system with a single Π-section cable model, the return path of the feedback loop is a first order improper transfer function, which has similar frequency characteristic property as the distributed parameter cable model in the low frequency band. The stability for both cable models is then analyzed, using the Nyquist criterion in a straight forward manner.

Two examples have been illustrated, showing that in both cases with either the rectifier or the inverter working as DC voltage controller, the VSC-HVDC system with distributed parameter cable model is stable for three different cable distances d=50km, 150km, 450km. Similarly, the VSC-HVDC system with a single Π-section cable model is also stable under above study cases.

Paper 2

> Y. Song and C. Breitholtz, Nyquist Stability Analysis of an AC-grid connected VSC-HVDC System Using a Distributed Parameter DC-cable Model, *submitted for publications in IEEE Tran. on Power Delivery, special issue: HVDC transmission systems for large offshore wind power plants.*

In this paper a two terminal VSC-HVDC system embedded in a weak grid AC-environment, represented by an inductance and a resistance in series, is considered. Modeling, controller design and small-signal stability analysis are emphasized.

Under assumption of weak grid AC environment, the dynamics of the PLL and the AC-grid have to be considered. The d-axis and q-axis currents are coupled due to the AC-grid dynamics. For the active power controlled VSC, the feedback loop stability would not be influenced by the weak AC-grid. Similarly, the stability of the active power controlled VSC could be analyzed without considering the DC-side influence. Consequently, the stability analysis of two terminal VSC-HVDC systems embedded in a weak AC-grid can be separated into two parts: the active power controlled VSC and the VSC-HVDC system while the active power controlled VSC is under steady state.

The stability of the first part is analyzed by the small gain theorem, which shows that for SCR > 2.7, provided the parameter values are taken from Table 4.1, the active power controlled VSC embedded in a weak AC-

environment will always be stable. The second part is analyzed by the Nyquist criterion. Similar to the strong AC-grid case, the system can be described by two cascaded blocks. The first block is a transfer function that will be different, due to which input and output variables that are considered but is in all realistic cases stable. The second block is a feedback loop, where the forward path is a rational function and the return path is a dissipative infinite dimensional function, that remains the same in all cases. Note that all blocks, however, will be a bit more complicated than in the strong AC-grid case.

One example has been illustrated, showing that the VSC-HVDC system with a single Π-section cable model is sufficient to prove system stability, independently of the DC-cable length and impedance density.

References

[1] N. Flourentzou, V. Agelidis, and G. Demetriades, "VSC-based HVDC power transmission systems: An overview," *IEEE Transaction Power Electronics*, vol. 24, no. 3, pp. 592–602, March, 2009.

[2] "VSC transmission," Cigre Working Group, Tech. Rep. B4.37-269, 2005.

[3] P. Bresesti, W. L. Kling, R. L. Hendriks, and R. Vailati, "HVDC connection of offshore wind farms to the transmission system," *IEEE Trans. Energy Conversion*, vol. 22, no. 1, pp. 37–43, March, 2007.

[4] L. Harnefors, M. Bongiorno, and S. Lundberg, "Input-Admittance Calculation and Shanping for Controlled Voltage-Source Converters," *IEEE Trans. Ind. Electron.*, vol. 54, no. 6, pp. 3323–3334, Dec., 2007.

[5] M. Durrant, H. Werner, and K. Abbott, "Design of Low Order Robust Controllers for a VSC HVDC Power Plant Terminal," *European Journal of Control*, vol. 13, no. 3, pp. 366–381, 2007.

[6] M. Andreasson, D. V. Dimarogonas, H. Sandberg, and K. H. Johansson, "Distributed Controllers for Multi-Terminal HVDC Transmission Systems," in *19th World Congress of the International Federation of Automatic Control*, Cape town, South Africa, August, 2014.

[7] J. Svensson, "Grid-Connected Voltage Source Converter Control Principles and Wind Energy Applications," Ph.D. dissertation, Chalmer University of Technology, Göteborg, Sweden, 1998.

[8] S. Cole, J. Beerten, and R. Belmans, "Generalized Dynamic VSC MTDC Model for Power System Stability Studies," *IEEE Trans. Power System*, vol. 25, no. 3, pp. 1655–1662, August, 2010.

[9] L. Zhang, "Modeling and Control of VSC-HVDC Links Connected to Weak AC System," Ph.D. dissertation, Royal Institute of Technology, Stockholm, Sweden, 2010.

[10] G. C. Hsieh and J. C. Hung, "Phase locked loop techniques - A survey," *IEEE Trans. Ind. Electron*, vol. 43, no. 6, pp. 609–615, Dec. 1996.

[11] B. T. Ooi and X. Wang, "Voltage angle lock loop control of the boost type PWM converter for HVDC application," *IEEE Trans. Power Electronics*, vol. 5, no. 2, pp. 229–235, April, 1990.

[12] K. J. Astrom and R. M. Murray, *Feedback System - An Introduction for Scientists and Engineers.* Princeton university press, 2008.

[13] J. M. Maciejowski, *Multivariable feedback design.* Wesley Publishing Company, 1989.

[14] N. Mohan, *Advanced electric drives: analysis, control and modeling using Simulink.* MNPERE, 2001.

[15] B. K. Bose, *Power Electronics and Variable Frequency Drives.* New York, USA: IEEE Press, 1997.

[16] A. Jain, K. Joshi, A. Behal, and N. Mohan, "Voltage regulation with STATCOMs: Modeling, control and results," *IEEE Trans. Power Delivery*, vol. 21, no. 2, pp. 726–735, April, 2006.

[17] R. Ottersten, "On control of back-to-back converters and sensorless induction machine drives," Ph.D. dissertation, Chalmer University of Technology, Göteborg, Sweden, 2003.

[18] L. F. Drbal, P. G. Boston, and K. L. Westra, *Power Plant Engineering.* Springer, 1996.

[19] H. K. Khalil, *Nonlinear Systems.* Prentice Hall, 2002.

Part II

Included papers

Paper 1

Nyquist stability analysis of a VSC-HVDC system using a distributed parameter DC-cable model

Y. Song and C. Breitholtz

19th World Congress of the International Federation of Automatic Control, August 2014, Cape Town, South Africa

Comment: The layout of this paper has been reformatted in order to comply with the rest of the thesis. The contents have not been altered.

Nyquist stability analysis of a VSC-HVDC system using a distributed parameter DC-cable model

Y. Song and C. Breitholtz

Abstract

In this paper a two terminal VSC-HVDC system embedded in a strong grid AC-environment is considered, emphasizing modeling, controllers design and small-signal stability analysis. Traditionally, DC cables are most often modeled by Π-sections, and when using them for higher frequencies or in case of transmission over long distances, approximation accuracy aspects must be considered. Here, a distributed parameter cable model, based on the damped wave equation, is used to overcome this limitation. It is shown that the VSC-HVDC system can be described by a forward transfer function cascaded with a feedback loop. The first transfer function will be different, due to which input and output variables that are considered but is in all realistic cases stable. The feedback loop, where the forward path is a rational function and the return path is a dissipative infinite dimensional system, remains the same in all cases. The stability is then analyzed, using the Nyquist criterion, in a straight forward manner. Numerical examples are given by MATLAB.

1 Introduction

The main purpose of the HVDC-systems (High Voltage Direct Current) invented in the 1950:th was the transmission of DC electric power over longer distances, not seldom across water, and at both terminals embedded in AC-environment. These systems were largely based on thyristor technology [1]. At the end of the 1990:th the thyristor systems were gradually replaced by so called voltage source converters, VSC:s, based on recent power transistor technology [2].

Various aspects of these VSC-HVDC systems have been addressed by several researchers and engineers from roughly 1997. In some of these contributions focus has been on short term operation of the VSC-HVDC systems,

emphasizing dynamics and control. From the system theory point of view the VSC:s involve several linear subsystems, for example PI-controllers and linear circuit elements, but also nonlinear subsystems, due to the relations between power and voltage (or current). If large changes in voltage levels, for example due to severe system faults, should be taken into account, nonlinear dynamical models must be used in analysis. A major interest has been in the dynamics close to steady state (implying sinusoidal steady state at the AC-side and constant steady state at the DC-side). Consequently linearized dynamical models then have been in focus [3].

One particular aspect of linear dynamics that has drawn much attention is the system stability. Naturally, state-space models are preferred to be used. Typically the DC-cable has been modeled by one simple Π-link [4], [5]. This is often sufficient, at least when considering short cables and low frequencies. If more general results are required, for example fast system excitation caused by abrupt disturbances and perhaps in very long cables (200 - 400 km), it would be more appropriate to use a distributed parameter cable model together with state-space (or transfer function) VSC-models.

In this paper a VSC-HVDC system is modeled, comprising VSC:s and AC-side dynamics, together with a distributed parameter cable model, based on the one dimensional damped wave equation. The system is linearized around an arbitrary operational point and the resulting linear infinitely dimensional model is based on the use of transfer functions. It turns out that the system can be described by two cascaded systems: One is a forward combination of transfer functions that will be different, due to which input signal and which output signal that are considered, but always be input to output stable. The second is a feedback system, where the forward subsystem is finite dimensional and the return subsystem only depends on the infinite dimensional cable model. The stability of this feedback system, that remains the same for all combinations of input and output signals, is analyzed by use of the Nyquist criterion. Schemes and equations are deduced in the paper and some simulations in frequency domain are showed as well. The purpose is to provide a tool for small-signal analysis of the total VSC-HVDC system, including a cable model that is valid independently of the cable length or which frequencies that can be considered due to a given cable model approximation. The focus is here on the strong AC-grid case, making some simplifications possible. However the weak-grid case can quite likely be treated by the same approach.

2 Problem formulation

A standard VSC-HVDC system is described by Fig. 1. It consists of two

three-phase AC sources, which represent the equivalent electrical systems that are connected by the DC cable. At the AC-side of the VSC:s, the series inductances (L_1, L_2) and resistances (R_1, R_2) represent the AC reactor and the power losses in the converter. The transmission line would be interpreted as a distributed parameter model. The shunt capacitors at the terminals are denoted by C_1, C_2 respectively.

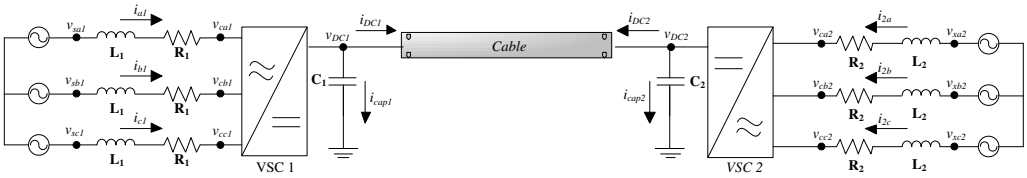

Figure 1: Standard VSC-HVDC system embedded in a strong AC environment

2.1 Model and Control objectives

In a standard VSC-HVDC systems, one converter station (VSC1) is assigned the duty as the DC voltage controller to secure the stability of the DC-Bus voltage; the other station (VSC2) operates as the active power controller to guarantee and balance the power exchanges [6]. Besides, in each VSC, it is possible to control the reactive power or grid voltage at the AC side; this is, however, not considered in this paper.

As the DC cable is modeled by a single Π-link, the stability of the system can be investigated through the eigenvalue calculation. However, the high frequency information is not well interpreted by the Π-scheme cable model and thus impossible to analyze the real dynamic influence from the DC cable. The new standard VSC-HVDC model includes the distributed parameter cable model and formulate the transfer function into the block diagram as shown at Fig.2. Therefore, if $g_1(s)$ is a rational function of 's' and the infinite dimensional transfer function $h_1(s)$ represents a dissipative system, the feedback loop stability could be analyzed by use of the Nyquist criterion.

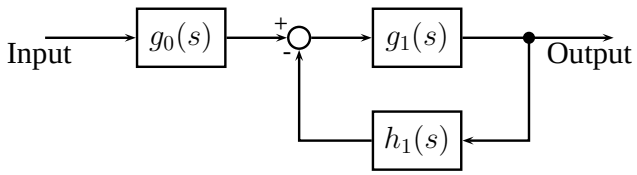

Figure 2: General block diagram of VSC-HVDC system

2.2 Assumptions and statements

The main assumptions and statements of the proposed model are the following:

- The connected AC grids are well balanced and strong, i.e. the nominal AC grid voltage is as most subject to small variation and the dynamics of Phase Locked Loop and low pass filter for feed forward terms are ignored.
- The model is derived in the so-called dq reference plane, which is oriented according to the robust Phase Locked Loop. The dynamic transformation from three phase abc-frame into dq-frame is given by, for example, [7].
- The two VSC:s are ideal and symmetrical, having a switching frequency of 1kHz. The relevant time delay is half of the switching period, around 0.5 ms. After design the system time constant is at least ten times larger then 0.5ms, the time delays of the VSC's are negligible.
- The units for voltage, current and active power are [kV], [kA] and [MW] respectively.
- All reference signals x are expressed as x^{ref}.
- The differential operator is expressed by 'p' and the Laplace form of time domain variable $x(t)$ is marked by $\tilde{x}(s)$.

3 System model

In this section, the dynamic equations of VSC is given in the power invariant *dq* reference frame, where the frame is chosen to be in alignment with the voltage direction i.e. $v_{sq0} = 0$. For balanced and strong AC grid, the grid frequency is assumed to be constant i.e. $\omega = 2\pi f_0$ and $f_0 = 50$Hz. Since the VSC:s are symmetric, the variables and parameters in this section would not be subscribed, i.e. index 1,2 are not used and which are applied to denote different VSC:s.

The local controller of the VSC is separated into two cascaded parts: inner current controller and outer controller. The inner current controller provides the voltage reference (v_{cd}^{ref} and v_{cq}^{ref}) to the pulse width modulator (PWM). The d-axis outer controller is used to track the reference of either DC voltage or active power and generates the d-axis current reference (i_d^{ref}) to the inner current loop. Since the q-axis current has no impact on the

dynamics at the DC side (after d- and q-dynamics decoupling), the q-axis current reference (i_q^{ref}) is thus assumed to be zero.

3.1 Inner current loop

The AC current dynamics in the dq frame is given by:

$$L \cdot \frac{\mathrm{d}i_d}{\mathrm{d}t} = -R \cdot i_d + \omega L \cdot i_q + v_{sd} - v_{cd} \tag{1}$$

$$L \cdot \frac{\mathrm{d}i_q}{\mathrm{d}t} = -R \cdot i_q - \omega L \cdot i_d + v_{sq} - v_{cq} \tag{2}$$

The current controller consists of one PI-controller and two feed forward signals i.e. the grid voltage and cross coupling current, which are given as following:

$$v_{cd}^{ref} = -(K_p + \frac{K_i}{p})(i_d^{ref} - i_d) + v_{sd} + \omega L \cdot i_q \tag{3}$$

$$v_{cq}^{ref} = -(K_p + \frac{K_i}{p})(i_q^{ref} - i_q) + v_{sq} - \omega L \cdot i_d \tag{4}$$

Due to the switching action of the PWM inside the converter, a delay of half a switching period appears, where $T_{sw} = 1/(2f_{sw}) = 0.5ms$. If the design time constant of the inner current loop is chosen ten times larger than the delay T_{sw}, it is reasonable to ignore the impact of the delay during the analysis of system dynamics i.e. $v_{cd}^{ref} \approx v_{cd}$ and $v_{cq}^{ref} \approx v_{cq}$ [8]. Consequently, the dynamics between the d- and q-axis are decoupled.

It is also important to notice that, in order to cancel the dominant pole $(-R/L)$ in the external circuit of the converter, the PI-parameters are designed as $K_p = \alpha_c L$ and $K_i = \alpha_c R$, where α_c is the bandwidth of inner current loop and the corresponding time constant is $\tau_c = 1/\alpha_c$. The linearized inner current closed loop is then simplified as a first order system with bandwidth α_c:

$$\Delta\tilde{i}_d(s) = \underbrace{\frac{\alpha_c}{s + \alpha_c}}_{G_c(s)} \Delta\tilde{i}_d^{ref}(s) \tag{5}$$

$$\Delta\tilde{i}_q(s) = \frac{\alpha_c}{s + \alpha_c} \Delta\tilde{i}_q^{ref}(s) \tag{6}$$

Note that the unavoidable uncertainties in the AC side model parameters, L and R, from a practical point of view are assumed to be quite small. Hence these uncertainties will have only a minor impact on the inner current loop performance. In addition, since the outer loop bandwidth usually

is designed to be at least ten times smaller than α_c, the effect caused by the inner loop parameter uncertainty would not influence the entire system dynamics very much. Therefore, the design of the inner current loop PI-controller based on model parameters is well justified.

However, even if the inner current feedback loop is cascaded by a slower system in the outer loop, the inner loop dynamics should not be ignored. This is due to that the inner current feedback loop performs as a low pass filter for the feed forwarded DC load power in the outer DC voltage control loop, which is shown in Fig. 3. It guarantees that no exceeded active power would be transmitted into the DC side due to high frequency resonance at the DC side.

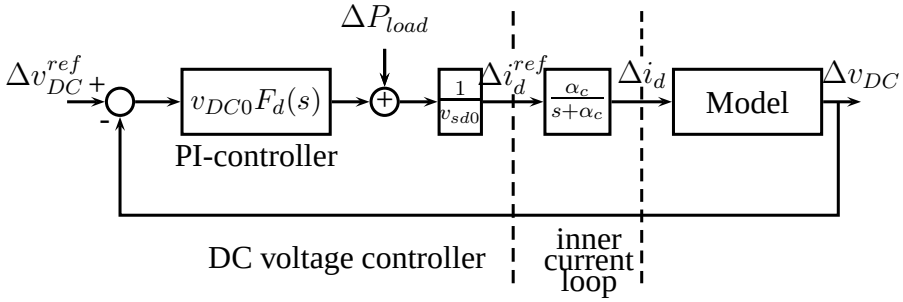

Figure 3: DC voltage control loop (Δv_{sd} is assumed to be zero)

3.2 Direct voltage control loop

The DC voltage is determined by the capacitor charging power that is the difference between input active power to the VSC (assume the VSC is power lossless) and DC load power:

$$\frac{\mathrm{d}}{\mathrm{d}t}(\frac{1}{2}C \cdot v_{DC}^2) = P - P_{load} \tag{7}$$

$$\Rightarrow \quad C \cdot v_{DC0} \cdot \frac{\mathrm{d}\Delta v_{DC}}{\mathrm{d}t} = \Delta P - \Delta P_{load} \tag{8}$$

Therefore, the linearized expression of the input active power and DC load power are required:

$$\begin{aligned} P &= Re\{(v_{sd0} + \Delta v_{sd} + j\Delta v_{sq})(i_{d0} + \Delta i_d - ji_{q0} - j\Delta i_q)\} \\ &\approx \underbrace{v_{sd0}i_{d0}}_{P_0} + \underbrace{v_{sd0}\Delta i_d + i_{d0}\Delta v_{sd} + i_{q0}\Delta v_{sq}}_{\Delta P} \end{aligned} \tag{9}$$

$$\begin{aligned} P_{load} &= (v_{DC0} + \Delta v_{DC})(i_{DC0} + \Delta i_{DC}) \\ &\approx \underbrace{v_{DC0}i_{DC0}}_{P_{load0}} + \underbrace{v_{DC0}\Delta i_{DC} + i_{DC0}\Delta v_{DC}}_{\Delta P_{load}} \end{aligned} \tag{10}$$

(9) shows that ΔP is proportional to Δi_d and independent with Δi_q. Therefore, the output of DC voltage controller, i.e. the d-axis reference current, could be designed through the reference input active power. The reference input active power is the sum of a PI-controller operating on the error of DC voltage square and feed forward DC load power:

$$P^{ref} = \underbrace{\left(K_{pd} + \frac{K_{id}}{p}\right)}_{F_d(p)} \cdot \nu + P_{load} \tag{11}$$

$$\nu = \frac{(v_{DC}^{ref})^2 - v_{DC}^2}{2}$$

$$i_d^{ref} = \frac{P^{ref}}{v_{sd}} \tag{12}$$

$$\Rightarrow \Delta\tilde{P}^{ref} = F_d(s) v_{DC0} (\Delta\tilde{v}_{DC}^{ref} - \Delta\tilde{v}_{DC}) + \Delta\tilde{P}_{load} \tag{13}$$

$$\Delta\tilde{i}_d^{ref} = \frac{1}{v_{sd0}} \Delta\tilde{P}^{ref} - \frac{P_0}{v_{sd0}^2} \Delta\tilde{v}_{sd} \tag{14}$$

Combining equations (8-10), (13-14) and the inner current loop (5), the linearized expression of DC voltage is given as following, where Δv_{sq} is assumed to be zero (due to fast PLL dynamics):

$$\begin{aligned}\Delta\tilde{v}_{DC} = (C v_{DC0} s + v_{DC0} F_d G_c + i_{DC0}(1 - G_c))^{-1} \cdot \\ \cdot [v_{DC0} F_d G_c \cdot \Delta\tilde{v}_{DC}^{ref} - v_{DC0}(1 - G_c) \cdot \Delta\tilde{i}_{DC} + \\ + i_{d0}(1 - G_c) \cdot \Delta\tilde{v}_{sd}]\end{aligned} \tag{15}$$

After designing the PI-controller parameters as $K_{pd} = 2C\zeta\omega_{nd}$ and $K_{id} = C\omega_{nd}^2$, the transfer function from Δv_{DC}^{ref} to Δv_{DC} is given at (16). The approximation is based on the assumption that the inner current loop is much faster than the outer loop and thus $G_c(s) \approx 1$. However, this assumption is only used to analyze the transfer function from Δv_{DC}^{ref} to Δv_{DC} but not for the entire two terminal VSC-HVDC system.

$$\begin{aligned}\frac{\Delta\tilde{v}_{DC}}{\Delta\tilde{v}_{DC}^{ref}} &= \frac{v_{DC0} F_d(s) G_c(s)}{C v_{DC0} s + v_{DC0} F_d(s) G_c(s) + i_{DC0}(1 - G_c(s))} \\ &\approx \frac{v_{DC0} F_d(s)}{C v_{DC0} s + v_{DC0} F_d(s)} \\ &= \frac{2\zeta\omega_{nd} s + \omega_{nd}^2}{s^2 + 2\zeta\omega_{nd} s + \omega_{nd}^2}\end{aligned} \tag{16}$$

A common requirement of the closed loop DC voltage dynamics is to have a bandwidth ten times smaller than the inner loop [8] so that the DC voltage would not be sensitive to the DC load power. In addition,

the damping ratio is chosen around 1 in order to decrease the DC voltage overshoot. As $\zeta = 1$, the relation between the natural frequency ω_{nd} and the DC voltage bandwidth α_d is:

$$\omega_{nd} = \sqrt{-(2\zeta^2+1) + \sqrt{(2\zeta^2+1)^2+1}} \cdot \alpha_d \approx 0.4\alpha_d \tag{17}$$

3.3 Active power control loop

For the outer controller of transmitted active power, again a PI-controller is used. The controller parameters are designed by inner current loop pole cancelation, choosing the bandwidth of the outer loop as $\alpha_p = 0.2\alpha_d$. Therefore, the DC voltage would not display large oscillations during the variations of transmitted active power. The linearized differential equations of the active power control loop are derived as following:

$$i_d^{ref} = (K_{pp} + \frac{K_{ip}}{p})(P^{ref} - P)/v_{sd} \tag{18}$$

$$\Rightarrow \Delta\tilde{i}_d^{ref} = \frac{1}{v_{sd0}}(K_{pp} + \frac{K_{ip}}{s})(\Delta\tilde{P}^{ref} - \Delta\tilde{P}) \tag{19}$$

Combining equations (8-10), (19) and the inner current loop (5), the linearized expression of active power and DC voltage is given as following, where Δv_{sq} is assumed to be zero and $K_{pp} = \alpha_p/\alpha_c$, $K_{ip} = \alpha_p$:

$$\Delta\tilde{P} = \underbrace{\frac{\alpha_p}{s+\alpha_p}}_{G_p(s)} \cdot \Delta\tilde{P}^{ref} + \frac{i_{d0}s}{s+\alpha_p} \cdot \Delta\tilde{v}_{sd} \tag{20}$$

$$\begin{aligned}\Delta\tilde{v}_{DC} = (Cv_{DC0}s + i_{DC0})^{-1}(&G_p(s) \cdot \Delta\tilde{P}^{ref} + \\ &+ i_{d0}(1 - G_p(s)) \cdot \Delta\tilde{v}_{sd} - v_{DC0} \cdot \Delta\tilde{i}_{DC})\end{aligned} \tag{21}$$

It can be seen from above equations that, for active power controller, the AC dynamics is independent with DC dynamics but not reversely.

3.4 DC cable

The conventional method of approximating a transmission line is to replace the line by cascaded lumped RLGC-sections, which is shown in Fig. 4. The terminal voltage and current are represented by v_{DC1}, v_{DC2}, i_{DC1} and i_{DC2}. The cable parameters are given by r, l, g, c and d, which are the cable density of resistance, inductance, conductance, capacitance and the cable length.

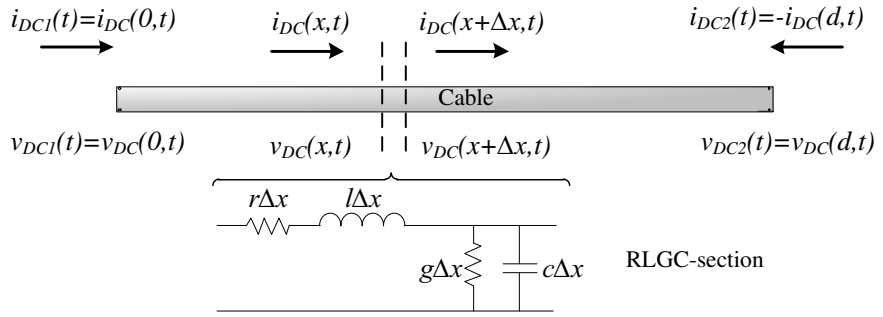

Figure 4: DC cable model

At an arbitrary distance 'x' from terminal 1, the voltage v_{DC} and current i_{DC} obey:

$$\frac{\partial v_{DC}(x,t)}{\partial x} + r \cdot i_{DC}(x,t) + l \cdot \frac{\partial i_{DC}(x,t)}{\partial t} = 0 \tag{22}$$

$$\frac{\partial i_{DC}(x,t)}{\partial x} + g \cdot v_{DC}(x,t) + c \cdot \frac{\partial v_{DC}(x,t)}{\partial t} = 0 \tag{23}$$

These well known transmission line equations are readily derived directly from Fig. 4, after letting the element Δx approach zero. Taking the Laplace transforms of these two linear PDE:s and eliminating i_{DC}, the following ordinary differential equation is obtained:

$$\frac{\mathrm{d}^2 \tilde{v}_{DC}(x,s)}{\mathrm{d}x^2} - (r + l \cdot s)(g + c \cdot s) \cdot \tilde{v}_{DC}(x,s) = 0 \tag{24}$$

The boundary conditions are:

$$\tilde{v}_{DC}(0,s) = \tilde{v}_{DC1}(s) \tag{25}$$

$$\tilde{v}_{DC}(d,s) = \tilde{v}_{DC2}(s) \tag{26}$$

Introducing the complex damping factor per unit length γ and the wave admittance Y_0:

$$\gamma(s) = \sqrt{(c \cdot s + g)(l \cdot s + r)} \tag{27}$$

$$Y_0(s) = \sqrt{\frac{c \cdot s + g}{l \cdot s + r}} \tag{28}$$

Define the current from the AC to DC side as positive, implying that the terminal currents $i_{DC1}(t) = i_{DC}(0,t)$ and $i_{DC2}(t) = -i_{DC}(d,t)$ (see Fig. 4). We can formulate a relationship between the terminal currents and voltages:

$$\begin{bmatrix} \tilde{i}_{DC1}(s) \\ \tilde{i}_{DC2}(s) \end{bmatrix} = \begin{bmatrix} h_1(s) & -h_2(s) \\ -h_2(s) & h_1(s) \end{bmatrix} \cdot \begin{bmatrix} \tilde{v}_{DC1}(s) \\ \tilde{v}_{DC2}(s) \end{bmatrix} \tag{29}$$

Further, letting $\Gamma(s) = \gamma(s) \cdot d$, the functions h_1 and h_2 are obtained as:

$$h_1(s) = Y_0(s) \coth(\Gamma(s)) \tag{30}$$

$$h_2(s) = \frac{Y_0(s)}{\sinh(\Gamma(s))} \tag{31}$$

As the cable system itself is dissipative, the functions $h_1(s)$ and $h_2(s)$ have infinite numbers of poles strictly located in the left half plane.

4 Block diagram of two terminal VSC-HVDC system

As previously mentioned, the VSC-HVDC system is assumed to be embedded in a strong AC environment. Here the DC cable is described by a distributed parameter model, not to be restricted to the study of short cables and low frequencies. In the control system, the converter VSC1 is assigned the duty of controlling the DC voltage and VSC2 of controlling the transmitted active power. The block diagram illustrating this case is found in Fig. 5.

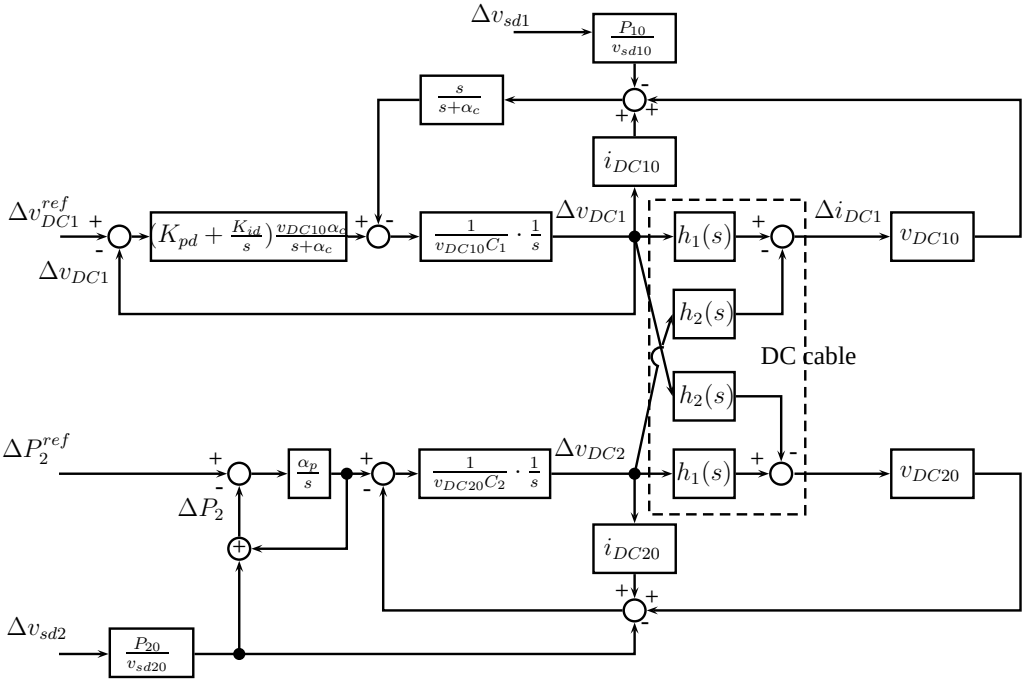

Figure 5: Linearized VSC-HVDC system

In the linearized system, there are two reference signals, Δv_{DC1}^{ref} and ΔP_2^{ref}, and two AC grid disturbances, Δv_{sd1} and Δv_{sd2}, considered as in-

puts. From (20), it is clear that the active power ΔP_2 is independent of DC side variations and depends on the inputs ΔP_2^{ref} and Δv_{sd2}. Therefore, the DC grid voltage Δv_{DC1} and Δv_{DC2} have been chosen as the system outputs.

Use Fig. 5, rewrite equations (15), (21) and combine with the DC cable dynamics (29):

$$\Delta\tilde{v}_{DC1} = g_{11}\Delta\tilde{v}_{DC1}^{ref} + \frac{i_{d10}g_{11}s}{v_{DC10}\alpha_c F_d}\Delta\tilde{v}_{sd1} - \frac{g_{11}s}{\alpha_c F_d}\Delta\tilde{i}_{DC1} \tag{32}$$

$$\Delta\tilde{v}_{DC2} = \frac{g_{12}G_p}{v_{DC20}}\Delta\tilde{P}_2^{ref} + \frac{i_{d20}(1-G_p)g_{12}}{v_{DC20}}\Delta\tilde{v}_{sd2} - g_{12}\Delta\tilde{i}_{DC2} \tag{33}$$

$$\Delta\tilde{i}_{DC1} = h_1\Delta\tilde{v}_{DC1} - h_2\Delta\tilde{v}_{DC2} \tag{34}$$

$$\Delta\tilde{i}_{DC2} = -h_2\Delta\tilde{v}_{DC1} + h_1\Delta\tilde{v}_{DC2} \tag{35}$$

Where,

$$g_{11} = \frac{v_{DC10}F_dG_c}{C_1v_{DC10}s + v_{DC10}F_dG_c + i_{DC10}(1-G_c)} \tag{36}$$

$$g_{12} = \frac{v_{DC20}}{C_2v_{DC20}s + i_{DC20}} \tag{37}$$

Insert (34) and (35) into (32) and (33):

$$\underbrace{\begin{bmatrix} 1+\frac{g_{11}s}{\alpha_c F_d}h_1 & -\frac{g_{11}s}{\alpha_c F_d}h_2 \\ -g_{12}h_2 & 1+g_{12}h_1 \end{bmatrix}}_{\Lambda(s)} \begin{bmatrix}\Delta\tilde{v}_{DC1}\\ \Delta\tilde{v}_{DC2}\end{bmatrix} =$$

$$\underbrace{\begin{bmatrix} g_{11} & 0 & \frac{i_{d10}g_{11}s}{\alpha_c v_{DC10}F_d} & 0 \\ 0 & \frac{g_{12}G_p}{v_{DC20}} & 0 & \frac{i_{DC20}(1-G_p)g_{12}}{v_{DC20}} \end{bmatrix}}_{\Phi(s)} \begin{bmatrix}\Delta\tilde{v}_{DC1}^{ref}\\ \Delta\tilde{P}_2^{ref}\\ \Delta\tilde{v}_{sd1}\\ \Delta\tilde{v}_{sd2}\end{bmatrix} \tag{38}$$

Thus, the MIMO transfer function between inputs and outputs is given by:

$$\begin{bmatrix}\Delta\tilde{v}_{DC1}\\ \Delta\tilde{v}_{DC2}\end{bmatrix} = \Lambda^{-1}\Phi \begin{bmatrix}\Delta\tilde{v}_{DC1}^{ref}\\ \Delta\tilde{P}_2^{ref}\\ \Delta\tilde{v}_{sd1}\\ \Delta\tilde{v}_{sd2}\end{bmatrix} \tag{39}$$

Noting from (29) that the DC cable dynamics is symmetric and as $h_1^2(s) - h_2^2(s) \equiv Y_0^2(s)$, the determinant of the matrix Λ is independent of the irrational function $h_2(s)$.

In addition, this conclusion can be extended to weak AC grid or the case considering the dynamics of PLL and the low pass filter for the feed forwards at each VSC, again see [8].

From what is mentioned above, it is possible to rewrite the block diagram of each input output combination into the form of Fig. 2, where $g_1(s)$ is determined by $\det(\Lambda)$ and unique for all input output combinations. The determinant of Λ and g_1 are then given by:

$$\det(\Lambda) = \underbrace{(1 + \frac{g_{11}g_{12}s}{\alpha_c F_d} Y_0^2)}_{g_{1d}(s)} + \underbrace{(g_{12} + \frac{g_{11}s}{\alpha_c F_d})}_{g_{1n}(s)} \cdot h_1 \tag{40}$$

$$g_1(s) = \frac{g_{1n}(s)}{g_{1d}(s)} \tag{41}$$

$$\frac{1}{\det(\Lambda)} = \frac{g_1}{1 + g_1 h_1} \cdot \frac{1}{g_{1n}} \tag{42}$$

Unlike $g_1(s)$ which remains the same, $g_0(s)$ depends on which element of the MIMO transfer function $\Lambda^{-1}\Phi$ that is picked out due to choice of input and output signals. As normally $\Delta v_{DC1}^{ref} = 0$ (implying that $v_{DC1}^{ref} = v_{DC10}$), the most encountered situation is a change in the desired transmitted power ΔP_2^{ref} and its impact on the DC line voltage Δv_{DC1}. At the same time, no AC disturbances are considered. Therefore, the transfer function from ΔP_2^{ref} to Δv_{DC1} is deduced below.

4.1 Dynamics from ΔP_2^{ref} to Δv_{DC1}

The forward path function $g_0(s)$ corresponding to the input ΔP_2^{ref} and output Δv_{DC1} is:

$$g_0(s) = \underbrace{\frac{g_{11}g_{12}G_p s}{v_{DC20}\alpha_c F_d g_{1n}}}_{f_1(s)} h_2(s) \tag{43}$$

The block diagram from ΔP_2^{ref} to Δv_{DC1} is illustrated at Fig. 6, where $f_1(s)$ is a rational function with respect to 's' and $h_2(s)$ has infinite number of stable poles.

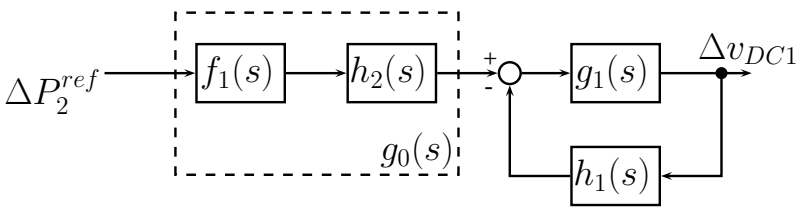

Figure 6: Block diagram from ΔP_2^{ref} to Δv_{DC1}

Insert (36), (37) into (43), the expression of $f_1(s)$ is given as following:

$$f_1(s) = \frac{\alpha_p s}{v_{DC20}(s+\alpha_p)Q_3(s)} \tag{44}$$

$$Q_3(s) = (C_1+C_2)s^3 + (C_1\alpha_c + \frac{i_{DC10}}{v_{DC10}} + \frac{i_{DC20}}{v_{DC20}})s^2 + \\ + \alpha_c K_{pd} s + \alpha_c K_{id} \tag{45}$$

In order to guarantee the roots of $Q_3(s)$ are located at the left half plane, the following inequality should be hold:

$$\frac{C_1\alpha_c + \frac{i_{DC10}}{v_{DC10}} + \frac{i_{DC20}}{v_{DC20}}}{C_1+C_2} > \frac{K_{id}}{K_{pd}} = \frac{\omega_{nd}}{2\zeta} \tag{46}$$

For the purpose of less transmission losses, the DC voltage drop between two terminals should be small, which implies that $i_{DC10}/v_{DC10}+i_{DC20}/v_{DC20}$ is much less than $C_1\alpha_c$. In addition, the bandwidth of inner current loop α_c is designed to be ten times larger than the DC voltage loop. Therefore the inequality holds for all reasonable design of PI-controllers and the poles of $f_1(s)$ have strictly negative real part and are thus stable.

Similarly, it can be proved that the feed forward path function $g_0(s)$ is stable for all the input output combinations. Therefore, the entire system stability in practice only depends on the feedback loop dynamics.

5 Closed loop stability assessment

As was previously concluded, for reasonably designed PI-parameters, the entire system stability only relies on the feedback loop $g_1(s)/[1+g_1(s)h_1(s)]$, where $g_1(s)$ is a rational function with respect to 's' and $h_1(s)$ is input to output stable. Therefore, the number of unstable poles of the open loop transfer function $g_1(s)h_1(s)$ is determined by $g_1(s)$, where $g_1(s)$ is:

$$g_1(s) = \frac{Q_3(s)(ls+r)}{P_5(s)} \tag{47}$$

$$P_5(s) = (ls+r)(C_2 s + \frac{i_{DC20}}{v_{DC20}})[C_1 s^3 + (C_1\alpha_c + \frac{i_{DC10}}{v_{DC10}})s^2 \\ + \alpha_c K_{pd} s + \alpha_c K_{id}] + s^2(cs+g) \tag{48}$$

Assuming a closed path Υ, enclosing all of the right half complex s-plane and having the clockwise positive direction, we can apply the Nyquist criterion: The number of anti-clockwise encirclements around the critical point (-1,0) in the $g_1(s)h_1(s)$-plane should, for a stable closed loop system,

equal the number of open loop unstable poles of $g_1(s)$, as $h_1(s)$ is already a stable function [9].

In the case study setup, the VSC-HVDC system parameters and initial states are listed in Table1. There are two cases that would be discussed in this section: one example is using the rectifier (AC→DC) as DC voltage controller (standard situation) and the other is using the inverter (DC→AC) as DC voltage controller.

Table 1: Parameter of VSC-HVDC system

Cable distance	d	50,150,450	km
Cable inductance density	l	0.189	mH/km
Cable capacitance density	c	0.207	μF/km
Cable resistance density	r	0.0376	Ω/km
Cable conductance density	g	0	S/km
Phase reactor inductance	L	53	mH
Phase reactor resistance	R	0.167	Ω
DC shunt capacitor	C	33	μF
Rated AC voltage (dq-frame)	v_{sd0}	200	kV
Rated DC voltage	v_{DC0}	300	kV
Rated transmission power	P_0	600	MW
System frequency	f	50	Hz

5.1 Rectifier performs as DC voltage controller

If the rectifier controls the DC voltage and the inverter controls the transmitted active power, the steady states are $v_{DC10} = 300kV$ and $P_{20} = -600MW$. The poles of $g_1(s)$ with different cable distances are given in Table 2. For all three cable distances, there is one unstable pole of the open loop transfer function $g_1(s)h_1(s)$.

Table 2: Poles of $g_1(s)$ with P_{20}=-600MW

d	Poles of $g_1(s)$				
50	23.9	-3.3+3.4j	-3.3-3.4j	-206.8+954j	-206.8-954j
150	25.3	-3.3+3.5j	-3.3-3.5j	-204.5+951j	-204.5-951j
450	31.3	-3.3+3.5j	-3.3-3.5j	-194.7+938j	-194.7-938j

The Nyquist plots of the transfer functions $g_1(j\omega)h_1(j\omega)$ with different cable distances are given in Fig. 7. It shows that for all three cases, $g_1(j\omega)h_1(j\omega)$ anti-clockwise encircles the critical point (-1,0) once, which is equal to the number of positive poles of $g_1(s)h_1(s)$. Consequently, for the different cable distances, d=50km, 150km, 450km, the VSC-HVDC system remains stable at the operational point v_{DC10}=300kV and P_{20}=-600MW.

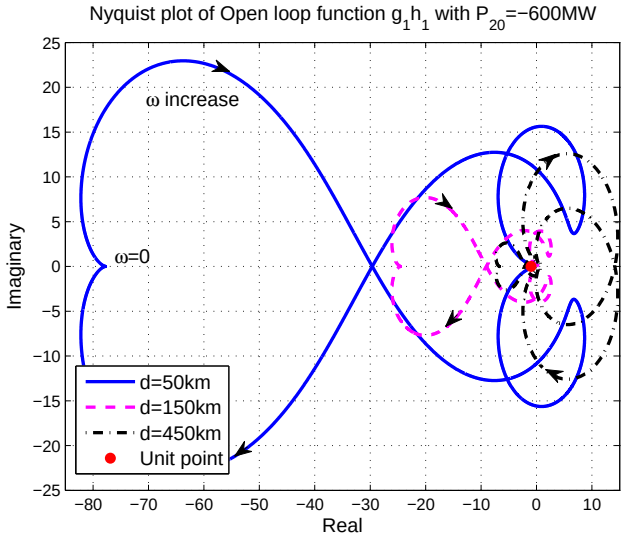

(a)Full curve of $g_1h_1(j\omega)$ with ω from $-\infty$ to ∞

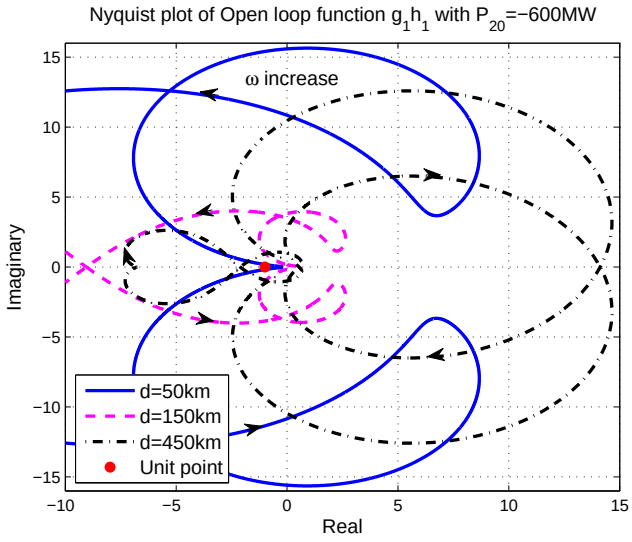

(b)Amplified curve around critical point (-1,0)

Figure 7: Nyquist plot of $g_1h_1(j\omega)$ with $P_{20} = -600MW$: d=50km (solid blue); d=150km (dashed red); d=450km (dashed dotted black)

5.2 Inverter performs as DC voltage controller

If instead the inverter controls the DC voltage and the rectifier controls the transmitted active power, the steady states are $v_{DC10} = 300kV$ and $P_{20} = 600MW$. The poles of $g_1(s)$ with different cable distances are given in Table 3. For all three cases, there are two unstable poles of the open loop transfer function $g_1(s)h_1(s)$.

Table 3: Poles of $g_1(s)$ with P_{20}=600MW

d	Poles of $g_1(s)$				
50	1.2+11.5j	1.2-11.5j	-3.6	-198+994j	-198-994j
150	1.1+11.3j	1.1-11.3j	-3.6	-195+995j	-195-995j
450	0.95+10.6j	0.95-10.6j	-3.6	-190+996j	-190-996j

The Nyquist plots of the transfer functions $g_1(j\omega)h_1(j\omega)$ with different cable distances are given in Fig. 8. It shows that for all three cases, $g_1(j\omega)h_1(j\omega)$ anti-clockwise encircles the critical point (-1,0) twice, which is equal to the number of positive poles of $g_1(s)h_1(s)$. Consequently, for the different cable distances, d=50km, 150km, 450km, the VSC-HVDC system remains stable at the operational point v_{DC10}=300kV and P_{20}=600MW.

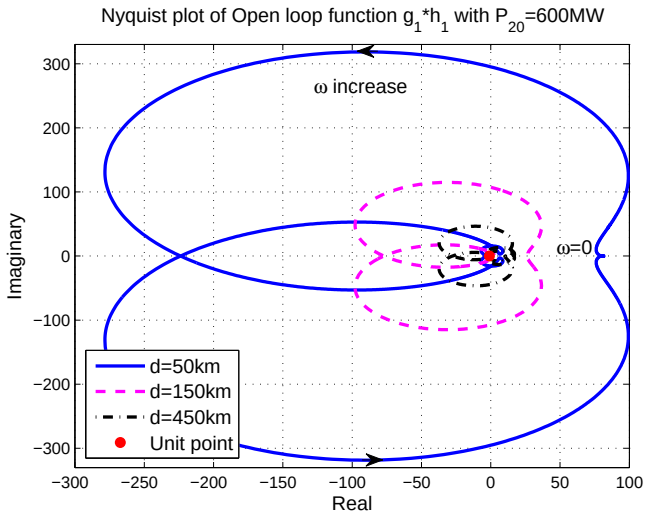

(a)Full curve of $g_1h_1(j\omega)$ with ω from $-\infty$ to ∞

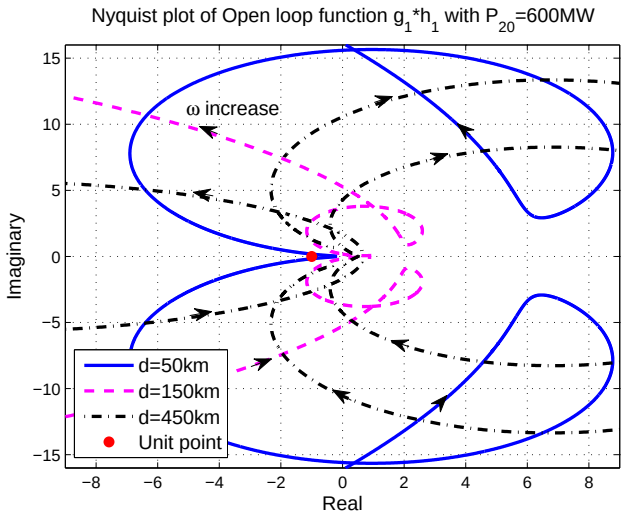

(b)Amplified curve around critical point (-1,0)

Figure 8: Nyquist plot of $g_1 h_1(j\omega)$ with $P_{20} = 600MW$: d=50km (solid blue); d=150km (dashed red); d=450km (dashed dotted black)

6 Conclusions

A mathematical model for small-signal stability analysis of a two terminal VSC-HVDC system with a distributed parameter DC cable model has been presented. Due to the symmetric properties of the cable model, the block diagram of each input output combination could be rewritten as in Fig. 2, where $g_0(s)$ is stable with reasonable design of the DC voltage PI-controller and the forward path of the feedback loop, $g_1(s)$, is a rational function of 's' and the return path $h_1(s)$ is dissipative. Using this approach, the small-signal stability could be analyzed by the Nyquist criterion. Two examples have been illustrated, showing that in both cases with either the rectifier or the inverter working as DC voltage controller, the system is stable for three different cable distances d=50km, 150km, 450km.

The proposed method enables the VSC-HVDC system stability to be determined with arbitrary DC cable length and not limited to short length cable model approximations. Further, no assumptions of low frequency bands are demanded by using the distributed parameter cable model. The proposed approach to stability analysis could in principle be extended into the weak grid AC environment case. Some more (rational) transfer functions have then to be taken into account as well.

References

[1] R. Rudervall, J. Charpentier, and S. Raghuveer, "High Voltage Direct Current (HVDC) Transmission Systems Technology Review Paper," *Energy Week 2000*, March, 2000.

[2] T. Larsson, A. Edris, D. Kidd, F. Aboytes, and R. Haley, "Eagle Pass Back-to-Back Tie : a Dual Purpose Application of Voltage Source Converter technology," *IEEE Power Enginnering Society Summer Meeting*, vol. 3, pp. 1686–1691, 2001.

[3] J. Svensson, *Grid-Connected Voltage Source Converter Control Principles and Wind Energy Applications*. Chalmer University of Technology, 1998, no. 331.

[4] P. Karlsson, *DC Distributed Power Systems - analysis, design and control for a renewable energy system*. Lund University, 2002.

[5] Y. Pipelzadeh, B. Chaudhuri, and T. C. Green, "Control Coordination Within a VSC HVDC Link for Power Oscillation Damping : A Robust Decentralized Approach Using Homotopy," *IEEE Transactions on Control Systems Technology*, vol. 21, no. 4, pp. 1270–1279, 2013.

[6] B. Ooi and X. Wang, "Voltage angle lock loop control of the boost type PWM converter for HVDC application," *IEEE Transactions on Power Electronics*, vol. 5, no. 2, pp. 229–235, Apr. 1990.

[7] N. Mohan, *Advanced electric drives: analysis, control and modeling using Simulink*. MNPERE, 2001.

[8] L. Harnefors, M. Bongiorno, and S. Lundberg, "Input-Admittance Calculation and Shaping for Controlled Voltage-Source Converters," *IEEE transactions on industrial electronics*, vol. 54, no. 6, pp. 3323–3334, 2007.

[9] K. J. Astrom and R. M. Murray, *Feedback System - An Introduction for Scientists and Engineers*. Princeton university press, 2008.

Paper 2

Nyquist Stability Analysis of an AC-grid connected VSC-HVDC System Using a Distributed Parameter DC-cable Model

Y. Song and C. Breitholtz

submitted for publications in IEEE Tran. on Power Delivery, special issue: HVDC transmission systems for large offshore wind power plants

Comment: The layout of this paper has been reformatted in order to comply with the rest of the thesis. The contents have not been altered.

Nyquist Stability Analysis of an AC-grid connected VSC-HVDC System Using a Distributed Parameter DC-cable Model

Y. Song and C. Breitholtz

Abstract

In this paper a two terminal VSC-HVDC system embedded in a weak grid AC-environment is considered, emphasizing modeling, controller design and small-signal stability analysis. Traditionally, the DC cable is modeled by one (or more) Π-section, implying that care has to be taken when using the model for higher frequencies or in case of higher cable impedance density such as submarine cables. Here, a distributed parameter cable model is used to overcome this problem. The VSC-HVDC system can be described by two cascaded blocks. The first block is a transfer function that will be different, due to which input and output variables that are considered but is in all realistic cases stable. The second block is a feedback loop, where the forward path is a rational function and the return path is a dissipative infinite dimensional function, remains the same in all cases. The stability is then analyzed, using the Nyquist criterion, in a straight forward manner. Numerical examples are given by the use of MATLAB.

1 Introduction

Voltage source converter based high voltage direct current transmission (VSC-HVDC) systems have now been in operation since 1997 as it is a reliable and flexible method of power transmission [1]. A typical application would be the integration of renewable energy resources over large geographical areas, such as wind farms [2]. Various aspects of these VSC-HVDC systems have been addressed, especially focusing on the control strategy and small signal stability analysis. In some of them focus has been on short term operation of the HVDC systems, emphasizing dynamics and control.

From the system theory point of view the VSCs involve several linear subsystems, for example PI-controllers and linear circuit elements, but also

nonlinear subsystems, due to the relations between power and voltage (or current). If large changes in voltage levels should be taken into account, for example due to severe system faults, nonlinear dynamical models must be used in analysis as well as simulation. A major interest has been in the dynamics close to steady state (implying sinusoidal steady state at the AC-side and constant steady state at the DC-side). Consequently linearized dynamical models have been in focus [3].

However, little attention has so far been paid to evaluate the influence of DC cable dynamics of VSC-HVDC system, especially when embedded within weak AC environment. Typically, DC cables have been modeled by one simple Π-section and thus the stability of linearized multi-terminal or two terminals VSC-HVDC systems could be analyzed by straightforward calculation of the system eigenvalues [4] [5]. This is often sufficient, at least when considering dynamics of short cables and low frequencies. If more general results are required, for example fast system excitation caused by abrupt disturbances and perhaps in submarine cables (due to increased impedance density i.e. inductance density, capacitance density and resistance density), it would be more appropriate to use a distributed parameter cable model together with transfer functions (or finite order state space) linearized VSC models.

In this article, the VSC-HVDC system embedded in a weak AC environment is modeled, comprising VSCs and AC-side dynamics, together with a distributed parameter DC-cable model, based on the one dimensional damped wave equation. The system is linearized around an arbitrary operational point and the resulting linear infinitely dimensional model is based on the use of transfer functions. The VSC-HVDC system can be described by two cascaded systems: One is a forward combination of transfer functions that will be different, due to which input signal and which output signal that are considered, which in cases of reasonably large AC-grid short circuit ratios (SCR) is input to output stable. The second is a feedback system, where the forward subsystem is finite dimensional and the return subsystem only depends on the infinite dimensional cable model. The stability of this feedback system, which remains the same for all combinations of input and output signals, is analyzed by use of the Nyquist criterion. Schemes and equations are deduced in the paper and simulation results in frequency domain will be showed as well. The purpose is to provide a tool for small signal analysis of the total VSC-HVDC system, including a cable model that is valid independently of cable length and impedance density or which frequencies that can be considered due to the cable model approximation.

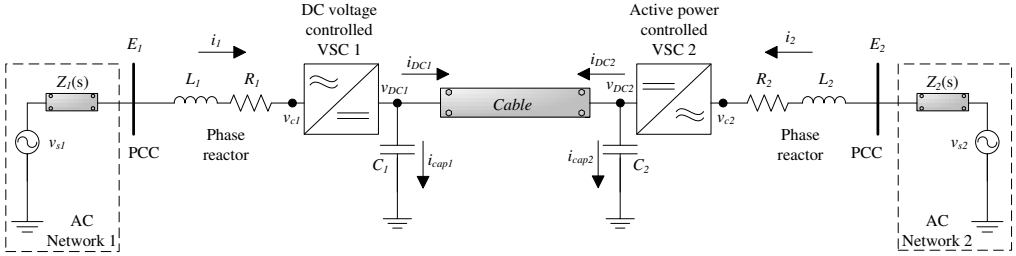

Figure 1: Standard HVDC-VSC system embedded in a weak AC environment. v_s is the source voltage; E is the PCC voltage; i is the converter input current; v_c is the converter voltage; E_c is the converter measured PCC voltage; i_c is the converter measured input current; $Z(s)$ is the AC-grid impedance.

2 Problem formulation

The system under study is depicted in Fig. 1., where the weak AC-grids are modeled by the impedance matrices Z_1(s) and Z_2(s) at the synchronous frame respectively. The so-called synchronous frame is oriented to be in alignment with the voltage direction, due to the Phase Locked Loops (PLL) [6]. The PLL dynamics would be considered to build converter-grid interconnection. At the AC-side of the VSCs, the series inductances (L_1, L_2) and resistances (R_1, R_2) represent the AC reactors and the power losses in the converters. The DC cable would be interpreted as a distributed parameter model. The shunt capacitors at the terminals are denoted by C_1, C_2 respectively.

In standard VSC-HVDC systems, one converter station (VSC1) is assigned the duty as the DC voltage controller to secure the stability of the DC-Bus voltage; the other station (VSC2) operates as the active power controller to guarantee and balance the power exchanges [7]. Moreover, in each VSC, it is possible to control the grid voltage at the AC-side, which in this paper is done by a P-controller.

If the DC cable is modeled by a simple Π-scheme, the stability of the system can be investigated by an eigenvalue calculation. However, the high frequency information is not necessarily well interpreted by the Π-scheme cable model and thus inconvenient to analyze the real dynamic influence of the DC cable. The new standard VSC-HVDC model includes the distributed parameter cable model and formulates the transfer function into the block diagram as shown in Fig. 2. Therefore, if $g_1(s)$ is a rational function of 's' and the infinite dimensional transfer function $h_1(s)$ represents a dissipative system, the feedback loop stability could be analyzed by use of the Nyquist criterion.

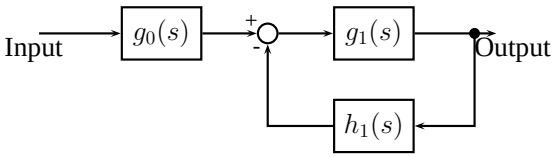

Figure 2: Block diagram: g_0 is the forward transfer function, g_1h_1 is the open loop function of the feedback loop $g_1/(1+g_1h_1)$.

The VSC-model is derived in the so-called dq reference plane as well. The two VSCs are assumed to be ideal and symmetrical, having a switching frequency of 1kHz. In the following, the units for voltage, current and active power are [kV], [kA] and [MW] respectively and all reference signals x are expressed as x^{ref}, the differential operator with respect to time is expressed by 'p' and the Laplace form of a time domain variable $x(t)$ is denoted $\tilde{x}(s)$.

3 System model

In this section, the dynamic equations of a VSC is given in the power invariant dq reference frame, where the frame is chosen to be in align with the voltage direction i.e. $E_{cq10} = E_{cq20} = 0$. E_{cq10} and E_{cq20} are the steady state of the converter measured point of common coupling (PCC) voltage. The AC-grid frequency is assumed to be constant i.e. $\omega_0 = 2\pi f_0$ and $f_0 = 50$ [Hz]. Since the VSCs are assumed symmetric, the variables and parameters in this section would not be subscribed by the numbers 1 and 2, used to denote the different VSCs.

The local controller of the VSC is separated into two cascaded parts: inner current controller and outer controller. The inner current controller provides the voltage reference (v_{cd}^{ref} and v_{cq}^{ref}) to the pulse width modulator (PWM). The d-axis outer controller is used to track the reference of either DC voltage or active power and generates the d-axis current reference (i_d^{ref}) to the inner current loop; The q-axis outer controller is used to limit the voltage drop of the PCC voltage by a P-controller [8] and therefore generates the q-axis current reference (i_q^{ref}) to the inner current loop as well.

3.1 Inner current loop

The AC current dynamics in the dq frame is given as follows, where i_{cd}, i_{cq} are the measured converter input currents; E_{cd}, E_{cq} are the measured PCC

voltages; v_{cd}, v_{cq} are the measured converter voltages:

$$L \cdot \frac{\mathrm{d}i_{cd}}{\mathrm{d}t} = -R \cdot i_{cd} + \omega_0 L \cdot i_{cq} + E_{cd} - v_{cd} \tag{1}$$

$$L \cdot \frac{\mathrm{d}i_{cq}}{\mathrm{d}t} = -R \cdot i_{cq} - \omega_0 L \cdot i_{cd} + E_{cq} - v_{cq} \tag{2}$$

The current controller consists of one PI-controller and two feed forward signals i.e. the PCC voltage and the cross coupling current [9]. The reference voltages (v_{cd}^{ref}, v_{cq}^{ref}) are given by:

$$v_{cd}^{ref} = -(K_p + \frac{K_i}{p})(i_d^{ref} - i_{cd}) + E_{cd} + \omega_0 L \cdot i_{cq} \tag{3}$$

$$v_{cq}^{ref} = -(K_p + \frac{K_i}{p})(i_q^{ref} - i_{cq}) + E_{cq} - \omega_0 L \cdot i_{cd} \tag{4}$$

Due to the switching action of PWM inside the converter, a delay of half a switching period appears, where $T_{sw} = 1/(2f_{sw}) = 0.5$ [ms]. After having designed the inner current loop relatively slow, the delay is reasonable to ignore during the analysis of system dynamics i.e. $v_{cd}^{ref} \approx v_{cd}$ and $v_{cq}^{ref} \approx v_{cq}$ [8]. Consequently, the dynamics between the d- and q-axis is decoupled at the inner current loop.

The PI-parameters are designed as $K_p = \alpha_c L$ and $K_i = \alpha_c R$, where α_c is the bandwidth of the inner current loop and the phase reactor pole of $-R/L$ is thus canceled by the inner current PI-controller. Note that the unavoidable uncertainties in the AC side model parameters, L and R, from a practical point of view are assumed to be quite small. Hence these uncertainties will have only a minor impact on the inner current loop performance. In addition, since the outer loop bandwidth usually is designed to be at least ten times smaller than α_c, the effect caused by the inner loop parameter uncertainty would not influence the entire system dynamics very much. Therefore, the design of the inner current loop PI-controller based on model parameters is well justified. Consequently, the linearized inner current closed loop in the Laplace domain is:

$$\Delta\tilde{i}_{cd}(s) = \frac{\alpha_c}{s + \alpha_c} \Delta\tilde{i}_d^{ref}(s) \tag{5}$$

$$\Delta\tilde{i}_{cq}(s) = \frac{\alpha_c}{s + \alpha_c} \Delta\tilde{i}_q^{ref}(s) \tag{6}$$

3.2 Direct Voltage control loop

The DC voltage is determined by the capacitor charging power that is the difference between the input active power to the VSC (assuming that the

VSC is power lossless) and the DC load power, which gives:

$$\frac{\mathrm{d}}{\mathrm{d}t}(\frac{1}{2}C \cdot v_{DC}^2) = P - P_{load} \tag{7}$$

$$\Rightarrow \quad C \cdot v_{DC0} \cdot \frac{\mathrm{d}\Delta v_{DC}}{\mathrm{d}t} = \Delta P - \Delta P_{load} \tag{8}$$

Therefore, the linearized expression of the input active power and the DC load power are required, where the conjugate value of x is denoted by x^*:

$$\begin{aligned} P &= Re\{(E_0 + \Delta E_{cd} + j\Delta E_{cq})(i_{d0} + \Delta i_{cd} + j(i_{q0} + \Delta i_{cq}))^*\} \\ &\approx \underbrace{E_0 i_{d0}}_{P_0} + \underbrace{E_0\Delta i_{cd} + i_{d0}\Delta E_{cd} + i_{q0}\Delta E_{cq}}_{\Delta P} \end{aligned} \tag{9}$$

$$\begin{aligned} P_{load} &= (v_{DC0} + \Delta v_{DC})(i_{DC0} + \Delta i_{DC}) \\ &\approx \underbrace{v_{DC0} i_{DC0}}_{P_{load0}} + \underbrace{v_{DC0}\Delta i_{DC} + i_{DC0}\Delta v_{DC}}_{\Delta P_{load}} \end{aligned} \tag{10}$$

Equation (9) shows that ΔP is proportional to Δi_{cd} and independent of Δi_{cq}. Therefore, the output of the DC voltage controller i.e. the d-axis reference current, could be designed through the reference input active power. The reference input active power is the sum of a PI-controller operating on the error of the DC voltage square and the filtered feed forward DC load power (with bandwidth α_f):

$$P^{ref} = (K_{pd} + \frac{K_{id}}{p}) \cdot \nu + \frac{\alpha_f}{p + \alpha_f} P_{load} \tag{11}$$

$$\nu = \frac{(v_{DC}^{ref})^2 - v_{DC}^2}{2} \text{ and } i_d^{ref} = \frac{P^{ref}}{E_{cd}} \tag{12}$$

$$\Delta\tilde{P}^{ref} = v_{DC0} F_d(\Delta\tilde{v}_{DC}^{ref} - \Delta\tilde{v}_{DC}) + F_f \Delta\tilde{P}_{load} \tag{13}$$

$$F_d = K_{pd} + \frac{K_{id}}{s} \text{ and } F_f = \frac{\alpha_f}{s + \alpha_f}$$

$$\Delta\tilde{i}_d^{ref} = \frac{1}{E_0}\Delta\tilde{P}^{ref} - \frac{P_0}{E_0^2}\Delta\tilde{E}_{cd} \tag{14}$$

After ignoring both the low-pass filter in (13) and the inner current loop dynamics i.e. $\Delta i_{cd} = \Delta i_d^{ref}$, designing the PI-controller parameters as $K_{pd} = 2\hat{C}\zeta\omega_{nd}$ and $K_{id} = \hat{C}\omega_{nd}^2$, the transfer function from $\Delta\tilde{v}_{DC}^{ref}$ to $\Delta\tilde{v}_{DC}$ is:

$$\frac{\Delta\tilde{v}_{DC}}{\Delta\tilde{v}_{DC}^{ref}} \approx \frac{2\zeta\omega_{nd}\frac{\hat{C}}{C}s + \omega_{nd}^2\frac{\hat{C}}{C}}{s^2 + 2\zeta\omega_{nd}\frac{\hat{C}}{C}s + \omega_{nd}^2\frac{\hat{C}}{C}} \tag{15}$$

The approximation is based on the fact that the inner current loop dynamics is designed ten times faster than the DC voltage loop and also assume that the DC load power signal has lower magnitude in the higher frequency band.

$\hat{C}$ is the estimated DC-shunt capacitance and C is the actual physical shunt capacitance. The damping ratio ζ and natural frequency ω_{nd} are amplified by $\sqrt{\hat{C}/C}$ compared to the designed parameters. Since the physical shunt capacitance C contains the DC-cable shunt capacitance, which is assumed to be larger than $\hat{C}$; then ζ and ω_{nd} should be higher than the designed value in order to compensate for the error. In this paper, the influence of such parameter uncertainty of C is not considered. ζ and ω_{nd} are chosen to be 1 and $0.4\alpha_d$, which guarantees the DC-voltage loop bandwidth of (15) is α_d.

3.3 Active power control loop

For the outer controller of transmitted active power, again a PI-controller is used. The controller parameters are designed by inner current loop pole cancelation i.e. $K_{pp} = \alpha_p/\alpha_c$, $K_{ip} = \alpha_p$. The bandwidth of the outer loop is chosen as $\alpha_p = 0.2\alpha_d$. Therefore, the DC voltage would not display large oscillations during the variations of transmitted active power. The linearized differential equations of the active power control loop are derived as follows:

$$i_d^{ref} = (K_{pp} + \frac{K_{ip}}{p})(P^{ref} - P)/E_{cd} \tag{16}$$

$$\Rightarrow \Delta\tilde{i}_d^{ref} = \frac{1}{E_0}(K_{pp} + \frac{K_{ip}}{s})(\Delta\tilde{P}^{ref} - \Delta\tilde{P}) \tag{17}$$

3.4 Alternating Voltage control loop

The idea of the AC voltage controller is to compensate for the AC voltage drop i.e. to increase the reactive power at PCC while the AC voltage is lower than the reference PCC voltage [10]. A P-controller is applied and thus the q-axis reference current is:

$$\Delta\tilde{i}_q^{ref} = K_{pa} \cdot (\Delta\tilde{E}^{ref} - \Delta\tilde{E}_{cd}) \tag{18}$$

It is also possible to use a PI-controller instead of a P-controller. The reason not to is that there is no accuracy specification for the AC voltage control and that the insert of an extra integral control action will not promote system stability. Therefore, in this paper, a P-controller is applied to control the AC voltage.

3.5 AC-grid and PLL

A PLL is applied to track the rotating phase angle θ^{ref}, which is used to transform the converter dq-frame from the stationary $\alpha\beta$-frame. At steady state, the q-part of the PCC voltage at the converter dq-frame is zero. Due to the assumption of constant AC-grid frequency, a P-controller is thus sufficient to track the reference AC-grid phase. The transfer function from ΔE_q to $\Delta\theta$ and relationships between voltages (ΔE_d, ΔE_q), currents (Δi_d, Δi_q) of the grid dq-frame and voltages (ΔE_{cd}, ΔE_{cq}), currents (Δi_{cd}, Δi_{cq}) of the converter dq-frame are given by [8]:

$$\Delta\tilde{\theta} = \frac{\alpha_{pll}}{s+\alpha_{pll}}\Delta\tilde{E}_q \tag{19}$$

$$\Delta\tilde{E}_{cd} = \Delta\tilde{E}_d, \text{ and } \Delta\tilde{E}_{cq} = \frac{s}{s+\alpha_{pll}}\Delta\tilde{E}_q \tag{20}$$

$$\Delta\tilde{i}_d = \Delta\tilde{i}_{cd} + \frac{Q_0}{E_0^2}\frac{\alpha_{pll}}{s+\alpha_{pll}}\Delta\tilde{E}_q \tag{21}$$

$$\Delta\tilde{i}_q = \Delta\tilde{i}_{cq} + \frac{P_0}{E_0^2}\frac{\alpha_{pll}}{s+\alpha_{pll}}\Delta\tilde{E}_q \tag{22}$$

For a strong AC-grid, the PCC voltage is independent of the current variation, while ΔE_d and ΔE_q are input disturbances of the VSC system. However, for a weak AC-grid, the PCC voltage is related to the current or power variation. In this case, the d-axis and q-axis dynamics are not independent of each other but correlated through the AC-grid impedance. The AC-grid is modeled by a series R_gL_g-circuit in the synchronous dq-frame. The AC-grid dynamics are:

$$\Delta\tilde{v}_{sd} - \Delta\tilde{E}_d = (L_g s + R_g)\Delta\tilde{i}_d - \omega_0 L_g \Delta\tilde{i}_q \tag{23}$$

$$\Delta\tilde{v}_{sq} - \Delta\tilde{E}_q = \omega_0 L_g \Delta\tilde{i}_d + (L_g s + R_g)\Delta\tilde{i}_q \tag{24}$$

3.6 DC-cable

The conventional method of approximating a transmission line is to replace the line by small cascaded lumped RLGC-sections, which is shown in Fig. 3. The terminal voltages and currents are represented by v_{DC1}, v_{DC2}, i_{DC1} and i_{DC2}. The current from the AC to DC side is defined as positive. The cable parameters are given by r, l, g, c and d, which are the cable density of resistance, inductance, conductance, capacitance and the cable length.

Define the complex damping factor per unit length γ and the wave ad-

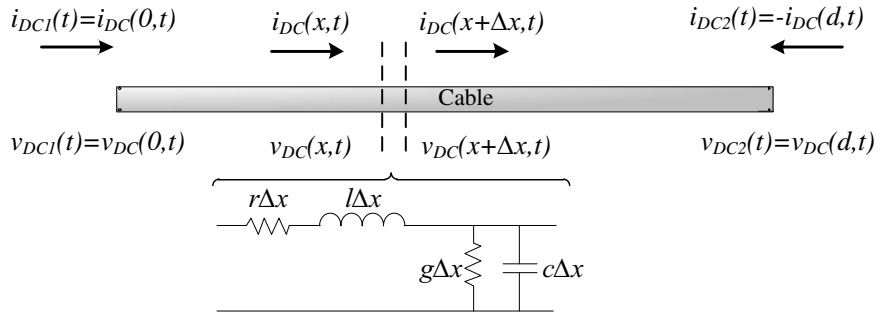

Figure 3: DC cable model: since the current from the AC to DC side is defined as positive, $i_{DC1} = i_{DC}(0,t)$ and $i_{DC2} = -i_{DC}(d,t)$

mittance Y_0 as:

$$\gamma(s) = \sqrt{(c \cdot s + g)(l \cdot s + r)},\ \Gamma(s) = d \cdot \gamma(s) \tag{25}$$

$$Y_0(s) = \sqrt{\frac{c \cdot s + g}{l \cdot s + r}} \tag{26}$$

By solving the readily derived linear partial differential equations, obtained from Fig. 3. after letting the element $\Delta x \to 0$ and taking Laplace transforms with respect to time, the relationship between the terminal currents and voltages are formulated [11]:

$$\begin{bmatrix} \tilde{i}_{DC1}(s) \\ \tilde{i}_{DC2}(s) \end{bmatrix} = \begin{bmatrix} h_1(s) & -h_2(s) \\ -h_2(s) & h_1(s) \end{bmatrix} \cdot \begin{bmatrix} \tilde{v}_{DC1}(s) \\ \tilde{v}_{DC2}(s) \end{bmatrix} \tag{27}$$

$$\text{where, } h_1(s) = Y_0(s) \coth(\Gamma(s)) \tag{28}$$

$$h_2(s) = \frac{Y_0(s)}{\sinh(\Gamma(s))} \tag{29}$$

As the cable system itself is dissipative, the functions $h_1(s)$ and $h_2(s)$ have infinite numbers of stable poles. In addition, the square difference between $h_1(s)$ and $h_2(s)$ is identically a rational function i.e. $h_1^2(s) - h_2^2(s) = Y_0^2(s)$.

4 Block diagram of two terminal VSC-HVDC system

In this section, the two terminal VSC-HVDC system embedded in strong or weak AC-environments are considered and transformed into the block diagram at Fig. 2.

4.1 Weak AC-grid environment

Under the situation of both VSCs are embedded in the weak AC-grid environment, for each VSC system, there are five input signals i.e. Δv_{sd}, Δv_{sq}, Δi_{DC} and reference signals Δv_{DC1}^{ref} or ΔP_2^{ref} and ΔE^{ref}. Note that Δi_{DC} is a state variable in the description of the entire system.

Choose the DC-voltage as the VSC system output. Both Δv_{DC} and Δi_{DC} constitute the interconnection between the VSC and the DC-grid. The preliminary transfer functions from those five inputs to the DC voltages are given by:

$$\begin{aligned}\Delta\tilde{v}_{DC1} =& g_{11}(s)\Delta\tilde{v}_{DC1}^{ref} + g_{12}(s)\Delta\tilde{E}_1^{ref} + g_{13}(s)\Delta\tilde{v}_{sd1} + \\ &+ g_{14}(s)\Delta\tilde{v}_{sq1} + g_{15}(s)\Delta\tilde{i}_{DC1} \\ \Delta\tilde{v}_{DC2} =& g_{21}(s)\Delta\tilde{P}_2^{ref} + g_{22}(s)\Delta\tilde{E}_2^{ref} + g_{23}(s)\Delta\tilde{v}_{sd2} + \\ &+ g_{24}(s)\Delta\tilde{v}_{sq2} + g_{25}(s)\Delta\tilde{i}_{DC2}\end{aligned}$$

Combine the relationship between the DC-terminal currents and voltages given at (27), the two-terminal VSC-HVDC system transfer function matrix is readily obtained from:

$$\begin{aligned}&\Lambda(s)\begin{bmatrix}\Delta\tilde{v}_{DC1}\\ \Delta\tilde{v}_{DC2}\end{bmatrix} = \Phi(s)\cdot u \qquad (30)\\ &\Lambda(s) = \begin{bmatrix}1-g_{15}h_1 & g_{15}h_2\\ g_{25}h_2 & 1-g_{25}h_1\end{bmatrix}\\ &\Phi(s) = \begin{bmatrix}g_{11} & g_{12} & 0 & 0 & g_{13} & g_{14} & 0 & 0\\ 0 & 0 & g_{21} & g_{22} & 0 & 0 & g_{23} & g_{24}\end{bmatrix}\end{aligned}$$

where, $u^T = [\Delta\tilde{v}_{dc1}^{ref}\ \Delta\tilde{E}_1^{ref}\ \Delta\tilde{P}_2^{ref}\ \Delta\tilde{E}_2^{ref}\ \Delta\tilde{v}_{sd1}\ \Delta\tilde{v}_{sq1}\ \Delta\tilde{v}_{sd2}\ \Delta\tilde{v}_{sq2}]$. The MIMO transfer function from inputs to outputs is given as follows, where $\mathrm{adj}(\Lambda)$ denotes the adjoint matrix of Λ and $G(s) = \mathrm{adj}(\Lambda)\Phi$:

$$\begin{aligned}\begin{bmatrix}\Delta\tilde{v}_{DC1}\\ \Delta\tilde{v}_{DC2}\end{bmatrix} &= \Lambda^{-1}\Phi\cdot u = \frac{1}{\det\Lambda}\mathrm{adj}(\Lambda)\Phi\cdot u\\ &= \underbrace{\frac{-\frac{g_{15}+g_{25}}{1+Y_0^2 g_{15}g_{25}}}{1-\frac{g_{15}+g_{25}}{1+Y_0^2 g_{15}g_{25}}\cdot h_1}}_{\text{Feedback loop } \frac{g_1}{1+g_1h_1}} \underbrace{\frac{-1}{g_{15}+g_{25}}G(s)}_{\text{Forward function } g_0}\cdot u \qquad (31)\end{aligned}$$

4.2 Strong AC-grid environment

While the connected AC-grids are well balanced and strong i.e. the nominal AC-grid voltage is as most subject to small variation, the dynamics of the

PLL is ignored. In addition, since the q-axis current has no impact on the dynamics at the DC-side (after d- and q-dynamics decoupling at the inner current loop), the q-axis current reference (Δi_q^{ref}) is thus assumed to be zero.

In this case, for each VSC, there are three input signals i.e. Δv_{sd}, Δi_{DC} and reference signal Δv_{DC1}^{ref} or ΔP_2^{ref}. As before, choose the D-C voltage as the VSC output. The transfer functions from inputs $\hat{u} = [\Delta\tilde{v}_{DC1}^{ref}\ \Delta\tilde{P}_2^{ref}\ \Delta\tilde{v}_{sd1}\ \Delta\tilde{v}_{sd2}]^T$ to the DC voltages are:

$$\Delta\tilde{v}_{DC1} = \hat{g}_{11}(s)\Delta\tilde{v}_{DC1}^{ref} + \hat{g}_{13}(s)\Delta\tilde{v}_{sd1} + \hat{g}_{15}(s)\Delta\tilde{i}_{DC1}$$
$$\Delta\tilde{v}_{DC2} = \hat{g}_{21}(s)\Delta\tilde{P}_2^{ref} + \hat{g}_{23}(s)\Delta\tilde{v}_{sd2} + \hat{g}_{25}(s)\Delta\tilde{i}_{DC2}$$

$$\begin{bmatrix}\Delta\tilde{v}_{DC1}\\ \Delta\tilde{v}_{DC2}\end{bmatrix} = \underbrace{\frac{-\frac{\hat{g}_{15}+\hat{g}_{25}}{1+Y_0^2\hat{g}_{15}\hat{g}_{25}}}{1-\frac{\hat{g}_{15}+\hat{g}_{25}}{1+Y_0^2\hat{g}_{15}\hat{g}_{25}}\cdot h_1}}_{\text{Feedback loop } \frac{\hat{g}_1}{1+\hat{g}_1 h_1}} \underbrace{\frac{-1}{\hat{g}_{15}+\hat{g}_{25}}\hat{G}(s)}_{\text{Forward function } \hat{g}_0} \cdot\hat{u} \tag{32}$$

$$\text{where, } \hat{G}(s) = \begin{bmatrix}\hat{g}_{11}(1-\hat{g}_{25}h_1) & -\hat{g}_{21}\hat{g}_{15}h_2\\ -\hat{g}_{11}\hat{g}_{25}h_2 & \hat{g}_{21}(1-\hat{g}_{15}h_1)\\ \hat{g}_{13}(1-\hat{g}_{25}h_1) & -\hat{g}_{23}\hat{g}_{15}h_2\\ -\hat{g}_{13}\hat{g}_{25}h_2 & \hat{g}_{23}(1-\hat{g}_{15}h_1)\end{bmatrix}$$

For both weak and strong AC-environment, the transfer functions of a two-terminal VSC-HVDC system, using a distributed parameter DC-cable model, can be written into the form $g_0 \cdot g_1/(1+g_1h_1)$. The forward function g_0 is determined by the choice of input and output, while the feedback loop is invariant of this choice. Using this approach, the small-signal stability of the infinite dimensional system could be analyzed by the Nyquist criterion.

5 Closed loop stability assessment

In order to guarantee the stability of the entire system, both the feedback loop and the forward transfer function should be stable. Even though the forward transfer function g_0 is determined by an input-output combination, it will always be a linear non-feedback combination of rational functions and of h_1 or h_2. Thus, the stability of g_0 is given according to the sign of the real parts of a limited number of poles. The stability of the feedback loop is analyzed by use of the Nyquist stability criterion.

Assuming that the closed path $\mathcal{C}$ enclosing all of the right half complex s-plane has the clockwise positive direction, we can apply the Nyquist criterion: The number of anti-clockwise encirclements around the point -1 in the

$g_1(s)h_1(s)$-plane should, for a stable closed loop system, equal the number of open loop unstable poles of $g_1(s)$, as $h_1(s)$ is already an input to output stable function [12].

5.1 Weak AC-grid environment

In this paper, the weak AC-grid is modeled by a series R_gL_g-circuit in the synchronous coordinates and their dynamics are given by (23)-(24).

For the active power controlled VSC, the transfer function g_{25} from Δi_{DC2} to Δv_{DC2} is the same as the VSC connected to a strong AC-grid. Therefore, $g_{25} = \hat{g}_{25}$ and the feedback loop stability would not be influenced by the weak AC-grid dynamics at the active power controlled VSC. Similarly, the stability of the active power controlled VSC could be analyzed without considering the DC-side influence. Consequently, the stability analysis of two terminal VSC-HVDC systems embedded in a weak AC-grid can be separated into two parts: the active power controlled VSC and the VSC-HVDC system while the active power controlled VSC is under steady state.

Stability of Active power controlled VSC

Combine the inner current loop dynamics (5)-(6), active power controlled outer loop dynamics (17) and the PLL dynamics (20)-(22), the state-space model of the active power controlled VSC is given by (33)-(34), where the state variables are $x_{ap}^T = [\Delta i_{cd}\ \Delta i_{cq}\ x_{pll}]$, the input variables are $u_{ap}^T = [\Delta P^{ref}\ \Delta E^{ref}\ \Delta v_{sd}\ \Delta v_{sq}]$ and the disturbance input variables are $d^T = [\Delta E_d\ \Delta E_q]$.

$$\dot{x}_{ap} = A_1 \cdot x_{ap} + B_{u1} \cdot u_{ap} + B_{d1} \cdot d \tag{33}$$

$$d = C_{d1} \cdot x_{ap} + D_{d1} \cdot u_{ap} \tag{34}$$

$$A_1 = \begin{bmatrix} -a_p & 0 & -a_p \cdot \frac{Q_0}{E_0^2} \\ 0 & -a_c & 0 \\ 0 & 0 & -a_{pll} \end{bmatrix}$$

$$B_{u1} = \begin{bmatrix} \frac{\alpha_p}{E_0} & 0 & 0 & 0 \\ 0 & \alpha_c K_{pa} & 0 & 0 \\ 0 & 0 & 0 & 0 \end{bmatrix} \quad B_{d1} = \begin{bmatrix} -a_p \cdot \frac{P_0}{E_0^2} & a_p \cdot \frac{Q_0}{E_0^2} \\ -a_c \cdot K_{pa} & 0 \\ 0 & a_{pll} \end{bmatrix}$$

The expressions of C_{d1} and D_{d1} are given in the Appx. Under strong AC-grid environment, the active power controlled VSC is stable and the system poles are $-\alpha_c$, $-\alpha_p$ and $-\alpha_{pll}$.

Since the input signals u_{ap} are independent of the state variables, the system stability has nothing to do with the value of u_{ap} and thus assume u_{ap}

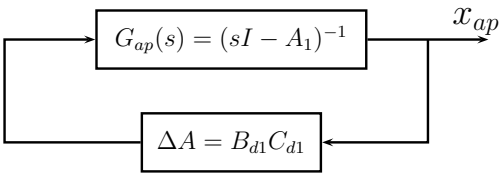

Figure 4: Block diagram of the active power controlled VSC with zero input signals

is the zero vector. Under weak-AC environment, the block diagram of the active power controlled VSC with zero input signals is depicted at Fig. 4.

According to small gain theorem [13], the sufficient condition of stable VSC system is: $||G_{ap}(j\omega)||_\infty \cdot ||\Delta A||_\infty < 1$, for any ω. By denoting the lowest and highest singular value of any matrix M as $\underline{\sigma}(M)$ and $\bar{\sigma}(M)$, the sufficient condition for a stable system is rewritten by (35), where T is an invertible scaling matrix and A_1 has only real eigenvalues:

$$\begin{aligned} & \bar{\sigma}((j\omega I - A_1)^{-1}) \cdot \bar{\sigma}(\Delta A) < 1,\ \omega \in \mathrm{R}^+ \\ \Leftrightarrow\quad & \bar{\sigma}(\Delta A) < \frac{1}{\bar{\sigma}((j\omega I - A_1)^{-1})} = \underline{\sigma}(j\omega I - A_1),\ \omega \in \mathrm{R}^+ \\ \Leftrightarrow\quad & \bar{\sigma}(T^{-1} \cdot \Delta A \cdot T) < \underline{\sigma}(T^{-1} \cdot A_1 \cdot T) \end{aligned} \tag{35}$$

Since the pole of the state Δi_{cq} is at least ten times further away from the imaginary axis compared with the other two states, the dynamics of Δi_{cq} is ignored i.e. $\Delta i_{cq} \approx K_{pa}(\Delta E^{ref} - \Delta E_{cd})$. The state-space model with new state variables $x_{apn} = [\Delta i_{cd}\ x_{pll}]$ is:

$$\dot{x}_{apn} = \tilde{A}_1 \cdot x_{apn} + \tilde{B}_{u1} \cdot u_{ap} + \tilde{B}_{d1} \cdot d \tag{36}$$

$$d = \tilde{C}_{d1} \cdot x_{apn} + \tilde{D}_{d1} \cdot u_{ap} \tag{37}$$

$$\tilde{A}_1 = \begin{bmatrix} -a_p & -a_p \cdot \frac{Q_0}{E_0^2} \\ 0 & -a_{pll} \end{bmatrix}$$

$$\tilde{B}_{u1} = \begin{bmatrix} \frac{\alpha_p}{E_0} & 0 \\ 0 & 0 \end{bmatrix} \quad \tilde{B}_{d1} = \begin{bmatrix} -a_p \cdot \frac{P_0}{E_0^2} & a_p \cdot \frac{Q_0}{E_0^2} \\ 0 & a_{pll} \end{bmatrix} \tag{38}$$

The expressions of $\tilde{C}_{d1}$ and $\tilde{D}_{d1}$ are given in Appx. Letting the scaling matrix T be

$$T = \begin{bmatrix} 0.008 & 0.002 \\ -1 & 1 \end{bmatrix}$$

the minimum singular value of $T^{-1} \cdot A_1 \cdot T$ and the maximum singular value of $T^{-1} \cdot \Delta A \cdot T$ with respect to $SCR = 1/L_g$ [p.u.] are given in Fig. 5,

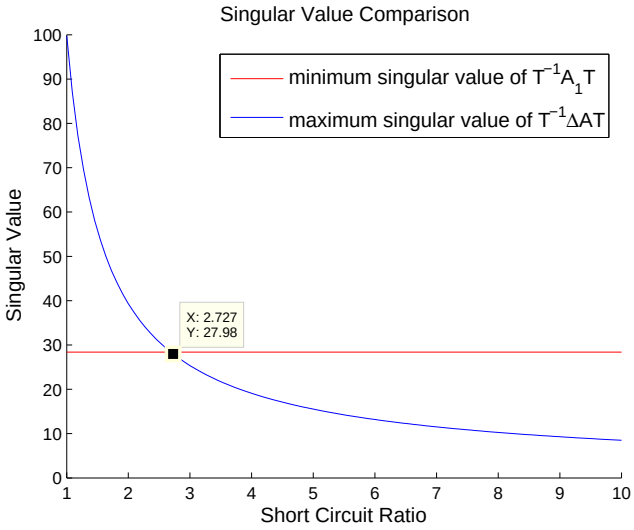

Figure 5: Singular value with respect to SCR: $\underline{\sigma}(T^{-1}A_1T)$ is a constant and marked by the red curve; $\bar{\sigma}(T^{-1}\Delta AT)$ decreases with respect to the increased SCR and marked by the blue curve. The cross point of those two curves is around SCR=2.69 and for $SCR \geq 2.7$, $\bar{\sigma}(T^{-1}\Delta AT) < \underline{\sigma}(T^{-1}A_1T)$ and thus the closed loop system (shows in Fig. 4.) is stable.

Table 1: Bandwidth design of VSC-HVDC system

Inner current loop	α_c	4p.u.	400π [rad/s]
Active power outer loop	α_p	0.1p.u.	10π [rad/s]
DC voltage outer loop	α_d	0.4p.u.	40π [rad/s]
PLL loop	α_{pll}	0.4p.u.	40π [rad/s]

where the parameters for the case study are listed in Table 1, Table 2 and the P-controller parameter of the AC-voltage controller is $K_{pa} = 0.1$.

Since A_1 and T are constant matrices, the minimum singular value of $T^{-1} \cdot A_1 \cdot T$ is constant and equal to 28.38. As shown in Fig. 5., for $SCR > 2.7$, the maximum singular value of $T^{-1} \cdot \Delta A \cdot T$ is smaller than the minimum singular value of $T^{-1} \cdot A_1 \cdot T$ and thus the active power controlled VSC is stable. Worth to be mentioned that, the inequality $SCR > 2.7$ is a sufficient condition for the stability of the VSC system. For SCR lower than 2.7, however, the system could be stable as well, which can be checked by eigenvalue calculation.

For weak AC-grids with other topology, such as shunt or series L_gC_g-circuits, the small gain theorem could also be applied and get a sufficient condition for the stability analysis. However, the disturbance matrix ΔA then needs to be reformulated according to the changed AC-grid dynamics.

Table 2: Parameter of VSC-HVDC system

Cable distance	d	50	km
Cable inductance density	l	9	mH/km
Cable capacitance density	c	0.207	μF/km
Cable resistance density	r	0.01	Ω/km
Cable conductance density	g	0	S/km
Phase reactor inductance	L	53	mH
Phase reactor resistance	R	0.167	Ω
Weak AC-grid inductance	L_g	53.1	mH
Weak AC-grid resistance	R_g	1.11	Ω
DC shunt capacitor	C	33	μF
Rated AC voltage (dq-frame)	v_{sd0}	200	kV
Rated DC voltage	v_{DC0}	300	kV
Rated transmission power	P_0	600	MW
System frequency	f_0	50	Hz

Stability of DC-voltage controlled VSC

As concluded above, the stability of the active power controlled VSC would not influence the stability of the feedback loop $g_1/(1+g_1h_1)$ since $g_{25} = \hat{g}_{25}$. In this subsection, assume that the active power controlled VSC is under steady state. On the other side, the DC-voltage controlled VSC is connected to a weak AC-grid, which is modeled by a series L_gR_g-circuit.

- One Π-section DC-cable model:

While the DC cable is modeled by one Π-section, the VSC-HVDC system without considering the dynamics of active power controlled VSC could be modeled by an eighth order state space model. The state variables are $x_{dv}^T = [\Delta i_{cd}\ \Delta i_{cq}\ \Delta v_{DC}\ x_{dv3}\ x_{dv4}\ x_{pll}\ \Delta i_{DC}\ \Delta v_{DC}^{ap}]$, where x_{dv3} is the integral action of the DC-voltage controller, x_{dv4} is the dynamics of the LPF of the forward DC-load power, Δv_{DC}^{ap} is the DC-voltage at the active power controlled VSC side. The input variables are $u_{dv}^T = [\Delta v_{DC}^{ref}\ \Delta E^{ref}\ \Delta v_{sd}\ \Delta v_{sq}]$ and the disturbance input variables are $d^T = [\Delta E_d\ \Delta E_q]$. u_{dv}^{ref} are the first two reference signals of the input vector u_{dv}.

Combine the inner current loop dynamics (5)-(6), the DC-voltage dynamics (8), the DC-voltage controlled outer loop dynamics (13)-(14), the PLL dynamics (20)-(22), the DC-current dynamics due to series $R_{DC}L_{DC}$-circuit and the active power controlled VSC dynamics given by $g_{25}(s)$, the state-space model of the VSC-HVDC system with one Π-section DC-cable

is:

$$\begin{aligned} \dot{x}_{dv} &= A_2 \cdot x_{dv} + B_{u2} \cdot u_{dv}^{ref} + B_{d2} \cdot d \\ d &= C_{d2} \cdot x_{dv} + D_{d2} \cdot u_{dv} \end{aligned} \tag{39}$$

Expressions of the matrices A_2, B_{u2}, B_{d2}, C_{d2} and D_{d2} are given in Appx. A_2, B_{u2} and B_{d2} do not depend on the SCR value, however, C_{d2} and D_{d2} rely on the SCR. The parameters of the DC cable are listed in Table 2, where $L_{DC} = l \cdot d$ and $R_{DC} = r \cdot d$. The stability of the VSC-HVDC system with one Π-section DC cable model can be analyzed by the eigenvalues of $A_2 + B_{d2}C_{d2}$. It is straight forward to be calculated that for $SCR < 4$, provided the parameter values from Table 2, the VSC-HVDC system would become unstable due to the weak AC-grid impedance but not for case with higher SCR.

- Distributed parameter DC-cable model:

While the DC-cable is modeled by (27), it is hard to use eigenvalue analysis to study the system stability since there are an infinite number of poles. Therefore, the Nyquist criterion is applied to analyze the stability of the system, which has the block diagram in Fig. 2.

As claimed in Section 5, the VSC-HVDC system can be described by two cascaded systems: one is a forward combination of transfer functions, which depends on the considered input and output. The second is a feedback loop which is unique for all input-output combinations. For an active power controlled VSC of this study case, the forward functions are stable at least for $SCR > 2.7$. For a DC-voltage controlled VSC, the forward function stability will be analyzed by a case study.

In the case study setup, the VSC-HVDC system parameters and nominal steady states are listed in Table 2. However, reset the cable inductance density to be 10.2 [mH/km], which render the one Π-section cable model based VSC-HVDC system unstable and the SCR of the AC-grid is still chosen to be 4. For the case with distributed parameter DC-cable model, the forward function stability and the function g_{15} are determined by the new state-space model, where x_{dvn} is the first six components of x_{dv}, the input signal is Δi_{DC} and the output signal is Δv_{DC}:

$$\dot{x}_{dvn} = A_3 \cdot x_{dvn} + B_3 \cdot \Delta i_{DC}$$

$$y = C_3 \cdot x_{dvn} \tag{40}$$

$$g_{15} = C_3(sI - A_3)^{-1}B_3 \tag{41}$$

where A_3 is the sub-square matrix of $A_2 + B_{d2}C_{d2}$ with the first 6 columns and first 6 rows and c=0 [μF] (since the cable capacitance should not be

included in the VSC dynamics itself), and B_3, C_3 are:

$$B_3^T = \begin{bmatrix} 0 & 0 & -\frac{1}{C} & 0 & a_f v_{DC0} & 0 \end{bmatrix}$$
$$C_3 = \begin{bmatrix} 0 & 0 & 1 & 0 & 0 & 0 \end{bmatrix}$$

It is straight forward to prove that the above system (40) is minimum order i.e. the system is both controllable and observable. Therefore, the stability of the forward function $g_0 = \frac{-1}{g_{15}+g_{25}} G(s)$ is determined by the zeros of $g_{15} + g_{25}$. The expression of g_{25} is given at (43) due to $g_{25} = \hat{g}_{25}$ and the expression of g_{15} is given by (41). In this case study, the zeros of $g_{15} + g_{25}$ are -30, $-41 \pm 66j$, -119, -1265, -466180 and thus the forward function $g_0(s)$ is always stable no matter what are the input and output signals.

The feedback loop stability is studied by the Nyquist criterion. The number of unstable poles of $g_1 h_1$ is determined by $g_1 = -\frac{g_{15}+g_{25}}{1+Y_0^2 g_{15} g_{25}}$ due to that $h_1(s)$ is dissipative, containing an infinite number of stable poles. The poles of g_1 are: 173, -0.98, $-25 \pm 22j$, -119, -434, -1125 and -449937. Therefore, there are one unstable pole of the open loop function of $g_1/(1 + g_1 h_1)$. In order to guarantee the stability of the closed loop function, the Nyquist plot should anti-clockwise encircle the critical point (-1,0) once. For one Π-section cable model, the equivalent cable function of $h_1(s)$ is depicted by $h_{pi}(s) = cs \cdot d/2 + 1/(ls + r)/d$. The Nyquist curve of open loop function $g_1 h_1(j\omega)$ and $g_1 h_{pi}(j\omega)$ is given by Fig. 6.

Fig. 6 (a). shows that in the low frequency band, both cable models provide similar Nyquist curves. However, in this study case, the Fig. 6 (b). shows that for the distributed parameter cable model, the Nyquist curve will anti-clockwise encircle the critical point (-1,0) but for the one Π-section cable model, the Nyquist curve will clockwise encircle the critical point once. Therefore, the VSC-HVDC system with distributed parameter DC cable is stable but the VSC-HVDC system with one Π-section DC cable model has two unstable poles i.e. $0.7 \pm 1.78j$, which are calculated by the eigenvalue of the weak AC-grid connected VSC-HVDC system state matrix $A_2 + B_{d2} C_{d2}$. This is because, for $\omega < 1/d/\sqrt{lc/2} = \omega_{rf}$ (resonance frequency of one Π-section cable), $|h_1(j\omega)| > |h_{pi}(j\omega)|$ and implies that the VSC-HVDC system with distributed parameter cable model has a larger gain margin.

Fig. 7. shows that if the VSC-HVDC system with one Π-section is stable, then the phase crossover frequency must be lower than ω_{rf} where $h_1(j\omega)$ is similar to $h_{pi}(j\omega)$ and since $g_1 h_1$ has a larger gain margin, the VSC-HVDC system with distributed parameter cable model is also stable. Consequently, the VSC-HVDC system with one Π-section DC cable is stable is a sufficient condition of the VSC-HVDC system with distributed parameter cable model is stable but not vice versa.

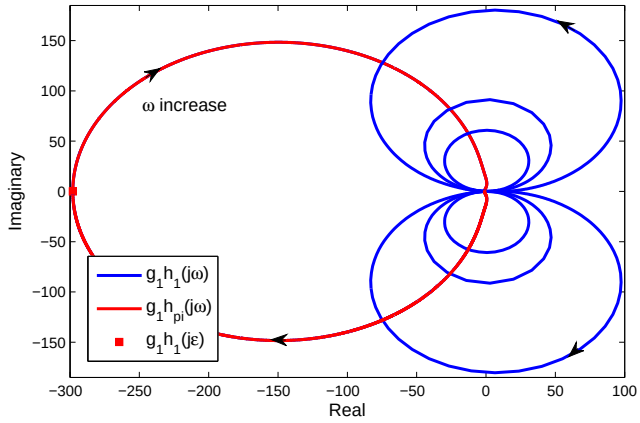

(a)Full curve

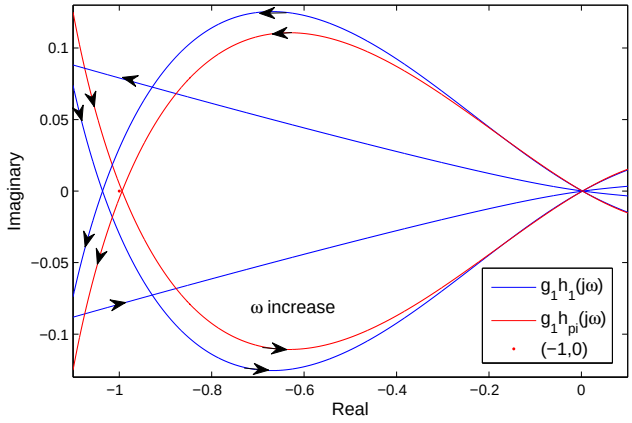

(b)Amplified around critical point (-1,0)

Figure 6: Nyquist plot of $g_1(j\omega)h_1(j\omega)$: red curve is the Nyquist plot of VSC-HVDC system with one Π-section DC-cable model; blue curve is the Nyquist plot of the VSC-HVDC system with distributed parameter DC-cable model; $\varepsilon = 0.01$ [rad/s]

5.2 Strong AC-grid environment

For a VSC-HVDC system embedded in strong AC-grid, the small signal stability analysis based on the Nyquist stability criterion is discussed in, for example [11]. It gives:

$$\hat{g}_{11} = \frac{\alpha_c \omega_{nd} C_1 (2\zeta s + \omega_{nd})}{C_1 s^2 (s + \alpha_c) + \alpha_c \omega_{nd} C_1 (2\zeta s + \omega_{nd}) + \frac{i_{DC10}}{v_{DC10}} s^2}$$
$$\hat{g}_{13} = \frac{\frac{P_{10}}{E_{10} v_{DC10}} s^2}{C_1 s^2 (s + \alpha_c) + \alpha_c \omega_{nd} C_1 (2\zeta s + \omega_{nd}) + \frac{i_{DC10}}{v_{DC10}} s^2} \quad (42)$$

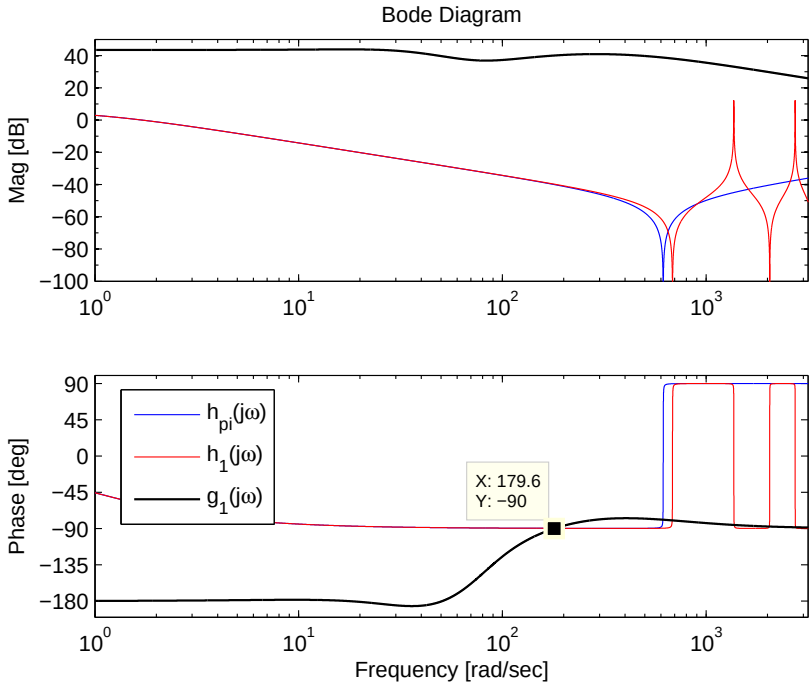

Figure 7: Frequency characteristic curve of $g_1(j\omega)$, $h_1(j\omega)$ and $h_{pi}(j\omega)$

$$\begin{aligned}
\hat{g}_{15} &= -\frac{s^2}{C_1 s^2(s+\alpha_c) + \alpha_c \omega_{nd} C_1(2\zeta s + \omega_{nd}) + \frac{i_{DC10}}{v_{DC10}} s^2} \\
\hat{g}_{21} &= \frac{\alpha_p}{(C_2 v_{DC20} s + i_{DC20})(s+\alpha_p)} \\
\hat{g}_{23} &= \frac{\frac{P_{20}}{E_{20}} s}{(C_2 v_{DC20} s + i_{DC20})(s+\alpha_p)} \\
\hat{g}_{25} &= -\frac{v_{DC20}}{C_2 v_{DC20} s + i_{DC20}}
\end{aligned} \tag{43}$$

The forward function $\hat{g}_0(s) = -1/(\hat{g}_{15} + \hat{g}_{25}) \cdot \hat{G}(s)$, whose stability depends on the zero polynomial $Q_3(s)$ of $\hat{g}_{15} + \hat{g}_{25}$:

$$\begin{aligned}
Q_3(s) = (C_1 + C_2)s^3 + (C_1\alpha_c + \frac{i_{DC10}}{v_{DC10}} + \frac{i_{DC20}}{v_{DC20}})s^2 + \\
+ \alpha_c K_{pd} s + \alpha_c K_{id}
\end{aligned} \tag{44}$$

To guarantee that the zeros of $Q_3(s)$ are located in the left half plane, the following inequality must hold:

$$\frac{C_1\alpha_c + \frac{i_{DC10}}{v_{DC10}} + \frac{i_{DC20}}{v_{DC20}}}{C_1 + C_2} > \frac{K_{id}}{K_{pd}} = \frac{\omega_{nd}}{2\zeta} \tag{45}$$

To minimize transmission losses, the DC voltage drop between two terminals should be kept small. Moreover, the bandwidth of the inner current loop α_c is designed to be ten times larger than the DC voltage loop. Therefore the inequality (45) holds for all reasonable designs of PI-controllers and the forward function $\hat{g}_0$ for all input-output combinations are thus stable in case of strong AC-grid environment.

In the paper [11], two examples have been investigated, showing that in both cases with either the rectifier or the inverter working as DC voltage controller, the VSC-HVDC system is stable for three different cable distances d=50km, 150km, 450km. The same result is obtained when the distributed parameter cable model is changed into one Π-section model.

6 Conclusions

A mathematical model for small-signal stability analysis of a two terminal VSC-HVDC system embedded in a weak AC-environment has been presented. The system could be separated into two parts: the active power controlled VSC and the DC-voltage controlled VSC with a DC-cable model. The stability of the first part is analyzed by the small gain theorem, which shows that for $SCR > 2.7$, provided the parameter values from Table 2, the active power controlled VSC embedded in a weak AC-environment always will be stable. The second part is analyzed by the Nyquist criterion. Due to the symmetric properties of the cable model, the block diagram of each input output combination can be rewritten as in Fig. 2., where $g_0(s)$ is stable with reasonable design of the DC voltage PI-controller and $SCR > 4$, $g_1(s)$, is a rational function of 's' and the return path $h_1(s)$ is dissipative. One case study have been illustrated, showing that If the VSC-HVDC system with one Π-section cable model is stable, then the VSC-HVDC system with distributed parameter DC cable model is also stable provided that $|h_1(j\omega)| > |h_{pi}(j\omega)|$ for $\omega < 1/d/\sqrt{lc/2}$.

The proposed method proves that for long distance VSC-HVDC transmission or larger cable impedance density, the VSC-HVDC system with one Π-section cable model is sufficient to prove the system stability. Also, the VSC-HVDC system with distributed parameter cable can provide accurate high frequency response.

7 Appendix

7.1 State space model of Active power controlled VSC

The disturbance matrices C_{d1} and D_{d1} of the third order state-space model of active power controlled VSC are:

$$
\begin{aligned}
d &= C_{d1} \cdot x_{ap} + D_{d1} \cdot u_{ap} \\
C_{d1} &= \frac{L_g}{k_1} \begin{bmatrix} 1 + a_{pll} L_g \frac{P_0}{E_0^2} & -(a_p + a_{pll}) L_g \frac{Q_0}{E_0^2} \\ a_c L_g K_{pa} & 1 - a_p L_g \frac{P_0}{E_0^2} \end{bmatrix} \cdot \\
&\quad \cdot \begin{bmatrix} a_p - \frac{R_g}{L_g} & \omega_0 & \omega_0 \frac{P_0}{E_0^2} + \frac{Q_0}{E_0^2}(a_p + a_{pll} - \frac{R_g}{L_g}) \\ -\omega_0 & a_c - \frac{R_g}{L_g} & (a_{pll} - \frac{R_g}{L_g}) \frac{P_0}{E_0^2} - \frac{Q_0}{E_0^2}\omega_0 \end{bmatrix} \\
D_{d1} &= \frac{1}{k_1} \begin{bmatrix} 1 + a_{pll} L_g \frac{P_0}{E_0^2} & -(a_p + a_{pll}) L_g \frac{Q_0}{E_0^2} \\ a_c L_g K_{pa} & 1 - a_p L_g \frac{P_0}{E_0^2} \end{bmatrix} \begin{bmatrix} -\frac{ap}{E_0} L_g & 0 & 1 & 0 \\ 0 & -acK_{pa} L_g & 0 & 1 \end{bmatrix} \\
k_1 &= 1 + L_g(a_{pll} - a_p)\frac{P_0}{E_0^2} - L_g^2[a_p a_{pll}\frac{P_0^2}{E_0^4} + a_c(a_p + a_{pll})K_{pa}\frac{Q_0}{E_0^2}]
\end{aligned}
$$

The disturbance matrices $\tilde{C}_{d1}$ and $\tilde{D}_{d1}$ of the second order state-space model of active power controlled VSC are:

$$
\begin{aligned}
d &= \tilde{C}_{d1} \cdot x_{apn} + \tilde{D}_d \cdot u_{ap} \\
\tilde{C}_{d1} &= \frac{L_g}{\tilde{k}_1} \begin{bmatrix} 1 + a_{pll} L_g \frac{P_0}{E_0^2} & -(a_p + a_{pll}) L_g \frac{Q_0}{E_0^2} \\ K_{pa} L_g \frac{R_g}{L_g} & 1 + (\omega_0 K_{pa} - a_p \frac{P_0}{E_0^2}) L_g \end{bmatrix} \cdot \\
&\quad \cdot \begin{bmatrix} a_p - \frac{R_g}{L_g} & \omega_0 \frac{P_0}{E_0^2} + \frac{Q_0}{E_0^2}(a_p + a_{pll} - \frac{R_g}{L_g}) \\ -\omega_0 & (a_{pll} - \frac{R_g}{L_g}) \frac{P_0}{E_0^2} - \frac{Q_0}{E_0^2}\omega_0 \end{bmatrix} \\
\tilde{D}_{d1} &= \frac{1}{\tilde{k}_1} \begin{bmatrix} 1 + a_{pll} L_g \frac{P_0}{E_0^2} & -(a_p + a_{pll}) L_g \frac{Q_0}{E_0^2} \\ K_{pa} L_g \frac{R_g}{L_g} & 1 + (\omega_0 K_{pa} - a_p \frac{P_0}{E_0^2}) L_g \end{bmatrix} \begin{bmatrix} -\frac{ap}{E_0} L_g & K_{pa}\omega_0 L_g & 1 & 0 \\ 0 & -\frac{R_g}{L_g} K_{pa} L_g & 0 & 1 \end{bmatrix} \\
\tilde{k}_1 &= 1 + L_g[(a_{pll} - a_p)\frac{P_0}{E_0^2} + \omega_0 K_{pa}] + \\
&\quad + L_g^2[a_{pll}(\omega_0 K_{pa} - a_p \frac{P_0}{E_0^2})\frac{P_0}{E_0^2} + K_{pa}\frac{R_g}{L_g}(a_p + a_{pll})\frac{Q_0}{E_0^2}];
\end{aligned}
$$

For a strong AC-grid, $L_g \to 0$ and thus both C_{d1} and $\tilde{C}_{d1}$ are zero matrix and $D_{d1} = \tilde{D}_{d1} = \begin{bmatrix} 0 & 0 & 1 & 0 \\ 0 & 0 & 0 & 1 \end{bmatrix}$. It means that for strong AC-grid, $\Delta E_d = \Delta v_{sd}$ and $\Delta E_q = \Delta v_{sq}$.

7.2 State space model of VSC-HVDC system with one Π-section cable model

The state-space model of VSC-HVDC system with one Π-section DC-cable model is given below, where $\hat{C} = C + d \cdot c/2$:

$$\dot{x}_{dv} = A_2 \cdot x_{dv} + B_{u2} \cdot u_{dv}^{ref} + B_{d2} \cdot d$$

$$d = C_{d2} \cdot x_{dv} + D_{d2} \cdot u_{dv}$$

$$A_2 = \begin{bmatrix} -a_c & 0 & -2\zeta\omega_{nd}\hat{C}\frac{v_{DC0}}{E_0}a_c & \omega_{nd}^2\hat{C}\frac{v_{DC0}}{E_0}a_c \\ 0 & -a_c & 0 & 0 \\ \frac{E_0}{\hat{C}v_{DC0}} & 0 & -\frac{i_{DC0}}{\hat{C}v_{Dc0}} & 0 \\ 0 & 0 & -1 & 0 \\ a_f E_0 \frac{d\cdot c/2}{\hat{C}} & 0 & a_f i_{DC0}\frac{C}{\hat{C}} & 0 \\ 0 & 0 & 0 & 0 \\ 0 & 0 & \frac{1}{L_{DC}} & 0 \\ 0 & 0 & 0 & 0 \end{bmatrix}$$

$$\begin{bmatrix} \frac{a_c}{E_0} & 0 & 0 & 0 \\ 0 & 0 & 0 & 0 \\ 0 & \frac{E_0}{\hat{C}v_{DC0}}\frac{Q_0}{E_0^2} & -\frac{1}{\hat{C}} & 0 \\ 0 & 0 & 0 & 0 \\ -a_f & a_f E_0 \frac{d\cdot c/2}{\hat{C}}\frac{Q_0}{E_0^2} & a_f v_{DC0}\frac{C}{\hat{C}} & 0 \\ 0 & -a_{pll} & 0 & 0 \\ 0 & 0 & -\frac{R_{DC}}{L_{DC}} & -\frac{1}{L_{DC}} \\ 0 & 0 & \frac{1}{\hat{C}} & \frac{i_{DC0}}{\hat{C}v_{DC0}^{ap}} \end{bmatrix}$$

$$B_{u2}^T = \begin{bmatrix} 2\zeta\omega_{nd}\hat{C}\frac{v_{DC0}}{E_0}a_c & 0 & 0 & 1 & 0 & 0 & 0 & 0 \\ 0 & a_c K_{pa} & 0 & 0 & 0 & 0 & 0 & 0 \end{bmatrix}$$

$$B_{d2}^T = \begin{bmatrix} -a_c\frac{P_0}{E_0^2} & -a_c K_{pa} & \frac{E_0}{\hat{C}v_{DC0}}\frac{P_0}{E_0^2} & 0 & a_f * E_0 * \frac{d\cdot c/2}{\hat{C}}\frac{P_0}{E_0^2} & 0 & 0 & 0 \\ 0 & 0 & -\frac{E_0}{\hat{C}v_{DC0}}\frac{Q_0}{E_0^2} & 0 & -a_f * E_0 * \frac{d\cdot c/2}{\hat{C}}\frac{Q_0}{E_0^2} & a_{pll} & 0 & 0 \end{bmatrix}$$

$$C_{d2} = \frac{L_g}{k_2}\begin{bmatrix} 1 + a_{pll}L_g\frac{P_0}{E_0^2} & -a_{pll}L_g\frac{Q_0}{E_0^2} \\ a_c L_g K_{pa} & 1 - a_c L_g\frac{P_0}{E_0^2} \end{bmatrix}\begin{bmatrix} a_c - \frac{R_g}{L_g} & \omega_0 & 2\zeta\omega_{nd}\hat{C}\frac{v_{DC0}}{E_0}a_c \\ -\omega_0 & a_c - \frac{R_g}{L_g} & 0 \end{bmatrix}$$

$$\begin{bmatrix} -\omega_{nd}^2\hat{C}\frac{v_{DC0}}{E_0}a_c & -\frac{a_c}{E_0} & \omega_0\frac{P_0}{E_0^2} + \frac{Q_0}{E_0^2}(a_{pll} - \frac{R_g}{L_g}) & 0 & 0 \\ 0 & 0 & (a_{pll} - \frac{R_g}{L_g})\frac{P_0}{E_0^2} - \frac{Q_0}{E_0^2}\omega_0 & 0 & 0 \end{bmatrix};$$

$$D_{d2} = \frac{1}{k_2}\begin{bmatrix} 1 + a_{pll}L_g\frac{P_0}{E_0^2} & -a_{pll}L_g\frac{Q_0}{E_0^2} \\ a_c L_g K_{pa} & 1 - a_c L_g\frac{P_0}{E_0^2} \end{bmatrix}\begin{bmatrix} -2\zeta\omega_{nd}\hat{C}\frac{v_{DC0}}{E_0}a_c L_g & 0 & 1 & 0 \\ 0 & -acK_{pa}L_g & 0 & 1 \end{bmatrix}$$

$$k_2 = 1 + L_g(a_{pll} - a_c)\frac{P_0}{E_0^2} + L_g^2 a_{pll}a_c(K_{pa}\frac{Q_0}{E_0^2} - \frac{P_0^2}{E_0^4});$$

References

[1] N. Flourentzou, V. Agelidis, and G. Demetriades, "VSC-based HVDC power transmission systems: An overview," *IEEE Trans. Power Electronics*, vol. 24, no. 3, pp. 592–602, March 2009.

[2] P. Bresesti, W. L. Kling, R. L. Hendriks, and R. Vailati, "HVDC connection of offshore wind farms to the transmission system," *IEEE Trans. Energy Conversion*, vol. 22, no. 1, pp. 37–43, March 2007.

[3] J. Svensson, *Grid-Connected Voltage Source Converter Control Principles and Wind Energy Applications*. Chalmer University of Technology, 1998, no. 331.

[4] S. Cole, J. Beerten, and R. Belmans, "Generalized Dynamic VSC MTDC Model for Power System Stability Studies," *IEEE Trans. Power System*, vol. 25, no. 3, pp. 1655–1662, August 2010.

[5] L. Zhang, *Modeling and Control of VSC-HVDC Links Connected to Weak AC System*. Stockholm, Sweden: PhD Thesis, Royal Institute of Technology, 2010.

[6] G.-C. Hsieh and J. C. Hung, "Phase-locked loop techniques – A survey," *IEEE Trans. Ind. Electron*, vol. 43, no. 6, pp. 609–615, Dec. 1996.

[7] B. Ooi and X. Wang, "Voltage angle lock loop control of the boost type PWM converter for HVDC application," *IEEE Transactions on Power Electronics*, vol. 5, no. 2, pp. 229–235, Apr. 1990.

[8] L. Harnefors, M. Bongiorno, and S. Lundberg, "Input-Admittance Calculation and Shaping for Controlled Voltage-Source Converters," *IEEE transactions on industrial electronics*, vol. 54, no. 6, pp. 3323–3334, 2007.

[9] B. K. Bose, *Power Electronics and Variable Frequency Drives*. New York, USA: IEEE Press, 1997.

[10] A. Jain, K. Joshi, A. Behal, and N. Mohan, "Voltage regulation with STATCOMs: Modeling, control and results," *IEEE Trans. Power Delivery*, vol. 21, no. 2, pp. 726–735, April 2006.

[11] Y. Song and C. Breitholtz, "Nyquist stability analysis of a VSC-HVDC system using a distributed parameter DC-cable model," in *19th World Congress of the International Federation of Automatic Control*, Cape town, South Africa, August 2014.

[12] K. J. Astrom and R. M. Murray, *Feedback System - An Introduction for Scientists and Engineers*. Princeton university press, 2008.

[13] H. K. Khalil, *Nonlinear Systems (3rd Edition)*. Prentice Hall,, 2002.